University of São Paulo
Institute of Astronomy, Geophysics and Atmospheric Sciences
Department of Atmospheric Sciences

Mario Eduardo Gavidia Calderón

From global to local: A multi-scale air quality modeling study over the Metropolitan Area of São Paulo

"De global ao local: Um estudo multi-escalas de modelagem de qualidade do ar na Região Metropolitana de São Paulo"

São Paulo 2020

Mario Eduardo Gavidia Calderón

From global to local: A multi-scale air quality modeling study over the Metropolitan Area of São Paulo

"De global ao local: Um estudo multi-escalas de modelagem de qualidade do ar na Região Metropolitana de São Paulo"

Thesis submitted in partial fulfillment of the requirements for the degree of Doctor of Sciences in the Institute of Astronomy, Geophysics and Atmospheric Sciences.

Major field: Atmospheric Sciences
Advisor: Prof. Dr. Maria de Fatima Andrade

Final version. The original copy is available at the library

São Paulo 2020

To my family: Lili, Napo, Carloncho, and Yor

Acknowledgements

Infinite thanks to my advisor, Professor Maria de Fatima Andrade, with whom I started to make my first steps in the air quality research field, and who taught me that optimism and patience are also important ingredients in science.

To the professors of IAG, special thanks to Professors Edmilson Freitas, Rita Yuri Inoe, Adalgiza Fornaro, and Humberto Rocha, who were the jury in the qualification exams during my master and Ph.D. studies. Every question, discussion, and suggestion was the equivalent of an intensive class.

To CAPES, CNPQ, and FAPESP for their financial support to develop this research.

To Yang Zhang, Youngseob Kim, and Yangyang Xu, for the opportunity to visit different laboratories in other countries, for the rich scientific discussion, and for taking care of me abroad, and to ensure to bring me be back to Brazil, safe and sound, to continue my research.

To my Latin American friends, Angel and Sergio. Angel, It was fun and terrifying to discover how to run WRF-Chem, your help was very important in the development of this work. Sergio, thanks for remembering me that not always the fault is in the emissions and for motivating me to code like a ninja and to share the knowledge.

To my Brazilian friends Ana, Carol, and Natalia, for all the awesome Portuguese conversation about the atmosphere, the life, and the future, and the indulgence during my first years in Brazil when I was destroying your beautiful language with my *portunhol*.

To the international friends that I met living in a *republica*, I'm sure we will meet again at any point of the globe. Shout out loud to *o grande* Yuugo and my shamanic brother Yadrán.

To my Peruvian friends at IAG and at the USP. Peru wasn't so far when we get together.

And to my Peruvian friends in Peru, because the time didn't pass when get together.

To my big brothers. Carlos (aka Carloncho), thanks a lot for your tips about coding and writing in science, you gave the last push to finish this thesis. Jorge (aka Yor), thanks a lot for taking care of my health remotely by answering all my health questions very patiently and for teaching me that the limit of Paracetamol in the body is 1 g. And thanks both of you for your great advice about adulthood.

To Mom and Dad, for always believe in me and encourage me. Dad, your pep talk is more than enough to deal with any monster than I can face (even the Ph.D.). Mom, thanks for your practical knowledge through sayings and for light a candle every time I struggle.

And to my beloved Sofi, who show me that life is easier in pairs.

Esta tese/dissertação foi escrita em LaTeX com a classe IAGTESE, para teses e dissertações do IAG.

"*...But then science is nothing but a series of questions that lead to more questions, which is just as well, or it wouldn't be much of a career path, would it? Well -whatever the answers to such questions, believe you me, everything is changing for mankind...*"

Terry Pratchett and Stephen Baxter, The Long Earth

"*Science is what we understand well enough to explain to a computer; art is everything else.*"

Donald E. Knuth, Things a Computer Scientist Rarely Talks About

Resumo

A poluição do ar é um problema ambiental que começa numa escala local, mas os seus efeitos vão além dos limites das cidades em diferentes escalas do espaço e tempo. As medições nas estações de qualidade do ar são a principal fonte de informação sobre o estado da atmosfera. Porém, elas possuem limitações na cobertura espacial, na interpretação da informação, e a sua implementação pode ser cara. Os modelos de qualidade do ar, através da solução das equações do movimento e das reações químicas da atmosfera, representam uma alternativa para investigar a qualidade do ar, fornecendo informação das concentrações de poluentes e as condições meteorológicas com diversa resolução espacial e temporal. Neste trabalho, diferentes modelos de qualidade do ar e inventários de emissões, em diferentes resoluções espaciais, são utilizados para estudar a qualidade do ar na região metropolitana de São Paulo (RMSP). Produtos do modelo global Community Atmosphere Model with Chemistry (CAM-Chem) são usados como condições de contorno químicas (CQC) para o modelo Weather Research and Forecasting with Chemistry (WRF-Chem). Em seguida, WRF-Chem é usado para simular a qualidade do ar na escala regional e urbana, através de domínios que cobrem a região sudeste do Brasil e a RMSP. Finalmente, o Model of Urban Network of Intersecting Canyons and Highways (MUNICH) é usado para simular ozônio e NO_X dentro dos cânions urbanos, considerando como exemplo o distrito de Pinheiros. Desenvolvemos uma nova metodologia para distribuir espacial e temporalmente as emissões veiculares baseada nas emissões totais e o comprimento das estradas; e criamos um programa para construir o arquivo de emissões antropogênicas do WRF-Chem. Também desenvolvemos um pacote no R para fazer download e gerar dados prontos para serem analisados da Rede de Estações de Qualidade do Ar da CETESB, permitindo a automatização da avaliação dos modelos de qualidade do ar utilizando toda a

informação disponível. Os resultados mostraram que o CAM-Chem, além de servir como CQC, representou adequadamente as concentrações de ozônio e $PM_{2.5}$ para toda a RMSP com coeficientes de correlação maiores que 0.7, enquanto os poluentes primários são altamente subestimados. O WRF-Chem atingiu as benchmarks meteorológicos para ambos os domínios (e.g. $\pm$ 0.5 K de sesgo médio para temperatura, $\pm$ 10 % para umidade relativa, e $\pm$ 1.5 ms^{-1} para velocidade do vento). WRF-Chem subestimou as concentrações dos poluentes primários com sesgos médio normalizado (NMB) menores que -35 %, enquanto que o O_3 atinge os benchmarks da acurácia com coeficiente de correlação de 0.83 e um NMB de -5 %. A simulação do MUNICH utilizando as simulações do domínio urbano do WRF-Chem melhoram a representação de NO_X dentro dos cânions urbanos com um NMB de -20 %. Os resultados exemplificam as capacidades dos modelos para resolver diferentes questões sobre a formação e transporte dos poluentes atmosféricos em diferentes escalas. Esse sistema multi-escala permite a avaliação da qualidade do ar e da eficácia das políticas de controle da poluição do ar, e a realização de estudos de impacto à saúde dos poluentes atmosféricos.

Palavras-chave: Poluição do ar, modelos de qualidade do ar, CAM-Chem, WRF-Chem, MUNICH, Região Metropolitana de São Paulo.

Abstract

Air pollution is a multi-scale environmental problem that starts at the local scale, but its effects surpass the limits of cities in different scales of space and time. Measurements from air quality and meteorological stations are the main source of information on the state of the atmosphere. However, they are restricted in spatial coverage, limited in data interpretation, and are expensive to implement. Air quality models, by solving atmospheric motion equations and chemical reactions, offer an alternative approach to study air pollution by providing high temporal and spatial information of air pollutant concentration and meteorology. We used air quality models and emission inventories at different scales to study air quality in the Metropolitan Area of São Paulo (MASP). Output from the Community Atmosphere Model with Chemistry (CAM-Chem) global model is downloaded to be applied as dynamic chemical boundary conditions (CBC) for the Weather Research and Forecasting with Chemistry (WRF-Chem) community model. Then, WRF-Chem is used to simulate air quality at a regional and urban scale, considering Southeast Brazil and the MASP as simulation domains. Finally, the Model of Urban Network of Intersecting Canyons and Highways (MUNICH) is used to perform the first air quality simulation inside São Paulo urban canyons. During this process, we developed a new methodology to spatially disaggregate vehicular emissions based on total emissions and road length; and created a new tool to build WRF-Chem anthropogenic emission files. We also coded an R package to download and get high-quality data ready for analysis from the São Paulo State Environmental Agency air quality network that allows the automatization of model evaluation using all the available information. Results showed that CAM-Chem is suitable as CBC for WRF-Chem and can simulate coherently O_3 and $PM_{2.5}$ over the whole MASP with a correlation coefficients greater than 0.7, but highly underestimates and fails to sim-

ulate primary pollutants. Both regional and urban WRF-Chem simulations achieved the meteorological benchmark of performance (e.g. ± 0.5 K mean bias of temperature, ± 10 % mean bias of relative humidity, and ± 1.5 ms^{-1} mean bias of wind speed). WRF-Chem presents an underestimation of primary pollutant with normalized mean bias (NMB) lower than -35 %, while O_3 is best simulated achieving goal benchmarks with correlation coefficient of 0.83 and NMB of -5 %. MUNICH air quality simulation using WRF-Chem urban domain results as input improves NO_X simulations with a NMB of -20 %. These simulations are an example of the capabilities that models have to address different scientific questions and how they can work to establish a multi-scale modeling system for air quality forecast. These tools allow the evaluation of air quality at different scales, the assessment of the efficacy of air pollution control policies, and the study of pollution health impact of pollutant exposure, even at street level.

Keywords: Air pollution, Air quality models, CAM-Chem, WRF-Chem, MUNICH, Metropolitan Area of São Paulo.

List of Figures

List of Tables

Contents

Chapter 1

Introduction

All models are wrong but some are useful.

George Box

1.1 Preface

Unlike our geopolitical boundaries, *there are no physical boundaries to air pollution* (Seigneur, 2005). Even when pollutant emissions start in the cities, they are transported outside their limits and impact the air quality and climate at local, regional, and global scales. One of the best examples is the increment of the global average of carbon dioxide (CO_2) concentration, produced mainly by the accumulation of all the city emissions (Briber et al., 2013). Similarly, there is evidence of intercontinental transport of pollutants, like the ozone (O_3) and particulate matter (PM) produced in Asia that can reach North America west coast (Tang et al., 2007).

A more local example, for our area of study, biomass burning emissions produced in the central and north areas of Brazil and inland the state of São Paulo can reach the metropolitan area of São Paulo (MASP) (Vara-Vela et al., 2018). The emissions and pollutants generated inside the MASP, like ozone precursors, can reach other suburban cities. As a matter of fact, higher ozone concentration was reported in air quality stations downwind the MASP (CETESB, 2015, 2020). This means that the study of air pollution requires a multi-scale approach.

Measurements are crucial to monitor the state of the atmosphere. These measurements are usually performed in an air quality station (AQS), and represent a snapshot of the atmosphere at a determined location and time. Thus, the information from AQS depends

on the coverage of the AQS network, which is limited as their installation and maintenance are expensive. Their data analysis is also constrained as they offer limited information about the sources and the reactions that lead to the measured concentrations (Zhong et al., 2016), For those reasons, Kumar et al. (2018) highlighted that optimally, there should be at least one AQS per urban neighborhood, and at least 100 AQS outside the city downtown to allow a bigger scope. On the other hand, remote sensing is a possibility that offers a great space cover but limited temporal resolution.

By solving atmospheric motion equations and chemical reactions, air quality models — or in a realistic-pessimistic way, air pollution models — surpass the space and time limitation of observations. They can provide high spatial and temporal pollutant concentration fields, offer air pollutant episode forecast capabilities, and answer scientific question by handling, paraphrasing Seinfeld (2004), the *exquisitely non-linearity* of atmospheric chemical reactions. Consequently, they provided a framework to address the multi-scale nature of air pollution.

This doesn't mean that measurements don't work and air quality models are the solution to address air pollution. Actually, Seinfeld and Pandis (2016) explained that there is an interconnection between air quality network measurements, air quality modeling, and laboratory experiments. Measurements provide the information to evaluate the air quality model. Laboratory measurements describe new process mechanisms and offer parameters for air quality models. And because the air quality model represents the understanding of the atmospheric system, their evaluation shows the limitation of our knowledge and pin-point where laboratory measurement are needed for model development. We can also add that modeling can suggest pollutant concentration hot-spots where air quality measurements are required (Fig 1.1).

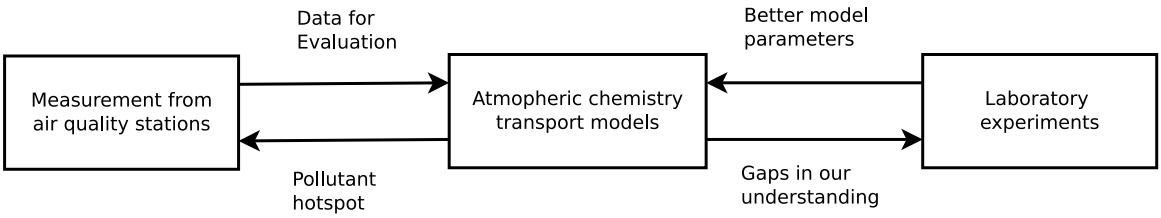

Figure 1.1: Interaction between air quality stations, air quality models, and laboratory measurements.

With this motivation, this work proposes a set of models that can be used to address different questions at different scales, how well they reproduced the observations, and a

set of tools to couple them in a way to create a multi-scale air quality modeling system.

1.2 Motivation and objectives

Air quality models offer a framework to evaluate the multi-scale nature of air pollution. Once validated, they can be used to estimate air pollutant concentrations at different temporal and spatial scales, that later can be used to perform air quality forecast or to assess the exposure to air pollutants. The MASP is the largest megacity in South America, and it counts with one of the most comprehensive air quality station network that offers enough data to verify the accuracy air quality models. It also suffers high concentrations of secondary pollutants, mainly ozone and $PM_{2.5}$, that usually present values above their respective state air quality standards. Previous studies do not account for representing high resolution description of pollutants at street-level, which is a need in a city where people spend many hours commuting.

For these reasons, the main objective is to develop a multi-scale modeling system for air quality and health exposure studies in the Metropolitan Area of São Paulo. To do that, we evaluate the Community Atmosphere Model with Chemistry (CAM-Chem) global chemistry transport model to represent pollutant concentrations in the MASP and to be used as chemical initial and boundary conditions. We then evaluate regional and urban scale simulations of regulated air pollutants, using the Weather Research and Forecasting Model with Chemistry (WRF-Chem). We take a step further and simulate ozone and nitrogen oxides inside urban canyons by using the Model of Urban Network of Intersecting Canyons and Highways (MUNICH). We also develop tools to enhance air quality analysis and air quality model verification that can be replicated in other cities.

1.3 Background and state of current research

1.3.1 Air quality models

A model is a representation of reality, or a part of it, like a system (the atmosphere) or a process (air pollution). There are typically two kinds of models, physical and mathematical models (Pielke, 2013). The physical model, also called scale or hardware model, is a physical replica of reality in a comprehensive way (Pielke, 2013; Oke et al., 2017). A wind

tunnel with a prototype of a city to study the effects of buildings in the wind flow is a good example of a physical model. Differently, mathematical models describe the world systems through mathematical equations derived from the laws of physics, chemistry, and biology (Brasseur and Jacob, 2017). These equations are usually differential equations that are solved through numeric approximations, that are translated into a computer language, resulting in a computer model. Figure 1.2 exemplifies the mathematical models: many natural phenomena are described through reactions and equations.

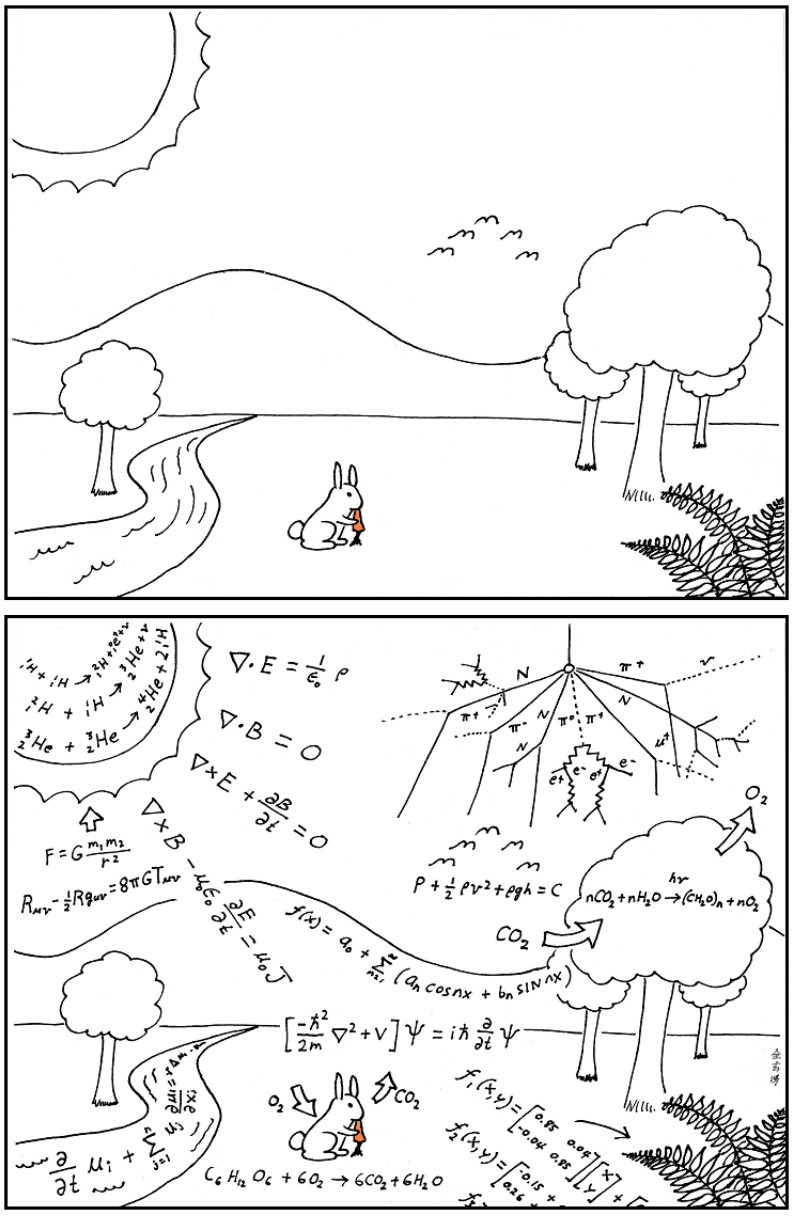

Figure 1.2: A world view by Abstruse Goose is licensed under CC BY-NC 3.0 US

Air quality models, also known as atmospheric chemistry transport model (CTM) or

photochemical models if they resolved O_3 and $PM_{2.5}$ concentrations (Seigneur and Dennis, 2011), are computer-coded representations of the dynamics, physics, radiative, and chemical processes in the atmosphere (Jacobson, 2005). Their main objective is to simulate the evolution of interacting chemical species in the atmosphere (Brasseur and Jacob, 2017). Time-dependent processes are solved through ordinary differential equations and time-space dependent processes by partial differential equations, which are solved by numerical approximations like finite-difference approximation (Jacobson, 2005).

The continuity equation, which explains the conservation of mass for different chemical species, is the base of atmospheric chemistry models (Brasseur and Jacob, 2017). The continuity equation in an Eulerian framework is shown in Eq.1.1

$$\frac{\partial C_i}{\partial t} = -\mathbf{v} \cdot \nabla C_i + P_i(\mathbf{C}) - L_i(\mathbf{C}) \tag{1.1}$$

Where $\mathbf{C} = (C_1, ..., C_n)^T$ is a vector that contains a group of chemical species ($i = 1, ..., n$) mole fractions (C_i), $\mathbf{v}$ is the 3-D wind velocity vector, P_i and L_i are the total production and total loss rates of species i. P_i and L_i include the increase or reduction by chemical reaction, emission, and deposition. So, the change in pollutant concentration in time depends on the pollutant advection ($\mathbf{v} \cdot \nabla$), the chemical production and loss, the emission and deposition, and subgrid-scale process included in $P_i - L_i$ (Seinfeld and Pandis, 2016).

Air quality models use a chemical mechanism to represent what chemical species the model will solve and how they'll react. A chemical mechanism is the component of the model that represents the pollutant chemistry. It incorporates the pollutant information about its reaction pathways and its chemical kinetics (Kaduwela et al., 2015). Also, air quality models will need the information on the emissions of these pollutants. Emissions are defined as the mass of pollutant released to the atmosphere (Pulles and Heslinga, 2007). Consequently, an emission inventory is a description of the quantity of these emissions by sources in a given period of time and space (Vallero, 2014). As noted by Pulles and Heslinga (2007), the calculation of emission inventories is not a simple task and they are usually pointed as guilty when an air quality simulation goes wrong.

Air quality models can be classified into different groups. According to their formulation, they can be Eulerian, Langragian, Statistical, and Gaussian. By their scales, they are grouped in global, continental, regional, and local/urban. By their coupling between

meteorology with chemistry, they can be online and offline.

Offline air quality models require an external meteorological input as they don't generate their own meteorological fields. On the contrary, online air quality models solve the chemistry continuity equation altogether with the meteorological conservation equation of mass, momentum, heat, and water (Brasseur and Jacob, 2017). For that reason, one great advantage of working with an on-line air quality model is the study of feedback effects between chemical composition and meteorology or vice-versa.

The other big classification group is based on the way the continuity equation is solved. Eulerian models solve it in a geographically fixed frame of reference, meanwhile, in a Lagrangian model, the frame of reference moves with the atmospheric flow. Eulerian models are better suited for air pollution modeling than the Lagrangian model. Eulerian models ensure a defined concentration field inside the simulation domain and deal better with mass conservation and the non-linear chemical reactions (Brasseur and Jacob, 2017). Nevertheless, Lagrangian models have lower errors in representing the transport of pollutants.

Air quality models have limitations. They are subjected to reducible and irreducible uncertainties. Reducible uncertainties arise from the errors in model inputs, like the meteorological and chemical initial and boundary conditions, emissions inventories, land use and cover, etc. They are also caused by the limitations on the knowledge about the atmosphere, for instance, there are still questions about a complete set of atmospheric chemical reactions, atmospheric turbulence, and secondary organic aerosol formation representation. On the other hand, irreducible uncertainties come from the limitation of representing the chaotic nature of the atmosphere and from the comparison of point measurements with model results which are volume average (Rao et al., 2020). Hence the need to evaluate the model capacity to replicate observations.

Air quality models once validated are typically used by the government and scientific community to evaluate air pollution scenarios, create national air pollution control actions, perform air quality forecast, answer scientific questions about physics and chemistry of the atmosphere, and to investigate air pollution impacts on health (Simon et al., 2012)

1.3.2 Atmospheric Scales of motions

Even when pollutant emissions are the main source of air pollution, the meteorological conditions will determine their level of concentration, their transformation to secondary

pollutants, their transport, and their removal from the atmosphere (Seinfeld and Pandis, 2016). Meteorological phenomena are classified by atmospheric scales of motions that vary in space and in time. In that sense, together with the pollutant properties and lifetimes, they will determine the scales that air pollutants can be transported (Monks et al., 2009). Figure 1.3 illustrates and summarizes all these factors.

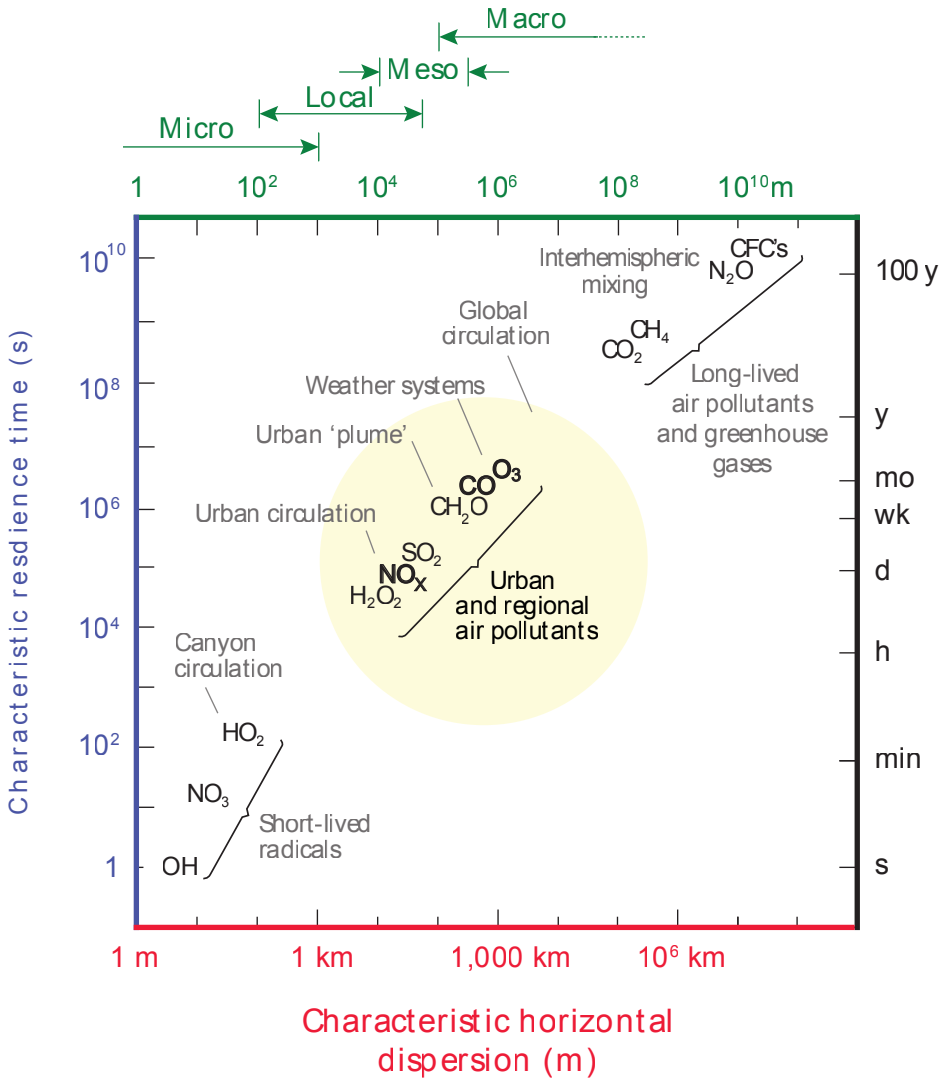

Figure 1.3: Characteristic horizontal scale of dispersion with characteristic residence time for selected gaseous species. The scale and pollutants of interest in this study are highlighted in a yellow circle (Adapted from Oke et al. (2017))

There are many examples of these interactions. At regional scales, the mixture of urban pollutants with the presence of urban breeze can create an urban plume, whereas without the breeze presence a polluted urban dome is created. At global and regional scales, long-lived atmospheric species, like greenhouse gases, can stay in the atmosphere for many years increasing the individual contribution from the cities. Greenhouse gases (GHG) are

well mixed in the hemisphere, and because the removal rate is lower than the emission rate, there is an increase in global background concentrations (Oke et al., 2017). The scales aren't isolated, they are actually integrated, and can affect the transport from one scale to another. For instance, deep convection can raise air pollution above the planetary boundary layer (PBL) which can be then transported by winds in the free troposphere on the hemispheric scales (Monks et al., 2009).

As time scales influence atmospheric dynamics, they also influence pollutant concentration (Rao et al., 2011). Intra-day concentration variations, especially for primary pollutants, depend on variation in emissions and in the development of the planetary boundary layer (PBL). Diurnal variation can be explained by the difference in emission during the night and day and the variation in meteorological conditions. Seasonal variation, as for example rainy and dry seasons, can affect photochemical reactions and deposition rates.

These scales can also be used to classify air quality models. The scale will affect the formulation of the model. Global models are hydrostatic and do not have boundary conditions, while regional and urban models are non-hydrostatic, and because they are limited area models, they require boundary conditions. For instance, WRF-Chem is a regional model, and MOZART-4 a global model (Zhang, 2008; Baklanov et al., 2014).

1.3.3 Air pollution in São Paulo

With a population of over 21 million inhabitants and with an area of 8000 km^2, the metropolitan area of São Paulo is the largest megacity in South America (United Nations, 2018). It is located in the state of São Paulo, one of the most important states of Brazil for its economic development, being responsible for 34% of Brazilian GDP (Instituto Brasileiro de Geografia e Estatistica, 2019). As every megacity, it faces the problem of air pollution (Baklanov et al., 2016), with ozone and $PM_{2.5}$ concentrations usually surpassing the Sao Paulo state air quality standards (i.e., 140 $\mu g\ m^{-3}$ of 8 h moving average and 60 $\mu g\ m^{-3}$ of daily mean, respectively).

The main source of air pollution in the MASP is the vehicular fleet (Andrade et al., 2017, 2015) (Fig. 1.4). The particularity of this vehicular fleet is the extensive use of biofuels: gasohol, ethanol and biodiesel. According to CETESB (2020), in 2019 vehicular emissions accounted for 96.5 % of carbon monoxide (CO) emissions, 73.5 % of hydrocarbons (HC), and 62.5 % of oxides of nitrogen (NO_X). Industrial sources dominate the emission of

sulfur dioxide (SO_2). For PM_{10}, 40 % is directly emitted by the vehicular fleet, and 25 % by pavement resuspension which is also related to the fleet (including tire and brake wear). In the case of $PM_{2.5}$, the vehicular fleet represents 37 % of the emission, nevertheless, 51 % of $PM_{2.5}$ correspond to secondary aerosol, which can be generated by the reaction of primary gases emitted mainly by vehicles (Vara-Vela et al., 2016). Also, the MASP atmosphere has a VOC-limited regime, which means the ozone formation is favorable to changes in VOC rather than NO_X emissions (Carvalho et al., 2015; Andrade et al., 2017).

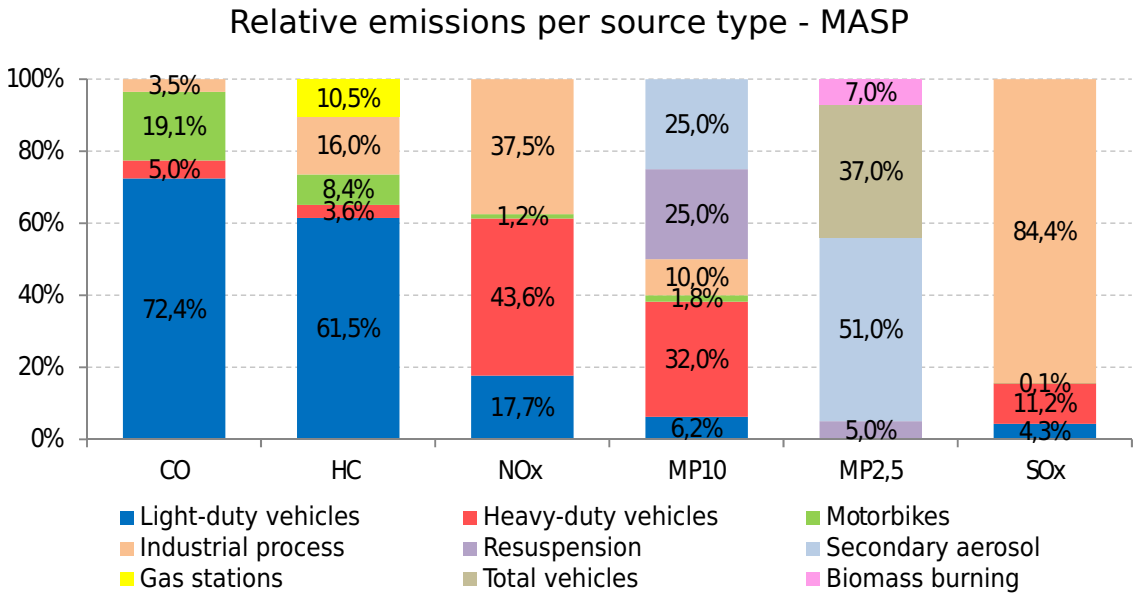

Figure 1.4: Relative emissions per source type (Adapted from CETESB (2020))

To reduce air pollution, emission control programs were established. The program for the Control of Air Pollution Emissions by Motor Vehicles (PROCONVE) is one of these programs. In the last 30 years, there was a reduction in the concentration of primary pollutants (e.g. CO, NO_X, and SO_2); however, secondary pollutants, such as ozone and fine particles have not presented a decline in concentration accordingly (Carvalho et al., 2015; Pérez-Martínez et al., 2015; Andrade et al., 2017).

Figure 1.5 shows the monthly variation of pollutant concentrations measured at the Ibirapuera air quality station (AQS). Ibirapuera AQS is located inside Ibirapuera Park, for this reason, it can be considered an urban background site (Oke et al., 2017). It clearly shows how in 20 years primary pollutants such as CO and NO_X have their concentration decreased in time, yet ozone concentration haven't, even during lock-down measures in the MASP during the COVID-19 pandemic in this year of 2020. Figure A.1, in the appendix

section, shows a similar behavior for Pinheiros AQS.

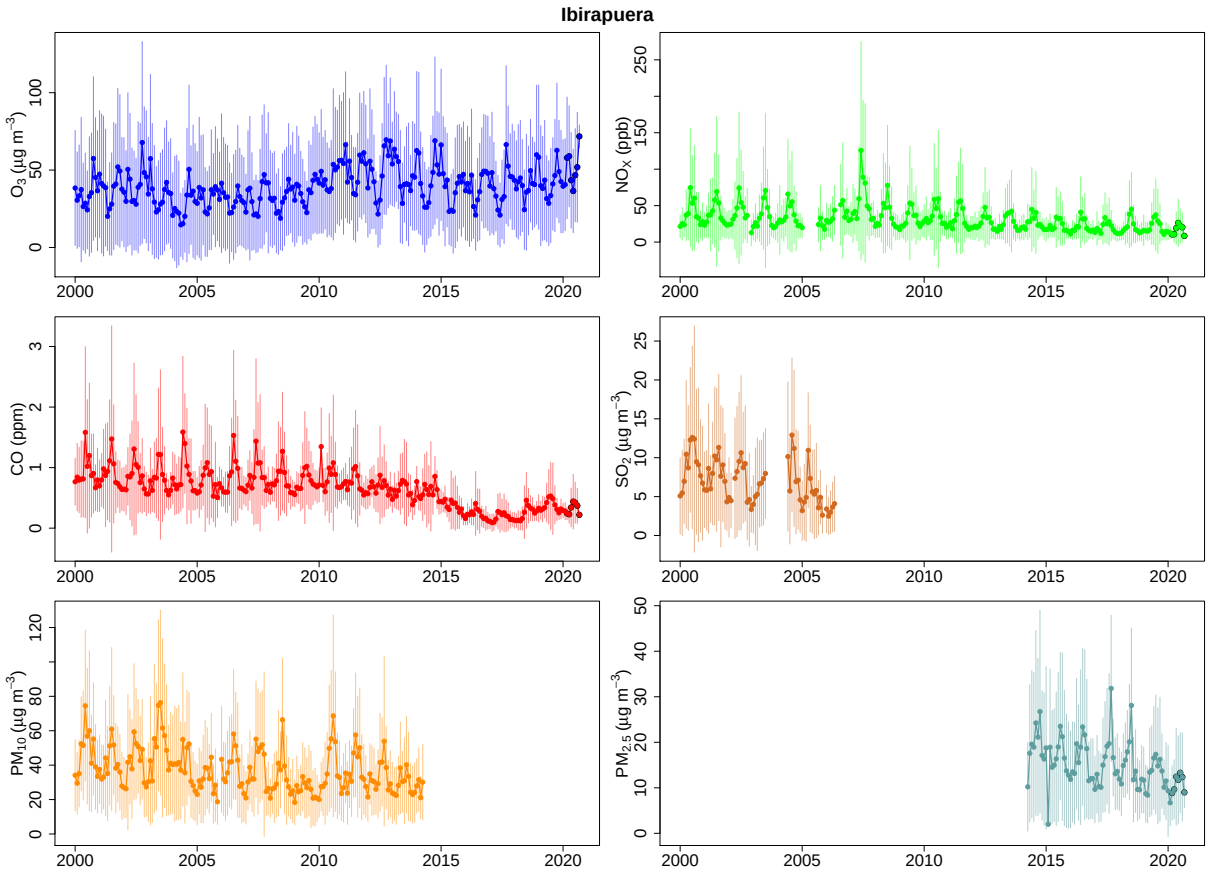

Figure 1.5: Monthly variation of air pollutants concentration at Ibirapuera air quality station. From January 2000 to September 2020

1.3.4 Air quality modeling studies in São Paulo

With the development of computer resources, it has been more affordable to run air quality models. In the MASP, many air quality models have been used to address different emerging questions.

By using the California Institute of Technology model (McRae et al., 1982), Sánchez-Ccoyllo et al. (2006) evaluated the impact of meteorology and NO_X and volatile organic compounds (VOC) limited scenarios on ozone formation, while Martins and Andrade (2008) studied the effect of VOC on ozone formation. De Freitas et al. (2005) developed a simplified photochemical module for RAMS (Regional Atmospheric Modeling System) to simulate ozone. CCATT-BRAMS model was also used to simulate ozone and $PM_{2.5}$ concentration in different ethanol consumption scenarios to see their impact on air quality and health (Scovronick et al., 2016).

The Community Multiscale Air Quality (CMAQ) modeling system, an offline air quality model, was also used. Albuquerque et al. (2018) used this model to evaluate emission reduction scenario on $PM_{2.5}$ concentrations, showing its non-linearity response to the reduction of inorganic precursors and their role in secondary organic aerosol formation. Albuquerque et al. (2019), proposed a modeling system using the Weather Research and Forecasting (WRF) model to provide the meteorological input, SMOKE as the emission preprocessor, and CMAQ to solve the atmospheric chemistry.

In recent years, WRF-Chem model has been used to simulate air quality in MASP. Andrade et al. (2015) detailed the methodology to perform air quality forecast for Southeast Brazil using WRF-Chem. The air quality forecast was performed considering vehicular emission spatially disaggregated by street length and the chosen chemical mechanism was CBM-Z. Hoshyaripour et al. (2016) compared WRF-Chem performance against an artificial neural networks (ANN) statistical model to represent surface ozone. WRF-Chem showed a better performance in simulating ozone mean and peak concentrations, the ANN model showed an advantage in simulating mean daily ozone and having lower computational cost.

Latter, Vara-Vela et al. (2016), used WRF-Chem to evaluate the impact of vehicular emission in the formation of fine particles, their results showed that 20 to 30 % of $PM_{2.5}$ total was secondary particles produced by emissions of primary gases. Gavidia-Calderón et al. (2018) evaluated the impact of using dynamic chemical boundary condition (CBC) from MOZART-4 model in the representation of ozone inside the MASP, instead of using the default WRF-Chem static CBC. They found that using dynamic CBC improves O_3 simulation, especially in the vertical levels, but the improvement is more significant in periods of lower photochemical activity. Vara-Vela et al. (2018), also used WRF-Chem to study the impact of biomass burning emission in aerosol properties inside the MASP. they found that biomass burning represent 20 % of the baseline particle number. Finally, Pellegatti Franco et al. (2019) evaluated the effect of different urban land-cover descriptions in ozone and meteorological parameter simulations, finding an improvement in the surface wind representation.

With the increase of the computer, better inputs for the modeling system was used, changing the meteorological inputs from one degree of spatial resolution to 0.5 degrees. Better tools for temporal and spatial disaggregation techniques were used to create the model emission input files. Field campaigns provided new emission factors, daily emission

profiles, and aerosol mass and number size distributions. The consideration of the global atmospheric models in regional simulation was added recently and it is limited only to their use as chemical initial and boundary conditions. The air quality modeling studies in São Paulo focused on the regional and urban scales, and there are not yet studies at street-level scale (i.e. urban canyons).

Chapter 2

Data and Methods

"Data! data! data!" He cried impatiently. "I can't make bricks without clay."

Arthur Conan Doyle, The adventure of the Copper Beeches

To create a multi-resolution platform modeling tool, we used three models: The Community Atmosphere Model with Chemistry (CAM-Chem) model (Emmons et al., 2020), the Weather Research and Forecasting with Chemistry (WRF-Chem) model (Grell et al., 2005), and the Model of Urban Network of Intersecting Canyons and Highways (MUNICH) (Kim et al., 2018), going from a Global to Regional/urban, and to a street-network model, respectively.

The experiment consists of first evaluate CAM-Chem, a global CTM, to represent atmospheric pollutants inside the MASP. Then, its output is used as chemical initial and boundary conditions to run WRF-Chem with two nested domains, one that covers Southeast Brazil (ΔX = 9 km) and the second domain, the MASP (ΔX = 3 km). This last domain then provide the meteorological input and chemical background concentration to MUNICH, a model to simulate air pollutants inside urban canyons. When putting together they represent a multi-scale air quality modeling system (Fig. 2.1).

We focused our study on the week of October 6^{th} to October 13^{th}, 2014. It was chosen for many reasons: it is a week of spring, where it is usually recorded high concentrations of ozone; no precipitation was registered, and the emission inventories used in this work were developed for that year. It also includes a holiday (October 12^{th}). The year 2014 wasn't favorable for air quality, the ozone air quality standard was surpassed 43 days, 13 of these days happened in October, and three of them happened on our study period according

to CETESB (2015). It is expected that if the evaluated model performs well during this week, they probably do better in not so extreme scenarios of pollutants concentrations.

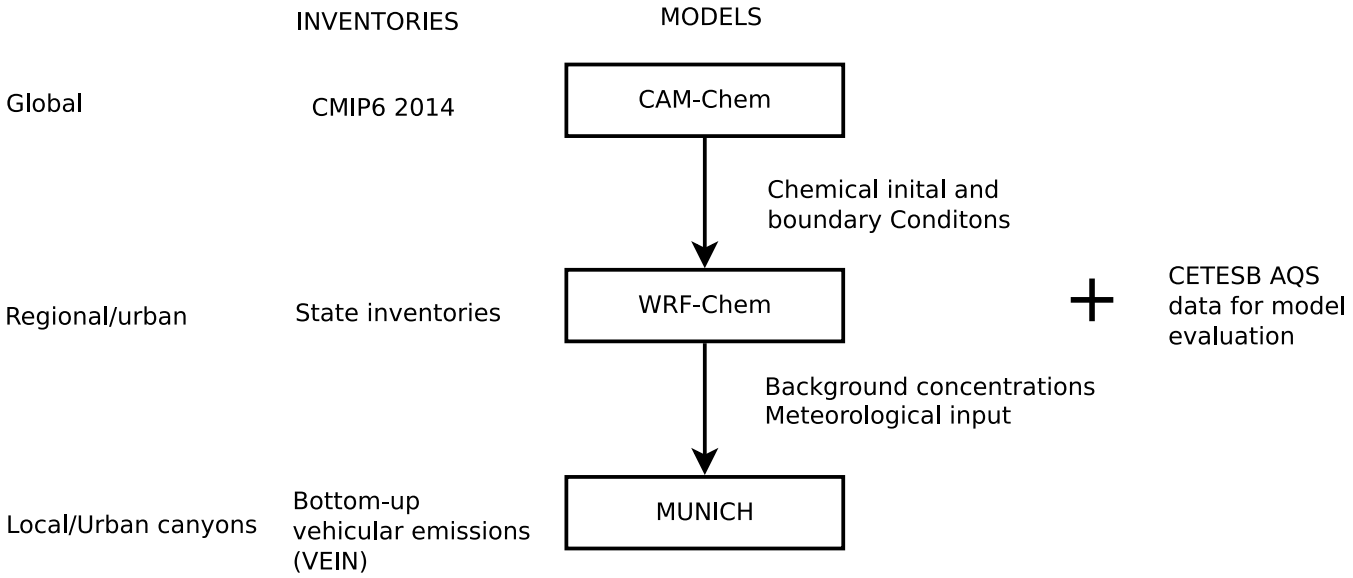

Figure 2.1: Schematics of methodology

2.1 Observations data: qualR

Air quality monitoring networks provide the concentration of air pollutants (and frequently meteorological surface data) in a specific time and space. This information is used to monitor the state of the atmosphere with the objective to protect human health. It can also provide insight into the effectiveness of emission control policies and also data for air quality model performance evaluation (Seinfeld and Pandis, 2016).

The São Paulo State Environmental Agency (CETESB) administrates the Air Quality Station network over the State of São Paulo. This network is one of the best air quality monitoring systems in the South American region (Riojas-Rodríguez et al., 2016). This network covers the MASP with more station density compared with the other regions of the São Paulo State. As noted in Andrade et al. (2017), the information from this network has been used in many studies that aim to understand air pollution over the MASP, from field campaigns to modeling studies.

Hourly pollutant and meteorological data are publicly available through a system developed by CETESB called QUALAR. QUALAR allows the user to download one variable from one air quality station (AQS) at a time in a comma-separated value file format. Be-

fore using this database, the data needs to be processed. For example, we need to change the time format, the decimal separator, and mainly, we need to complete the database as sometimes there are missing dates due to instruments calibration or malfunctions.

As around 80% of the time in data analysis is devoted to data preparation (Dasu and Johnson, 2003), we developed *qualR*[1], an R package to download São Paulo air pollution data. *qualR* streamlines this process producing complete data ready for analysis. It's built in R (R Core Team, 2020) and uses functions from *XML* and *httr* packages. A version of *qualR* in Python is also available[2].

In this work, we used *qualR* to download all the available information for all the air quality stations in São Paulo state for the period between October 6^{th} to October 13^{th}, 2014. For the meteorological database, we used hourly data of temperature at 2 meters (T2), relative humidity (RH2), wind speed and wind direction at 10 m (WS and WD). For air pollutants, we considered hourly data for Ozone (O_3), nitric oxide (NO), nitrogen dioxide (NO_2), carbon monoxide (CO), and fine particles ($PM_{2.5}$[3]).

2.2 Model performance evaluation

Model evaluation is required to create confidence in the regulatory and scientific community, this confidence is built by comparing model results against observations of meteorological and air quality data (McNider and Pour-Biazar, 2020; Rao et al., 2020).

To verify model accuracy it's common to use performance statistics or metrics and then compare them against benchmarks. Emery et al. (2001) described the benchmarks that meteorological simulation must pass to be used for air quality models. Monk et al. (2019) went further in updating these benchmarks to be used in complex terrain (see Table 2.1). Finally, to evaluate pollutant concentration simulation performance, Emery et al. (2017) increased the sample of evaluated models used by Simon et al. (2012) and recommended a set of the most used performance metrics in the evaluation of photochemical grid models. Even when these benchmarks are based on model results for Contiguous United States (CONUS), they are a good starting point, however, it is important to develop benchmarks for Brazil.

[1] Available in: `https://github.com/quishqa/qualR`

[2] Available in: `https://github.com/quishqa/qualR.py`

[3] Only used in CAM-Chem model evaluation

We used the following performance statistics (See also Table B.1 in Appendix B for their formulation):

- Mean bias (MB).
- Mean gross error (ME[4]).
- Root mean square error (RMSE).
- Normalized mean bias (NMB).
- Normalized mean error (NME).
- Correlation coefficient (R).
- Index of agreement (IOA).

Table 2.1 - Recommended performance statistics benchmark for meteorological parameters to be used in air quality modeling from Emery et al. (2001) and Monk et al. (2019)

Parameter	For simple terrain	For complex terrain
Temperature at 2m	$MB < \pm 0.5K$	$MB < \pm 1.0K$
	$ME < 2.0K$	$ME < 3.0K$
	$IOA \geq 0.8K$	
Relative humidity at 2m	$MB < \pm 10.0\%$	
	$ME < 20\%$	
	$IOA > 0.6$	
Wind speed at 10 m	$MB < \pm 0.5 ms^{-1}$	$MB < \pm 1.5 ms^{-1}$
	$RMSE \leq 2.0 ms^{-1}$	$RMSE \leq 2.5 ms^{-1}$
Wind direction at 10 m	$MB < \pm 10.0°$	$MB < \pm 10.0°$
	$ME < 30°$	$ME < 55°$

For evaluation of the pollutant concentration modelling estimates, we used the statistical indicators and benchmarks suggested by Emery et al. (2017). Table 2.2 shows these benchmarks.

[4] Also known as Mean absolute gross error (MAGE)

Table 2.2 - Recommended performance statistics benchmarks for air pollutants concentrations

Species	NMB		NME		R	
	Goal	Criteria	Goal	Criteria	Goal	Criteria
1-hr or MDA8[5] Ozone	$< \pm 5\%$	$< \pm 15\%$	$< 15\%$	$< 25\%$	> 0.75	> 0.50
24-hr $PM_{2.5}$, SO_4, NH_4	$< \pm 10\%$	$< \pm 30\%$	$< 35\%$	$< 50\%$	> 0.70	> 0.40
24-hr NO_3	$< \pm 15\%$	$< \pm 65\%$	$< 65\%$	$< 115\%$	-	-
24-hr OC	$< \pm 15\%$	$< \pm 50\%$	$< 45\%$	$< 65\%$	-	-
24-hr EC	$< \pm 20\%$	$< \pm 40\%$	$< 50\%$	$< 75\%$	-	-

A python module called *wrf_sp_eval* was coded to perform all the model evaluation for WRF-Chem in São Paulo state following these recommendations, performance statistics and benchmarks [6]. It was based on *modStats* function from the openair R package (Carslaw and Ropkins, 2012).

We used the nearest grid point to the station location to form the model - observation pairs for applying these statistics. We also transformed model units (i.e. CAM-Chem and WRF-Chem) to $\mu g\ m^{-3}$ for the case of O_3, NO, NO_2, and to *ppb* for the case of NO_X as these are the units reported from CETESB [7].

2.3 Model system and setup

In this section, we detail the models' description, configurations, and the methodology to create their input files.

2.3.1 Global scale: CAM-Chem

The Community Atmosphere Model with Chemistry (CAM-Chem) is part of the NCAR Community Earth System Model (CESM). It is used to simulate tropospheric and stratospheric composition at a global scale (Emmons et al., 2020). For this study, we downloaded a CAM-Chem simulation output[8] to be used as chemical initial and boundary conditions

[5] Maximum daily 8-h average

[6] Available in: `https://github.com/quishqa/WRF-Chem_SP`

[7] CETESB reports CO in *ppm*, the same units as WRF-Chem CO results

[8] Available in: `https://www.acom.ucar.edu/cam-chem/cam-chem.shtml`

(CBC) (Buchholz et al., 2019). This model output has a horizontal resolution of 0.9 x 1.25°, 56 vertical levels, and a temporal resolution of 6 hours. The Modern-Era Retrospective Analysis for Research and Applications (MERRA2) reanalysis was used as meteorological input. For chemistry, it used the MOZART-T1 chemistry mechanism and the Modal Aerosol Model with 4 modes with a Volatility Basis Set (MAM4-VBS) scheme as an aerosol module. The following emission inventories were considered: the Coupled Model Intercomparison Project Phase 6 (CMIP6) for anthropogenic emissions (Hoesly et al., 2018), the Model of Emissions of Gases and Aerosols from Nature version 2.1 (MEGAN2.1) for biogenic emissions (Guenther et al., 2012), and Quick Fire Emission Dataset (QFED CO2 x FINN) emission rates for fire emissions (Darmenov and Silva, 2015).

Previously, MOZART-4 output was available to be used as CBC (Emmons et al., 2009). It provided coarser horizontal resolution than CAM-Chem output (i.e. 1.9 x 2.5°) (Fig. 2.2). In MOZART-4, the chemical mechanism solver considered 85 gas-phase species, 39 photolysis, and 157 kinetic reactions; while MOZART-T1 in CAM-Chem, solves 151 gas-phase species, 65 photolysis, and 287 kinetic reactions. In a span of 10 years, it almost doubled the number of considered chemical reactions. This is a proof of the rapid advance of atmospheric chemistry and computational resources in the past years.

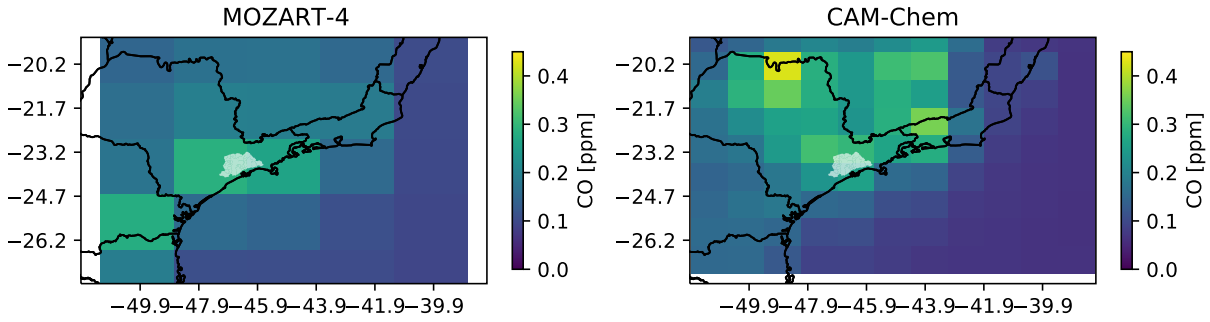

Figure 2.2: Comparison between MOZART-4 and CAM-Chem output for CO mean concentration for the study period

Global emission inventories are available in the Emissions of Atmospheric Compounds and Compilation of Ancillary Data (ECCAD)[9]. In Emmons et al. (2020), CMIP6 anthropogenic emissions are based on the Community Emissions Data System (CEDS), which is available in ECCAD.

mozbc tool[10] is used to incorporate CAM-Chem concentrations into WRF-Chem. *mozbc*

[9] Available in: https://eccad.aeris-data.fr/

[10] Available in: `https://www2.acom.ucar.edu/wrf-chem/wrf-chem-tools-community`

spatially interpolate the global model concentrations into WRF-Chem lateral boundary file (i.e. wrfbdy_d01). It does not interpolate in time, for that reason, wrfbdy_d01 has the same temporal resolution as the global model output. It also required a mapping of the global model chemical species to WRF-Chem chemical species based on the selected chemical mechanism. This mapping is performed by editing the chemical mechanism mapping template (i.e CBMZ-MOSAIC_4bins.inp) available inside *mozbc* folder. Finally, *mozbc* is also used to update initial condition concentration in WRF-Chem for both domains.

2.3.2 Regional/urban scale: WRF-Chem

The Weather Research and Forecasting with Chemistry (WRF-Chem) model is an eulerian online air quality model (Grell et al., 2005). WRF-Chem consists of a dynamical solver coupled with a chemical module. The dynamical module is the Advanced Research WRF (ARW), which is a mesoscale numerical weather prediction model for atmospheric research and operational forecast (Skamarock et al., 2019). The dynamical module offers different parameterization schemes to solve subgrid processes for longwave and shortwave radiation, planetary boundary layer (PBL) turbulence, microphysics, cumulus convection, and land surface process. Chemical modules deal with transport, chemical transformation, wet and dry deposition, photolysis, and aerosol chemistry and dynamics. As an on-line model, the chemical module uses the same transport, physics schemes, and grid as the meteorological module. In this study, we used WRF-Chem v 4.2.1.

2.3.2.1 Domain and configuration

We run WRF-Chem with two nested domains in two-way nesting (Fig. 2.3). The coarser domain (D01), with a horizontal resolution of 9 km, is the same domain used to perform the air quality forecast for Southeast Brazil (Andrade et al., 2015). The nested domain (D02) covers the MASP and it has a horizontal resolution of 3 km, satisfying the threshold value of horizontal resolution proposed by Tie et al. (2010). They proposed that to simulate O_3 correctly, the ratio between the grid resolution and the length of the city should be at least 1:6. In our case, MASP has an approximate length of $\sim$ 90 km, which gave us a grid resolution of at least 15 km to correctly simulate O_3. Table 2.3 summarizes the configurations of WRF-Chem simulations.

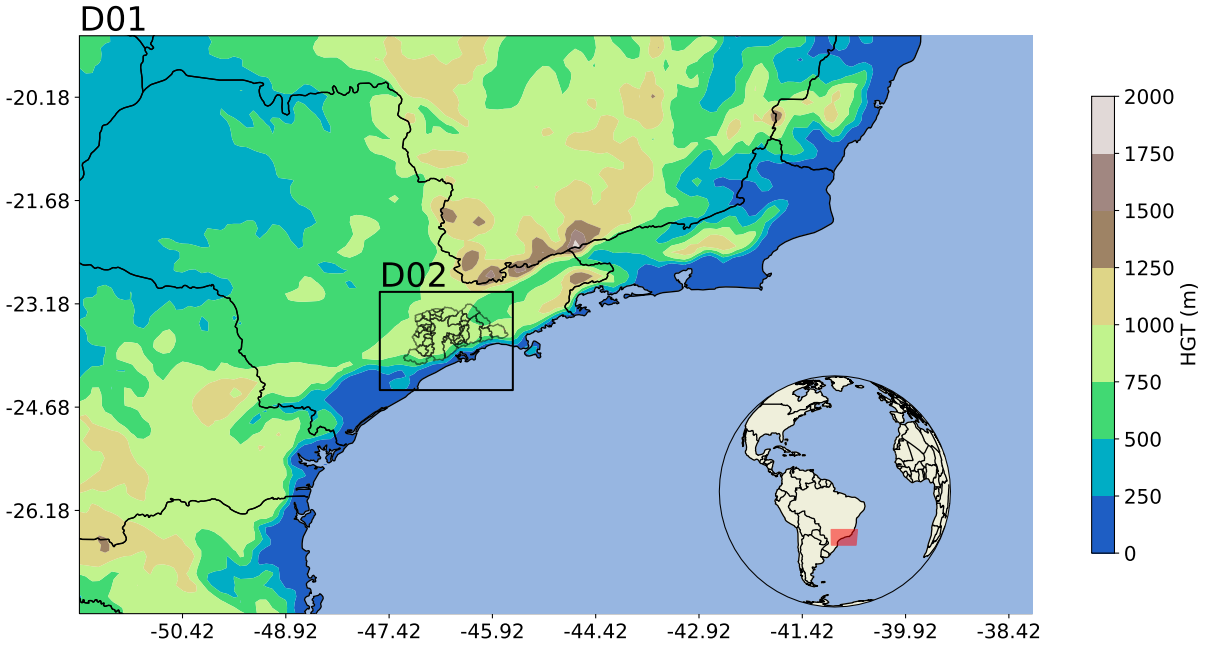

Figure 2.3: WRF-Chem simulation domains. The Metropolitan Area of São Paulo is indicated in the D02.

Table 2.3 - WRF-Chem simulation configuration.

Attribute	Configuration
WRF-Chem version	4.2.1
Domains	D01 ΔX = 9 km D02 ΔX = 3 km
Simulation period	October 4^{th} to October 13^{th}, 2014 (first two days are discarded as spin-up time)
Meteorological IC/BC	Historical Unidata Internet Data Distribution (IDD) Gridded Model Data (dds335.0)
Longwave Radiation	Rapid Radiative Transfer Model G (RRTMG) (Iacono et al., 2008)
Shortwave Radiation	Rapid Radiative Transfer Model G (RRTMG) (Iacono et al., 2008)
PBL	Yonsei University PBL (Hong et al., 2006)
Surface layer	Noah (Tewari et al., 2004)

Continued on next page

Table 2.3 – continued from previous page

Attribute	Configuration
Urban surface	3-category Urban Canopy Model (Chen et al., 2011)
Cumulus cloud	Multi-scale Krain-Fritsch (Zheng et al., 2016)
Cloud Microphysics	Morrison double-moment (Morrison et al., 2009)
Advection	Positive-definite and monotonic
Chemical mechanism	Carbon bond mechanism version Z (CBM-Z) (Zaveri, 1999)
Chemical IC/BC	CAM-Chem
Photolysis	Fast-J (Barnard et al., 2004)
Biogenic emissions	Model of Emissions of Gases and Aerosols from Nature (Guenther et al., 2006)
Anthropogenic emissions	Vehicular emissions
Species for verification	O_3, NO, NO_2, and CO

2.3.2.2 Emissions inventories

To create WRF-Chem emission file, we first need to temporally and spatially disaggregate the emission inventories. As noted by Harrison (2018), errors in emission disaggregation can cause major problems rather than the underestimation or overestimation of total emission in urban models.

Because more than 70 % of anthropogenic emissions are caused by vehicular fleet, we considered that all anthropogenic emissions are produced by the vehicular fleet as was previously assumed in Andrade et al. (2015); Gavidia-Calderón et al. (2018); Pellegatti Franco et al. (2019). We proposed a simplified approach than presented in (Andrade et al., 2015), where first a total emission is calculated by using information of emissions factors, vehicular fraction, use intensity, and fuel type. In our case, we spatially and temporally distribute the total emission reported from CETESB (2015) on WRF-Chem

domain cells based on the total road length in each cell retrieved from Open Street Map. The assumptions are as followed:

$$Total\ vehicles = \alpha \times Total\ road\ length \tag{2.1}$$

$$Total\ emission = \beta \times Total\ vehicles \tag{2.2}$$

Therefore:

$$Emission\ in\ cell = \beta \times Vehicles\ in\ cell \tag{2.3}$$

$$Emission\ in\ cell = \beta \times \alpha \times Road\ length\ in\ cell \tag{2.4}$$

The temporal distribution of emissions along the day is done by using a profile for light-duty and heavy-duty vehicles. The hourly variation of light-duty vehicle traffic was used to distribute CO and Volatile Organic Compounds (VOC) emissions, while heavy-duty vehicle traffic profile, to distribute NO_X emission. Figure 2.4 shows these emission profiles, for both type of vehicles the morning peak start at 6 hours and there is also an afternoon peak at 16 hours, which coincide with the commuting hours. However heavy-duty vehicle emissions remain relatively constant during the day. We used the VOC speciation from the air quality forecast emission file (Table G.1 in appendix G).

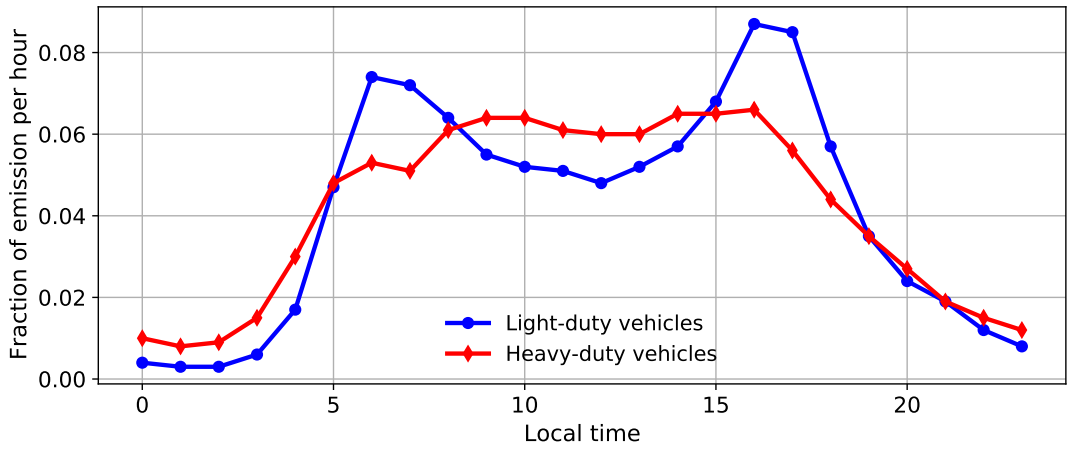

Figure 2.4: Emission temporal distribution for light-duty and heavy-duty vehicles, adapted from Andrade et al. (2015)

We think that this approach is easier to apply in other cities where their emission inventories are estimated by using top-down methodologies, or with limited emissions information, where total emissions are accumulated by year. On the other hand, we think that emission calibration is easier to perform as there are fewer variables to deal with. This approach follows the advise from Spiegelhalter (2019), where sometimes it is better to trade off *some accuracy for comprehension*[11].

Once we have the local emission spatially and temporally disaggregated, the emission file is built using PyChEmiss.

Figure 2.5 shows the roads inside the second domain and the resulted emission file after using PyChEmiss. As the proxy to disaggregate the vehicular emission is the total road length inside a model cell, the denser the road length in the cell, the higher emissions rate we will get. For this reason, São Paulo downtown have higher emission rates.

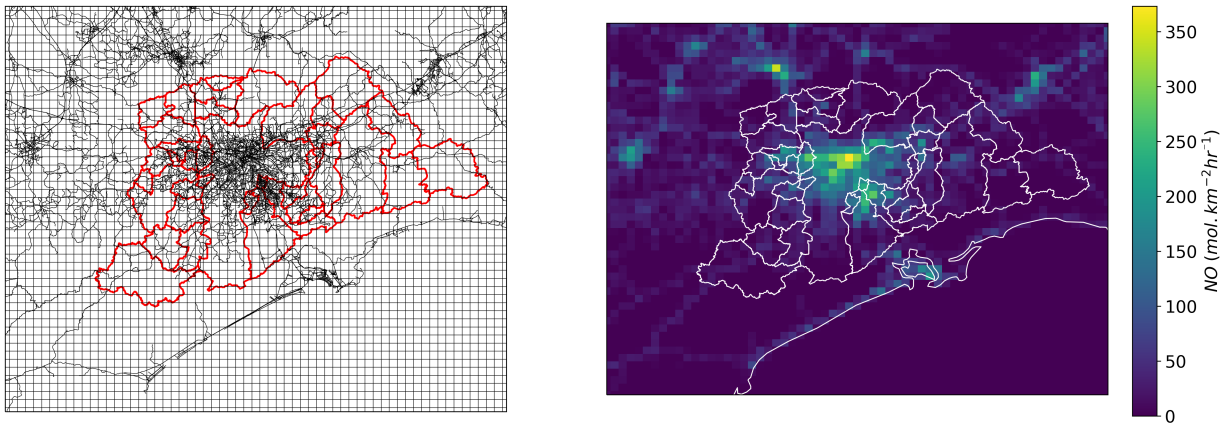

Figure 2.5: Roads inside D02 and NO emissions from wrfchemi file for 7:00 (LT)

2.3.2.3 PyChEmiss

PyChEmiss[12] is a program built in Python to create the WRF-Chem emission file from a text file that contains spatial and temporal desegregated emission fluxes. We choose Python for its language design (clear and easy reading code), its open-source philosophy, and its wide application in atmospheric sciences (Lin, 2012). The software uses functions from Numpy (Harris et al., 2020), pandas (Wes McKinney, 2010), xarray (Hoyer and

[11] More details in: `https://github.com/quishqa/FromGlob2LocSP/tree/main/04_Vehicular_Emissions`

[12] Available in: `https://github.com/quishqa/PyChEmiss`

Hamman, 2017), and xESMF (Zhuang et al., 2020) packages. PyChEmiss is based on the structure of AAS4WRF preprocessor which was coded in NCL language (Vara-Vela et al., 2017).

As input data, the software uses the WRF-Chem initial condition file (wrfinput_d01) and the local emission file. The latter is a text file with emission fluxes separated at one-hour temporal resolution and with the same spatial resolution as wrfinput_d01. PyChEmiss uses a control file (pychemiss.yml), where the location of the input files and the information to correctly read the local emission file are specified. Hence, in pychemiss.yml the user should specify the number of grid points of the spatially resolved emissions, the temporal range of the emissions (initial and end date), and the considered species (columns).

PyChEmiss was designed to: (1) Read the local emission file, reshape and transform it to a xarray Dataset data structure; (2) Store the wrfinput_d01 grid information as a xarray Dataset to create the destination grid; and (3) Perform the regridding by using xESMF package. PyChEmiss uses xEMSF source to destination nearest neighbor regridding method. Global attributes and variables attributes are added to format the regridded emission as WRF-Chem emission file requirements, to finally be exported in NetCDF format. To ensure emission mass conservation, the current version of the emission preprocessor works for surface emissions spatially resolved with the same spatial resolution of the WRF-Chem modeling domain.

2.3.3 Local scale: MUNICH

The Model of Urban Network of Intersecting Canyons and Highways (MUNICH) is a street-network model (Kim et al., 2018). A street-network model is mainly a box-model but enhanced in its formulation to explicitly model the exchange of flow and pollutants at the street intersections (Carpentieri et al., 2012). MUNICH is conceptually based on SIRANE street-network model (Soulhac et al., 2011, 2012). Nevertheless, it can use air quality measurements or chemical transport models as background concentrations. It also uses three types of urban canyons[13] based on their aspect ratios to determine the wind speed inside the urban canyon, and the vertical mass transfer between the urban canyon and the atmosphere (Lugon et al., 2020).

MUNICH has two main components, one that deals and solve pollutant concentrations

[13] An urban canyon is the structure formed by a street and its flanked buildings (Oke et al., 2017)

inside an urban-canopy volume (street-canyon component) and a second component to calculate the concentration inside an intersection volume (intersection component). Currently, MUNICH only solves gas-phase pollutants and uses CB05 chemical mechanism (Kim et al., 2018).

To get familiar with the model and to calibrate MUNICH inputs, we first performed a control simulation by running MUNICH using a WRF meteorology simulation with a horizontal resolution of 1 km in the finest domain (See in Appendix Fig. F.1 and Table F.1), and using background concentration from Ibirapuera air quality station. We then tested MUNICH using the meteorological information and background concentration from the previously described WRF-Chem urban simulation (ΔX = 3 km) as a part of the multi-resolution platform modeling tool.

One of the difficulties to run urban canyon models is the detailed input information, such as street geometry and building height. The performance of the model will depend on the quality of these in formations (Vardoulakis et al., 2003). Table 2.4 summarizes the model input used in the control MUNICH run. More details of MUNICH control simulation are described in Gavidia-Calderón et al. (2020).

2.3.3.1 Domain and configuration

For MUNICH simulations we chose Pinheiros neighborhood, a residential-commercial area in the West part of São Paulo City. From Figure 2.6 we can see that there is a variety of building heights. Pinheiros AQS is located near the roads (which is a reason for selecting this neighborhood), and it is located inside an urban canyon that has a mean building height of 5 meters (Local Climate Zone 6 - Open low rise).

2.3.3.2 Emissions: VEIN model

This kind of model requires emission rates inside each street. We can not use the previously emission approach used for WRF-Chem because the MUNICH domain is the size of one cell of WRF-Chem urban domain ($\Delta X = 3$ km), so we would only get the same emission rate for each street. Nevertheless, VEIN model uses information from traffic flow, street morphology (i.e. coordinates of intersection), and emission factors to calculate vehicular emissions. This made VEIN model suitable to create the emission input in street-network models.

Table 2.4 - MUNICH input data for diagnosis simulation

Input	Source
Meteorological simulation	WRF 3.7.1 simulation with three nested domains
Street links coordinates and width	VEIN emission model (Ibarra-Espinosa et al., 2018)
Street links emissions	VEIN emission model (Ibarra-Espinosa et al., 2018)
Building height	WUDAPT data base for MASP
Background concentration	O_3, NO and NO_2 from Ibirapuera AQS
VOC speciation	Ethanol, Formaldehyde, and acetaldehyde from WRF-Chem emission file from Andrade et al. (2015), other species were based from concentrations showed in Dominutti et al. (2016)

VEIN can be used to estimate vehicular in other cities. For example, in Ibarra-Espinosa et al. (2020) VEIN was used in urban areas located in south-east Brazil. Furthermore, VEIN was also used in Northeast China (Ibarra-Espinosa et al., 2021). The challenge is to adapt local information to VEIN input format.

For our case, emission inside the streets in VEIN model are estimated using 104 million GPS vehicle coordinates recorded in southeast Brazil, as shown by Ibarra-Espinosa et al. (2019). The GPS data is distributed to the OpenStreetMap (2017) data to obtain a traffic flow, to later generate the vehicular compositions and associate them with the emission factors reported by CETESB (2015). To obtain more representative emissions at each hour of a week, VEIN used the averaged speed calculated at each street which was previously estimated from a speed function calculated from the emission factors. Additionally, these emissions were calibrated using fuel consumption for the year 2014. More information regarding the estimations are found in Ibarra-Espinosa et al. (2020) with the emissions dataset in g h^{-1} available at `https://github.com/ibarraespinosa/ae1`.

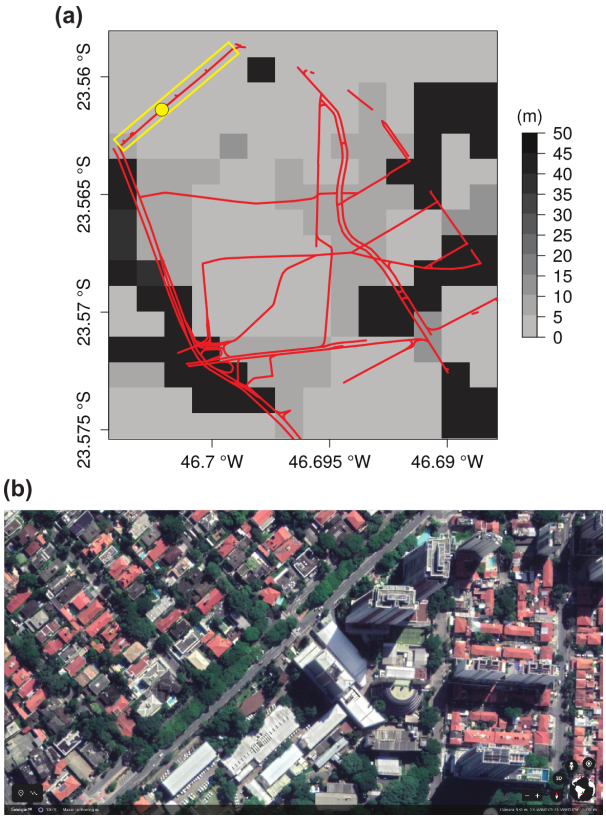

Figure 2.6: (a) MUNICH domain and building height, yellow point show Pinheiros AQS and the yellow rectangle shows the urban canyon for this study. The domains consist of a street network of 677 street links. In (b) a photo of the urban canyon in the yellow square.

MUNICH requires emission for a typical weekday and for a typical weekend. VEIN produces emission for a typical week, therefore we selected Wednesday as our typical weekday, and Saturday, as our typical weekend day. Figures 2.7 shows NO and HC emission rates at 7 hours (LT) distributed in Pinheiros streets during weekday.

2.3.3.3 Additional information: Building height and background concentration

Building height information was estimated from the World Urban Database and Access Portal Tools project (WUDAPT) for MASP (Ching et al., 2018). It is a raster file with a spatial resolution of 120 m and was previously used in Pellegatti Franco et al. (2019) (Fig. 2.8). WUDAPT categorizes urban areas in 17 Local Climate Zones (LCZ). These LCZ are divided into two groups: Build types, which are LCZ from 1 to 10; and Land Cover types, which go from A to G. Every LCZ has different surface cover, geometric, thermal, and radiative properties (Stewart and Oke, 2012).

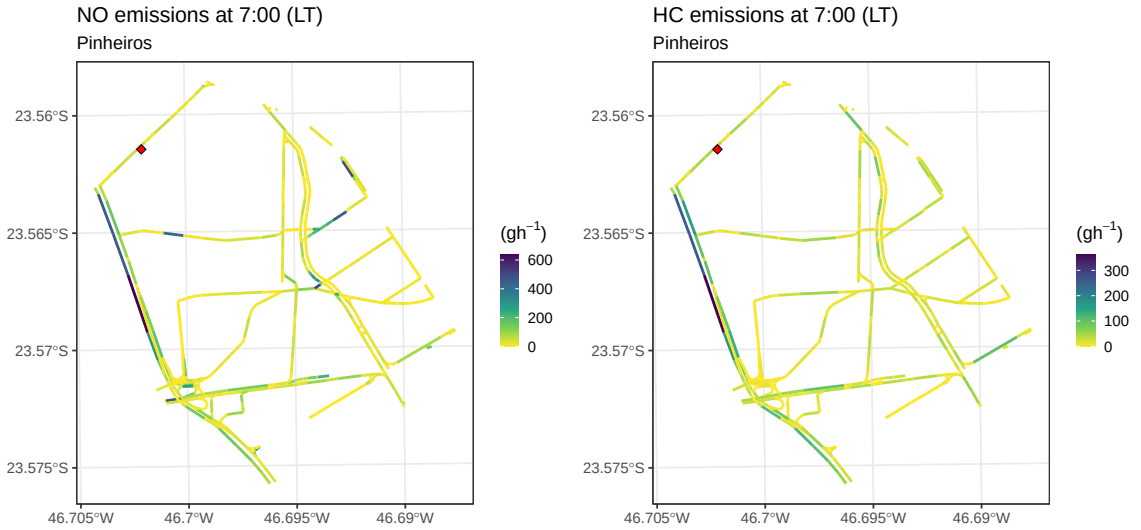

Figure 2.7: NO and HC emission from VEIN for Pinheiros MUNICH domains at 7:00 (Local time) during weekday. Red diamond points the location of Pinheiros Air quality station.

Vardoulakis et al. (2003) suggested that the background concentration in street air quality modeling is required to describe the proportion of air pollutant that is not emitted inside the urban canyons. In Street-in-Grid model, background concentrations come from Polair3D air quality model (Boutahar et al., 2004). Wu et al. (2020) chose measurements from a station located close to the study zone. Consequently, by using the mean wind field from WRF simulation for our study period, we selected Ibirapuera AQS measurements as background concentration, considering the pollutants advection from Ibirapuera to Pinheiros station.

Lastly, the number of lanes was provided by VEIN, the street width was computed by using 3 m of lane width and by adding, to each side of the street, 1.9 m as sidewalk width.

2.3.3.4 Performance statistics

To evaluate MUNICH we also used the suggested statistics from Hanna and Chang (2012) for urban dispersion model evaluation: Fractional mean bias (FB), Normalized mean-square error (NMSE), Fraction of prediction within a factor of two (FAC2), and Normalized absolute difference (NAD) (See table B.1 in appendix for their formulation). The acceptance criteria for urban modeling are $|FB| \leq 0.67$, NMSE ≤ 6, FAC2 ≥ 0.3, and NAD ≤ 0.5

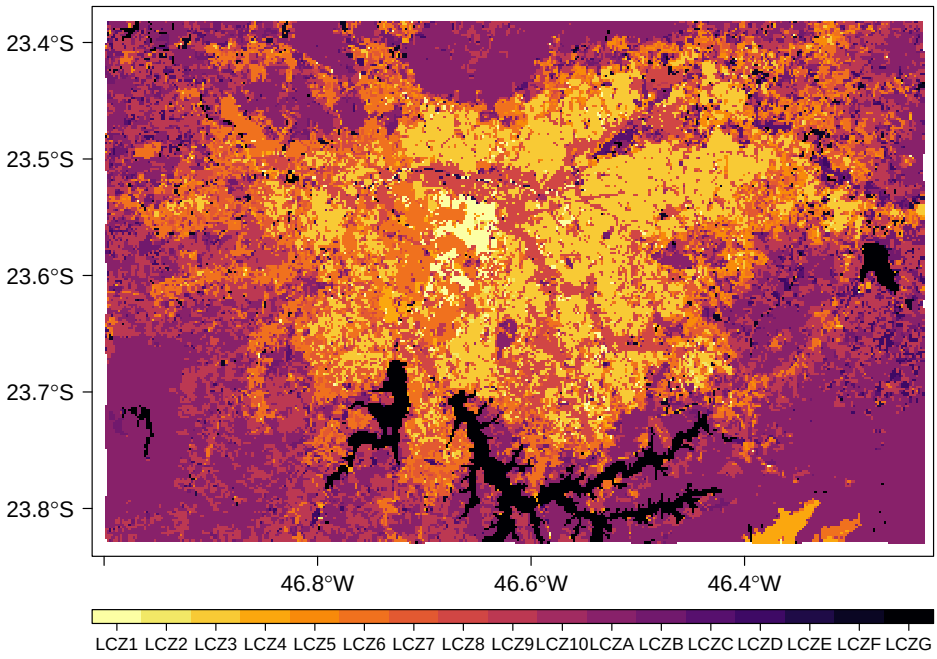

Figure 2.8: Local Climate Zone for MASP

2.3.4 A summary of emissions inventories

According to the revised literature, MASP presents a VOC limited regime, which means that ozone formation is more sensitive to the available VOC rather than NO_X. This regime is also known as high NO_X regime (Oke et al., 2017). In this regime, if we increased VOC emissions, more ozone will be formed. It seems that CETESB underpredicts the total emissions for VOC, possibly due to the underprediction of evaporative sources. During the process of emission calibration, we found that to form ozone in our simulated regional and urban domains (i.e. WRF-Chem simulations) the NO_X/VOC emission ratio needs to be around 0.4 (Table 2.5). This ratio is more important rather the amount of total emissions. We increased the emissions of WRF-Chem domains because it is bigger than São Paulo state (D01), and to compensate for other anthropogenic sources that were not included (i.e. industry and domestic emission).

We tried to include other sources using global emission inventories such as EDGAR-HTAP, by following the approach suggested by Hoshyaripour et al. (2016). First, we used the ANTRO_EMISS[14] tool to create a WRF-Chem emission file for each source type to finally added to the vehicular emissions[15]. However, it produces unrealistic concentrations

[14] Available in: `https://www2.acom.ucar.edu/wrf-chem/wrf-chem-tools-community`

[15] A script to add these wrfchemi files is available in: `https://github.com/quishqa/FromGlob2LocSP/`

of NO_X and CO.

For the case of emission inside the urban canyons, VEIN produces higher emissions of NO_X than VOC (See Fig. 2.7).

Table 2.5 - Total emissions

	CETESB (2015)[1]	CEDS (CAM-Chem)[2]	Emissions for D01[3]
NO_X (kTn)	171.4	207	340
VOC (kTn)	85.2	617	855
NO_X/VOC	2.01	0.33	0.39

[1] Vehicular emissions for 2014 for São Paulo State

[2] Total anthropogenic emissions for 2014 for São Paulo city

[3] Total emissions after calibration distributed on roads for WRF-Chem domain 1

blob/main/04_Vehicular_Emissions/utils/total_anthro_sum.py

Chapter 3

Results

Trust but verify.

A Russian proverb

3.1 CAM-Chem over the Metropolitan Area of São Paulo

3.1.1 CAM-Chem at continental scale

We start our analysis by examining CAM-Chem results over South America. Figure 3.1 shows surface O_3, NO, NO_2, CO, and $PM_{2.5}$ averaged for our study period. CAM-Chem simulated the highest values of ozone in MASP with an averaged concentration value of 108.0 $\mu g\ m^{-3}$. Meanwhile the lowest values are recorded in the Amazon. According to Williams et al. (2016), this difference in concentration is attributable to the low concentration of NO_X to catalyze photochemical O_3 formation, as the main sources of NO_X in the Amazon are soil bacterial emissions. Another factor is that NO_X and VOC are emitted in cities at, approximately, the same period of day by vehicles. Finally, the deposition efficiency of O_3 and NO_2 on vegetation surface is higher than on concrete.

NO values are low, São Paulo marks an average of 2.4 $\mu g\ m^{-3}$, Buenos Aires, and Santiago de Chile registered the highest values. NO_2 is a good tracer for anthropic activities in urban areas, and the main capital cities of South America are easily discerned in the simulation. NO_2 in MASP reaches 15.9 $\mu g\ m^{-3}$. Carbon monoxide and Fine Particles ($PM_{2.5}$) have a similar spatial distribution inside Brazil, especially in the central area. These concentrations are related to biomass burning emissions. In MASP, the CO concentration was 0.26 ppm and $PM_{2.5}$ was 30.5 $\mu g\ m^{-3}$.

CAM-Chem O_3 concentration in the ocean part in front of São Paulo state is $\sim$ 50

$\mu g\ m^{-3}$ ($\sim$ 25 ppb), which is consistent with values for ozone in South Atlantic Ocean: Lelieveld et al. (2004): 10 - 30 ppb ($\sim$ 20 - 60 $\mu g\ m^{-3}$) for annual average from 1995 - 2002; Boylan et al. (2015): 30 ppb ($\sim$ 60 $\mu g\ m^{-3}$) for October monthly mean 2009; and oceanic background level (Seinfeld and Pandis, 2016): 20 - 40 ppb ($\sim$ 40 - 80 $\mu g\ m^{-3}$). Overall, CAM-Chem shows us the macro picture of different compounds concentrations.

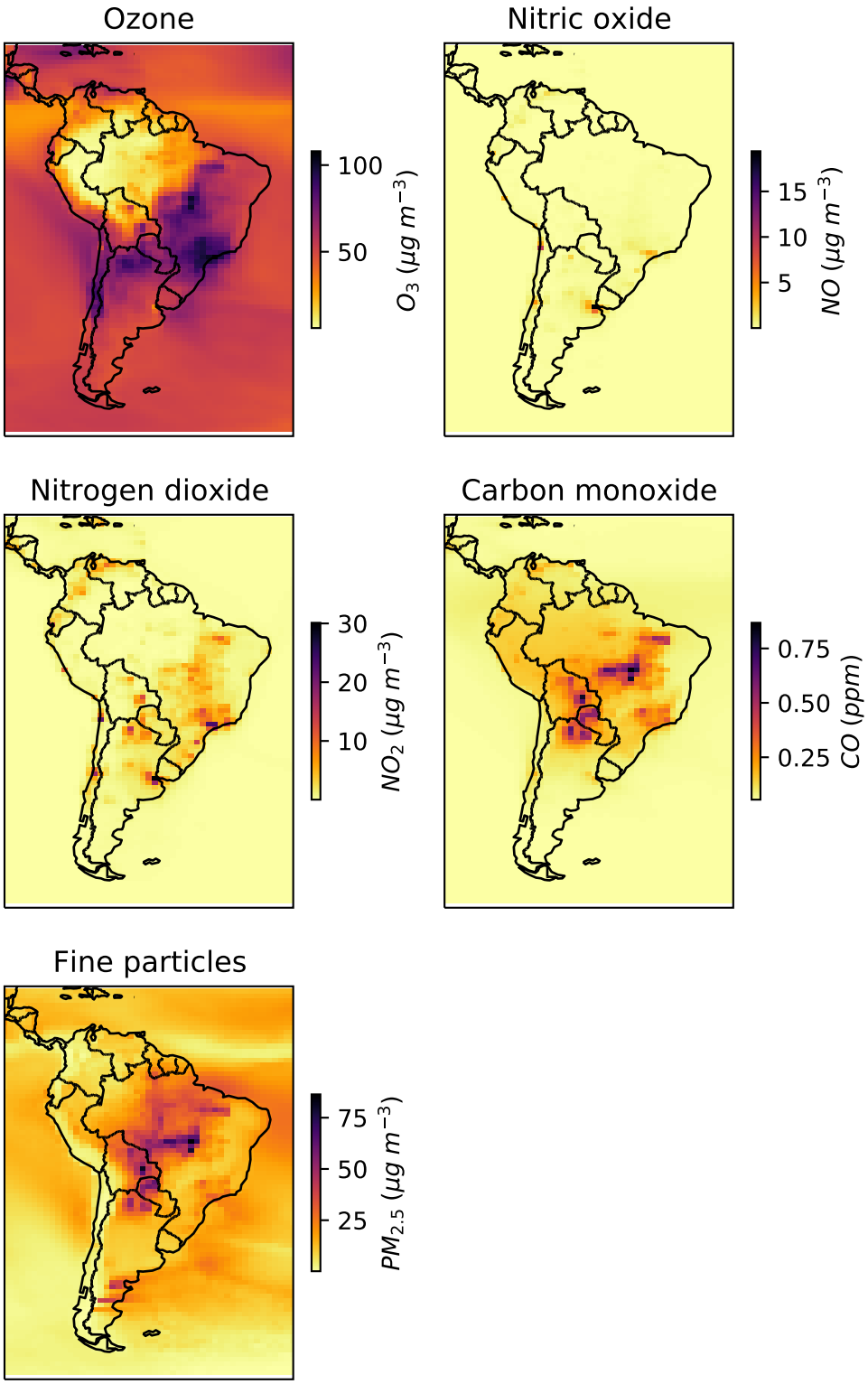

Figure 3.1: CAM-Chem surface mean simulated concentration for our study period.

3.1.2 CAM-Chem over MASP

CAM-Chem covers MASP with four grid cells, shown at Figure 3.2. We compared CAM-Chem simulations in each cell against the averaged measurement of air quality stations inside each cell, and the averaged of these four cells against the averaged of all air quality stations inside MASP. We compared CAM-Chem predictions against hourly and daily averaged CETESB measurements, and their diurnal profile. Cell A represents the suburban area outside MASP; cell B, north MASP; and Cell D, south MASP. There are no air quality stations in cell C.

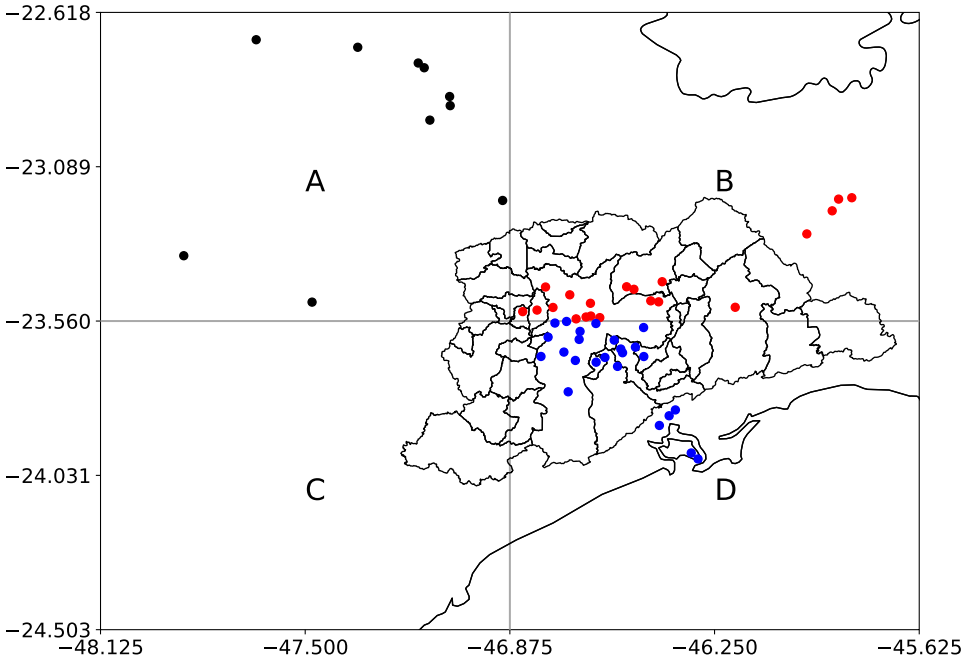

Figure 3.2: Distribution of CETESB air quality stations inside CAM-Chem cells. Black points denote air quality station inside cell A; red points, air quality stations inside cell B; and blue points, air quality stations inside cell D.

As shown in figure 3.3, considering all MASP region, CAM-Chem represent well O_3, even reaching the daily maximum concentration. Likewise, $PM_{2.5}$ trend along the week is well represented. Primarily pollutants as NO and CO, are highly underestimated in the model.

Table 3.1 shows the performance statistics for model evaluation. The positive MB for O_3 indicates an overestimation, but there is an underestimation for the other pollutants. It is worth noting that all the evaluated species are positively correlated and that O_3 and $PM_{2.5}$ present R above 0.7.

Table 3.1 - Performance statistics for predicted pollutant concentrations against averaged CETESB measurements in four CAM-Chem cells

	N	$\bar{O}$	$\bar{M}$	σ_O	σ_M	MB	ME	RMSE	NMB	NME	R	IOA
O_3 ($\mu g\ m^{-3}$)	28	54.67	87.08	45.86	54.46	32.81	33.47	44.55	60.46	61.67	0.83	0.81
NO ($\mu g\ m^{-3}$)	28	28.74	2.10	28.64	3.32	-20.37	20.37	27.24	-90.67	90.67	0.30	0.45
NO_2 ($\mu g\ m^{-3}$)	28	47.07	18.91	17.02	12.87	-28.35	28.43	32.01	-59.99	60.17	0.56	0.52
CO (ppm)	28	0.92	0.24	0.42	0.12	-0.67	0.67	0.74	-73.28	73.28	0.54	0.44
$PM_{2.5}$ ($\mu g\ m^{-3}$)	28	30.68	23.17	12.27	13.80	-6.85	10.03	11.75	-22.82	33.41	0.73	0.79

N : numbers of observation (O) and prediction (M); $\bar{O}$: observations mean; $\bar{M}$: prediction mean; σ_O: observation standard deviation; σ_M: prediction standard deviation; MB: mean bias; MAGE: Mean absolute gross error; RMSE: Root mean square error; NMB: Normal mean bias (%); NME: Normal mean error (%); R: Pearson correlation coefficient; IOA: index of agreement.

When we evaluate the daily average, it is clearer the overestimation of O_3 concentrations and the underestimation of NO, NO_2, CO and, $PM_{2.5}$ concentrations. The worst simulation was for NO species (Fig. 3.4).

Figure 3.5 shows the daily pattern of these pollutants. Although CAM-Chem provides pollutant concentrations at 6 hours, which can't be enough to describe a diurnal cycle, CAM-Chem O_3 and $PM_{2.5}$ diurnal cycles are close to observation. For the case of NO and CO, CAM-Chen can't reproduce the concentration peaks at rush hour, probably by the limited temporal resolution of the simulations and the temporal resolution of the global emission inventories.

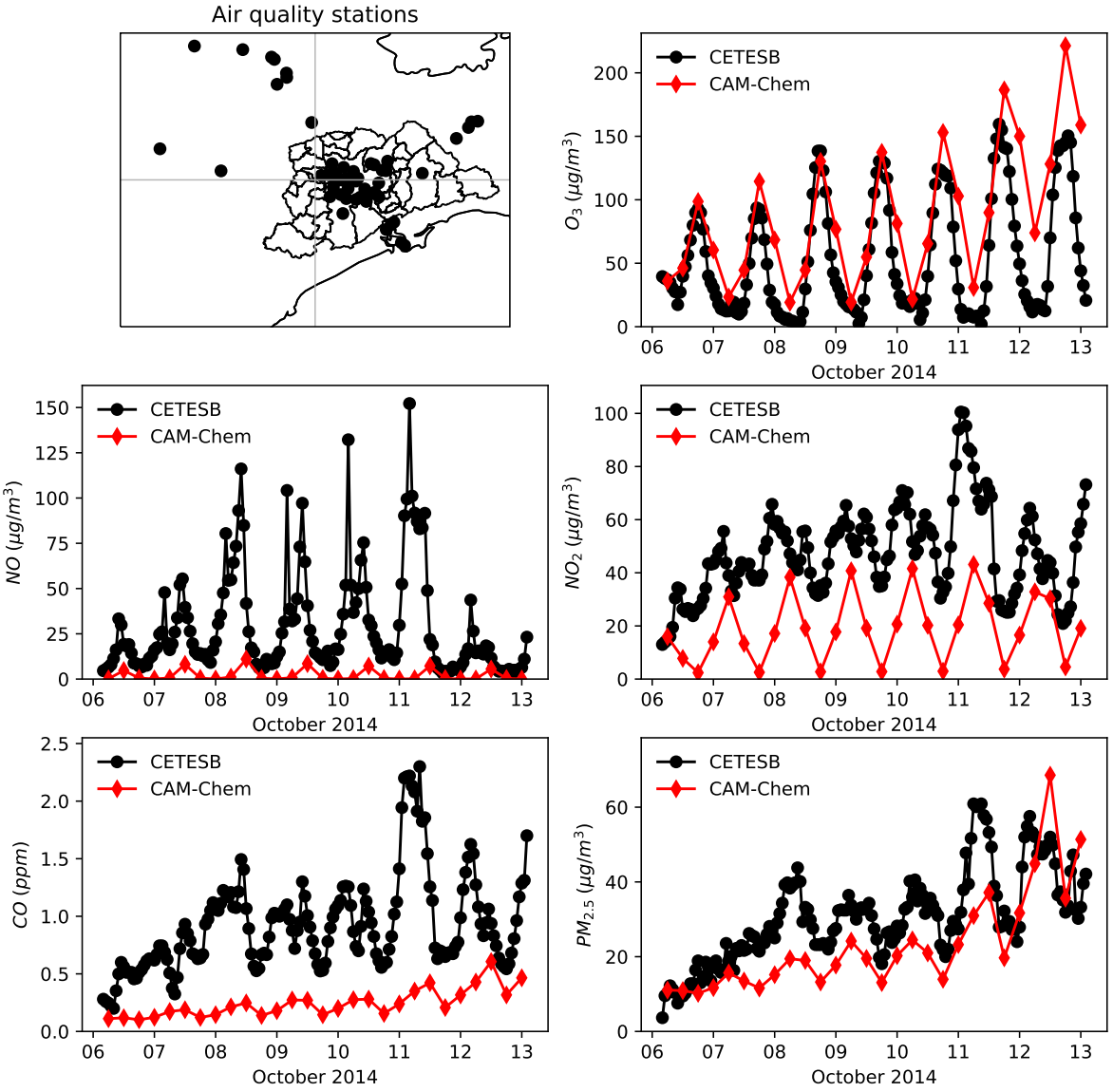

Figure 3.3: Comparison between spatial average of CAM-Chem simulations over all the MASP and spatial average of CETESB air quality stations hourly measurements. The Top-left map shows the air quality stations used to calculate the pollutants averages.

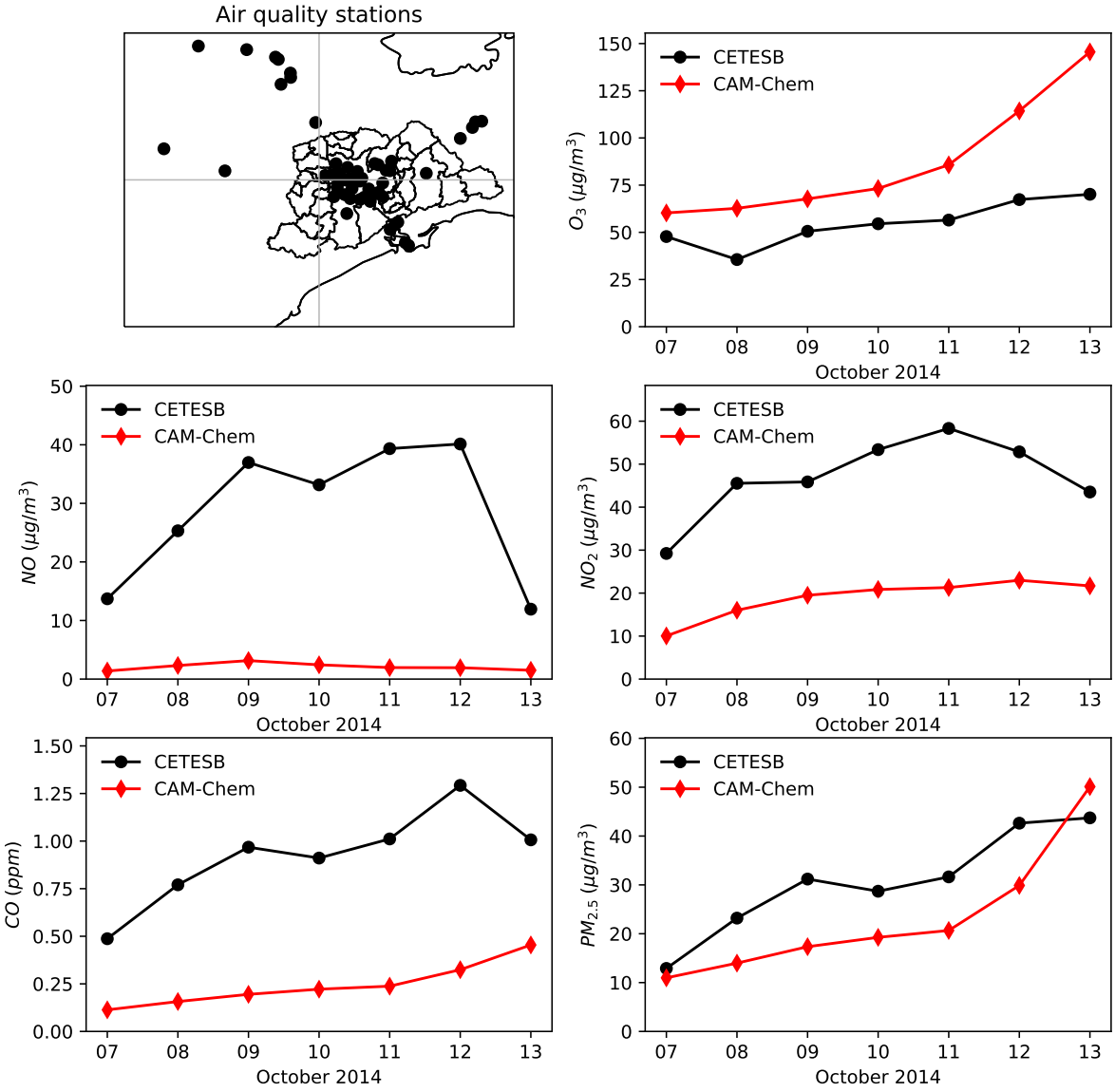

Figure 3.4: Comparison between spatial average of CAM-Chem simulations over all the MASP and spatial average of CETESB air quality daily averages. The Top-left map shows the air quality stations used to calculate the pollutants averages.

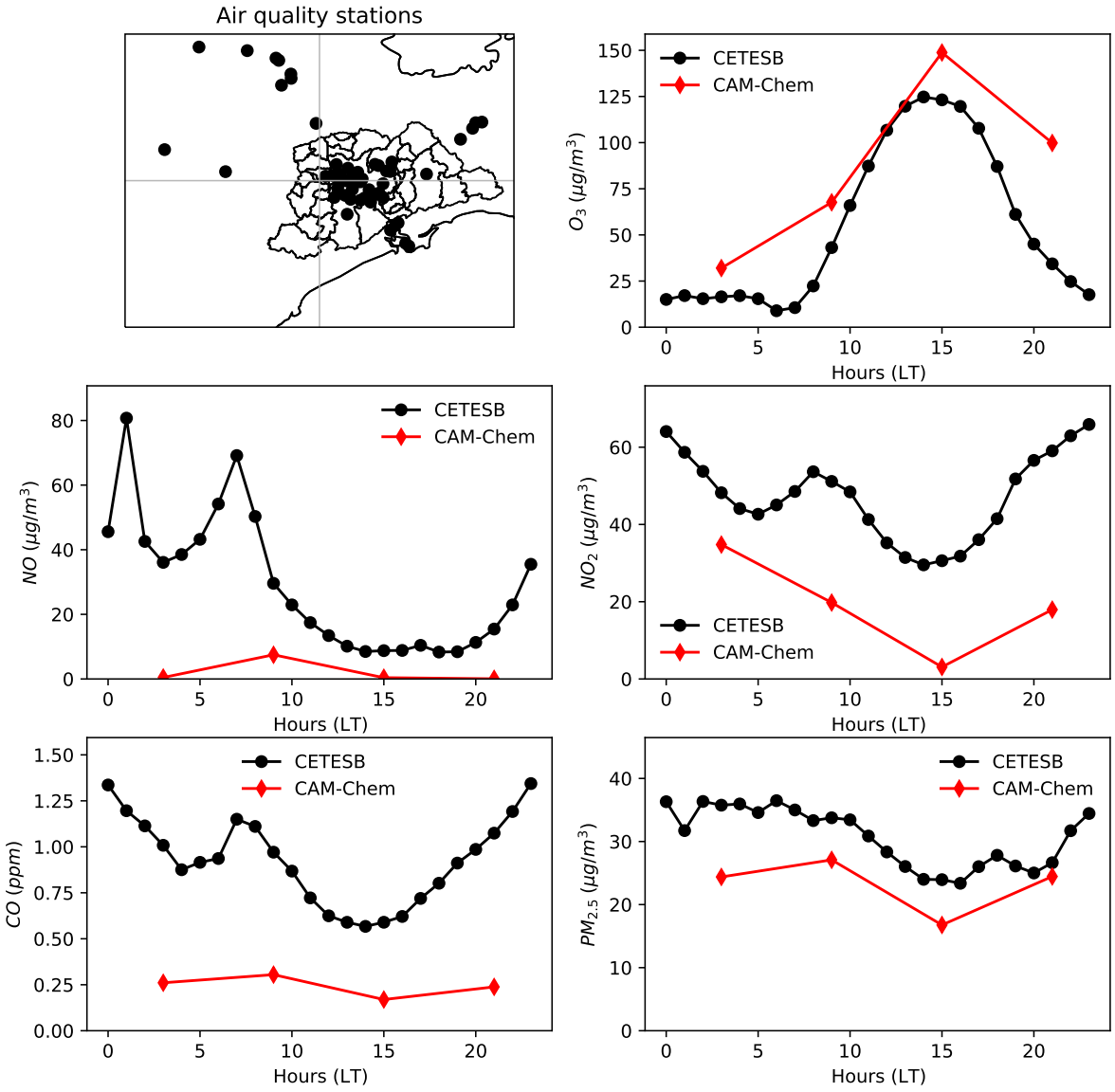

Figure 3.5: Diurnal cycle of CAM-Chem results over all the MASP and CETESB air quality measurements. The Top-left map shows the air quality stations used to calculate the pollutants averages.

3.1.3 Suburban and urban areas represented in CAM-Chem

Figure 3.6 shows the comparison between CAM-Chem results and the average concentration of CETESB AQS inside cell A. CAM-Chem correctly simulate O_3, NO, NO_2, and $PM_{2.5}$. CO is still underpredicted. In this case, daily averages of O_3, NO_2, and $PM_{2.5}$ concentrations are correctly simulated and their increment along the week (Fig. 3.7). Likewise, CAM-Chem estimates very well the diurnal profile of O_3, NO, NO_2 and $PM_{2.5}$, although in the case of NO, CAM-Chem estimates the diurnal peak one hour later. O_3 maximum hourly value, minimum NO_2 and $PM_{2.5}$ concentration values are correctly simulated, but CO diurnal variation is not well represented. Table 3.2 shows the statistical indicators, O_3 presents a significant linear correlation, but CO presents a negative linear correlation. It is important to mention, that in cell A, there is only one station that measure CO and $PM_{2.5}$, and six station measure O_3 and NO_X.

In cell D, the most populated area in MASP, is located a higher number of air quality stations. In this cell, a bigger difference appears between CAM-Chem and the observation as can be seen in figure 3.9. O_3 is overestimated, while the other pollutants are underestimated. As seen in table 3.3 bigger errors are registered in this case. In this cell, 17 stations measure O_3, 16 measure NO_X, nine measure CO, and seven $PM_{2.5}$

Results of cell B are shown in appendix C (Table C.1 and Figure C.1). In cell B, errors are lower than in cell D but higher than cell A.

Table 3.2 - Performance statistics for predicted pollutant concentrations against averaged CETESB measurements at CAM-Chem Cell A

	N	$\bar{O}$	$\bar{M}$	σ_O	σ_M	MB	ME	RMSE	NMB	NME	R	IOA
O_3 ($\mu g\ m^{-3}$)	28	69.70	76.77	40.35	49.16	10.47	19.65	27.10	15.80	29.64	0.86	0.90
NO ($\mu g\ m^{-3}$)	28	6.97	2.93	10.09	4.85	-3.47	4.74	9.95	-54.23	74.07	0.16	0.45
NO_2 ($\mu g\ m^{-3}$)	28	27.64	24.68	18.15	17.42	-3.18	13.31	18.78	-11.40	47.80	0.45	0.66
CO (ppm)	26	0.85	0.29	0.39	0.14	-0.56	0.57	0.76	-65.53	66.62	-0.17	0.36
$PM_{2.5}$ ($\mu g\ m^{-3}$)	27	27.15	23.70	15.53	13.28	-1.57	9.32	14.96	-6.22	37.02	0.39	0.63

N : numbers of observation (O) and prediction (M); $\bar{O}$: observations mean; $\bar{M}$: prediction mean; σ_O: observation standard deviation; σ_M: prediction standard deviation; MB: mean bias; MAGE: Mean absolute gross error; RMSE: Root mean square error; NMB: Normal mean bias (%); NME: Normal mean error (%); R: Pearson correlation coefficient; IOA: index of agreement.

Table 3.3 - Performance statistics for predicted pollutant concentrations against averaged CETESB measurements at CAM-Chem Cell D

	N	$\bar{O}$	$\bar{M}$	σ_O	σ_M	MB	MAGE	RMSE	NMB	NME	R	IOA
O_3 ($\mu g\ m^{-3}$)	28	50.94	99.80	45.73	74.84	49.12	49.12	70.98	96.94	96.94	0.73	0.67
NO ($\mu g\ m^{-3}$)	28	33.13	1.84	31.61	3.16	-24.92	24.92	34.29	-93.11	93.11	0.08	0.43
NO_2 ($\mu g\ m^{-3}$)	28	49.61	16.12	16.76	12.30	-33.44	33.44	36.18	-67.48	67.48	0.58	0.46
CO (ppm)	28	0.93	0.22	0.44	0.15	-0.68	0.68	0.78	-75.43	75.43	0.38	0.42
$PM_{2.5}$ ($\mu g\ m^{-3}$)	28	29.89	24.00	11.92	18.50	-5.08	11.86	15.00	-17.48	40.78	0.63	0.74

N : numbers of observation (O) and prediction (M); $\bar{O}$: observations mean; $\bar{M}$: prediction mean; σ_O: observation standard deviation; σ_M: prediction standard deviation; MB: mean bias; MAGE: Mean absolute gross error; RMSE: Root mean square error; NMB: Normal mean bias (%); NME: Normal mean error (%); R: Pearson correlation coefficient; IOA: index of agreement.

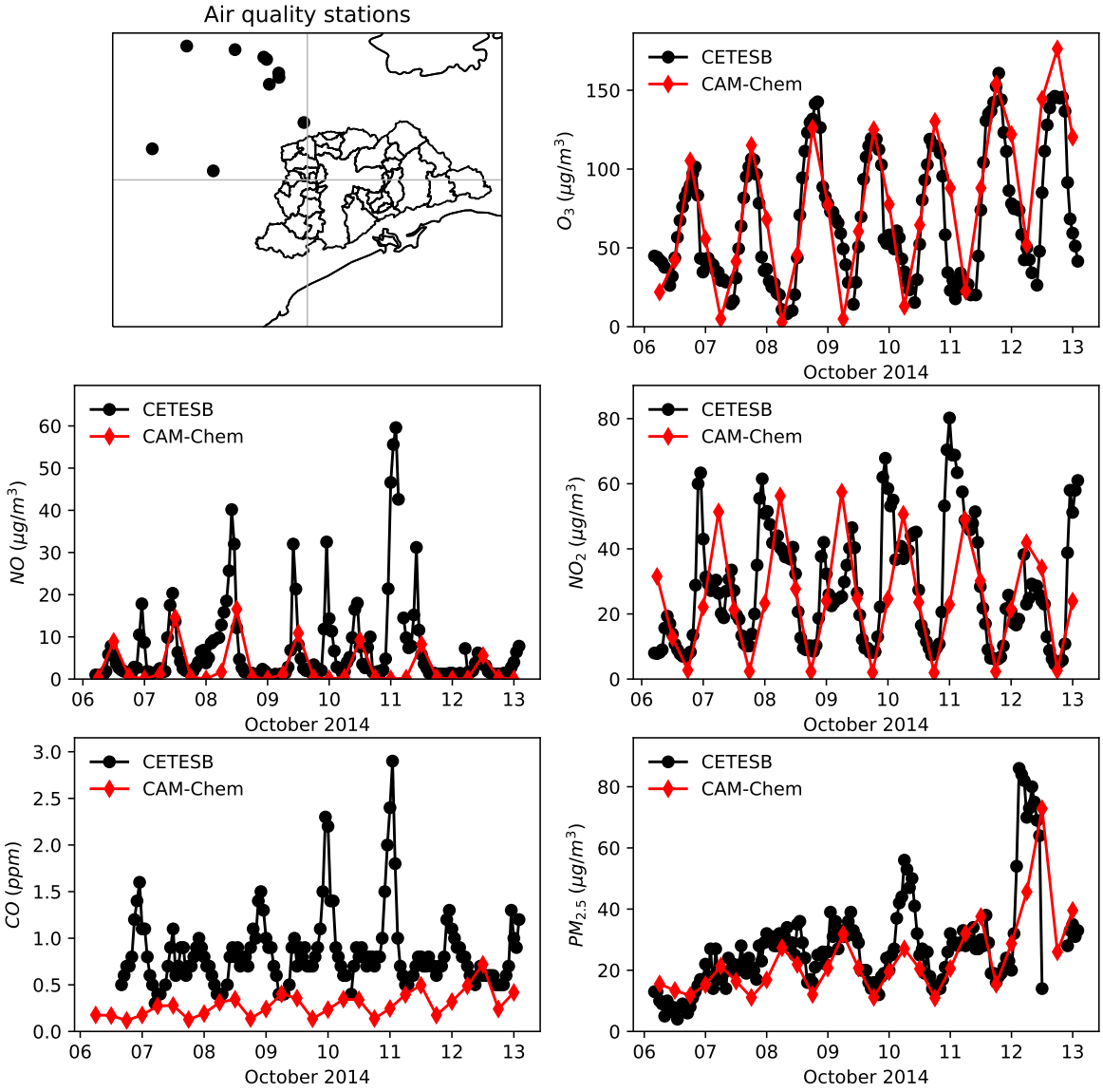

Figure 3.6: Comparison between spatial average of CAM-Chem simulations in cell A and spatial average of CETESB air quality stations hourly measurements.The Top-left map shows the air quality stations used to calculate the pollutants averages in cell A.

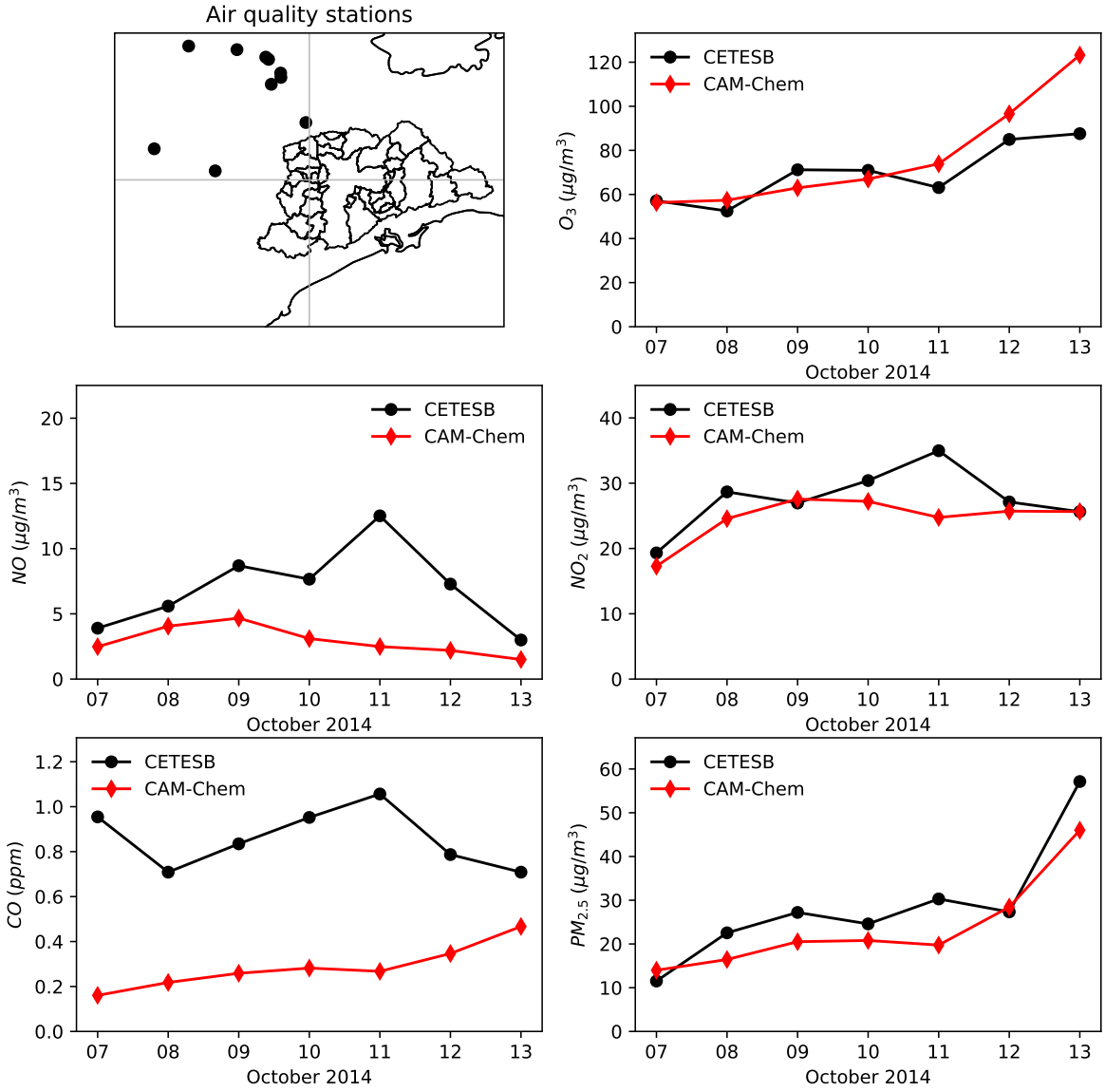

Figure 3.7: Comparison between spatial average of CAM-Chem daily average simulations in cell A and spatial average of CETESB air quality daily averages. The Top-left map shows the air quality stations used to calculate the pollutants averages in cell A.

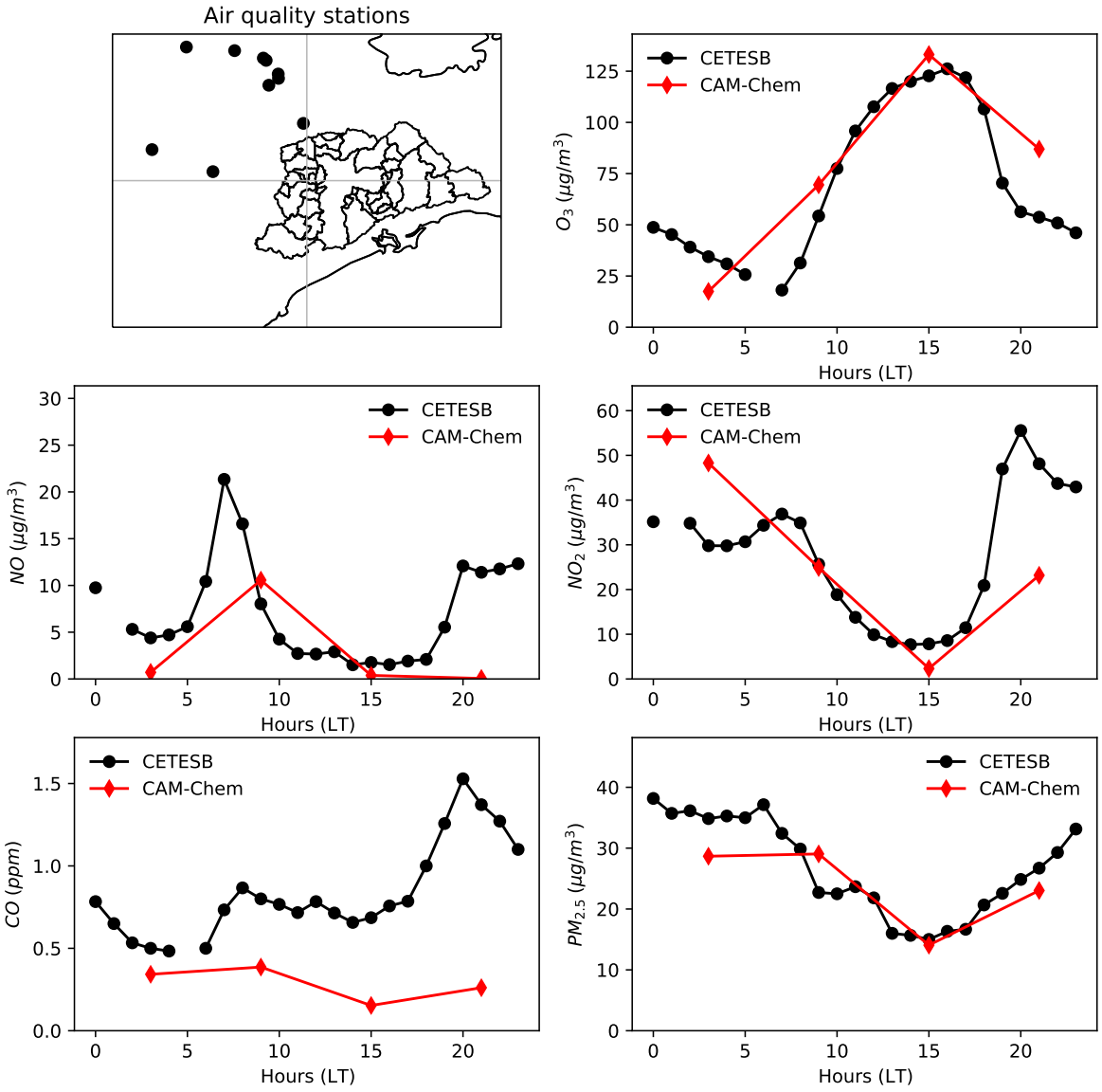

Figure 3.8: Diurnal cycle of CAM-Chem results in cell A and CETESB air quality measurements. The Top-left map shows the air quality stations used to calculate the pollutants averages in cell A.

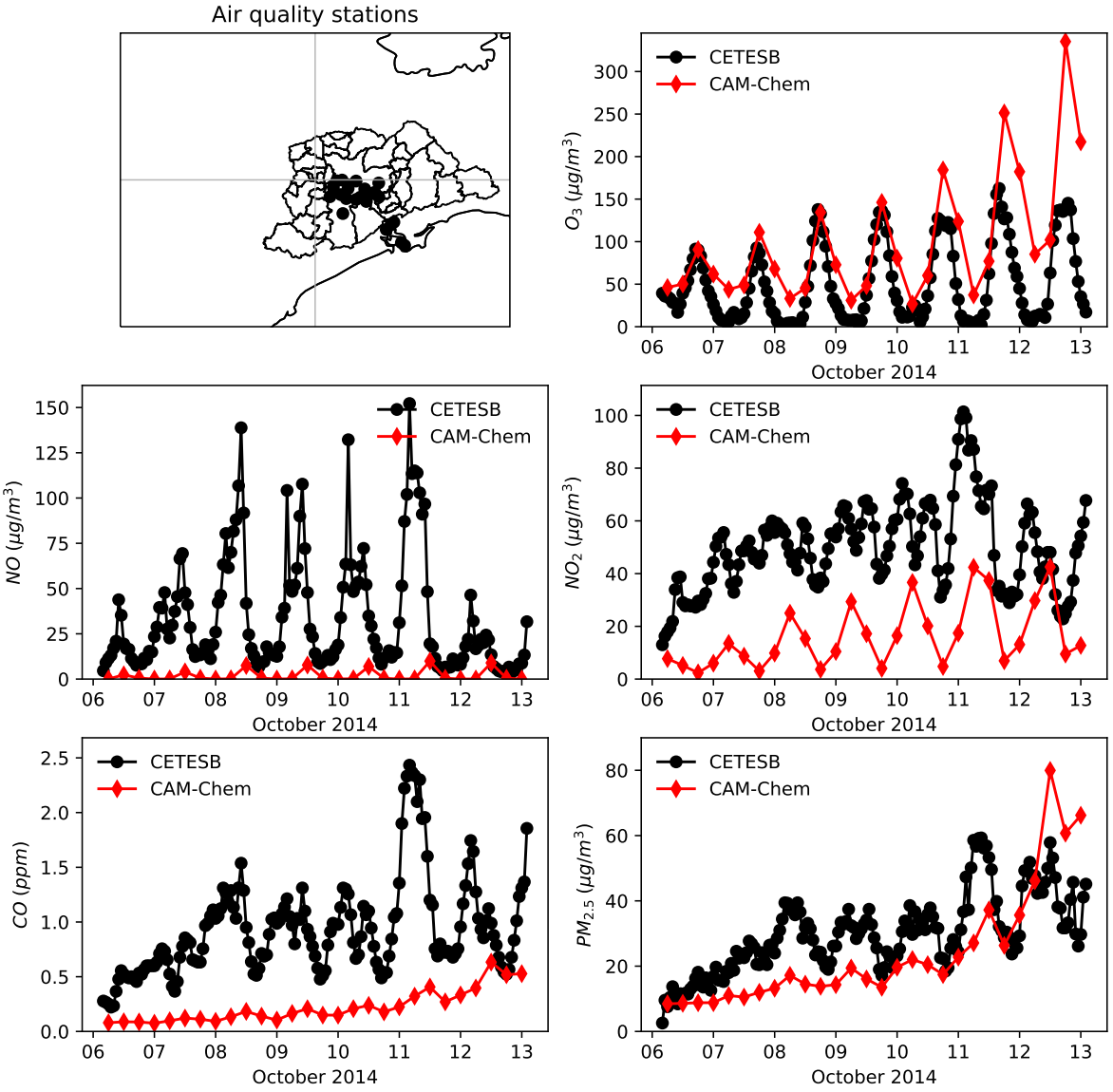

Figure 3.9: Comparison between spatial average of CAM-Chem simulations in cell D and spatial average of CETESB air quality stations hourly measurements. The Top-left map shows the air quality stations used to calculate the pollutants averages in cell D.

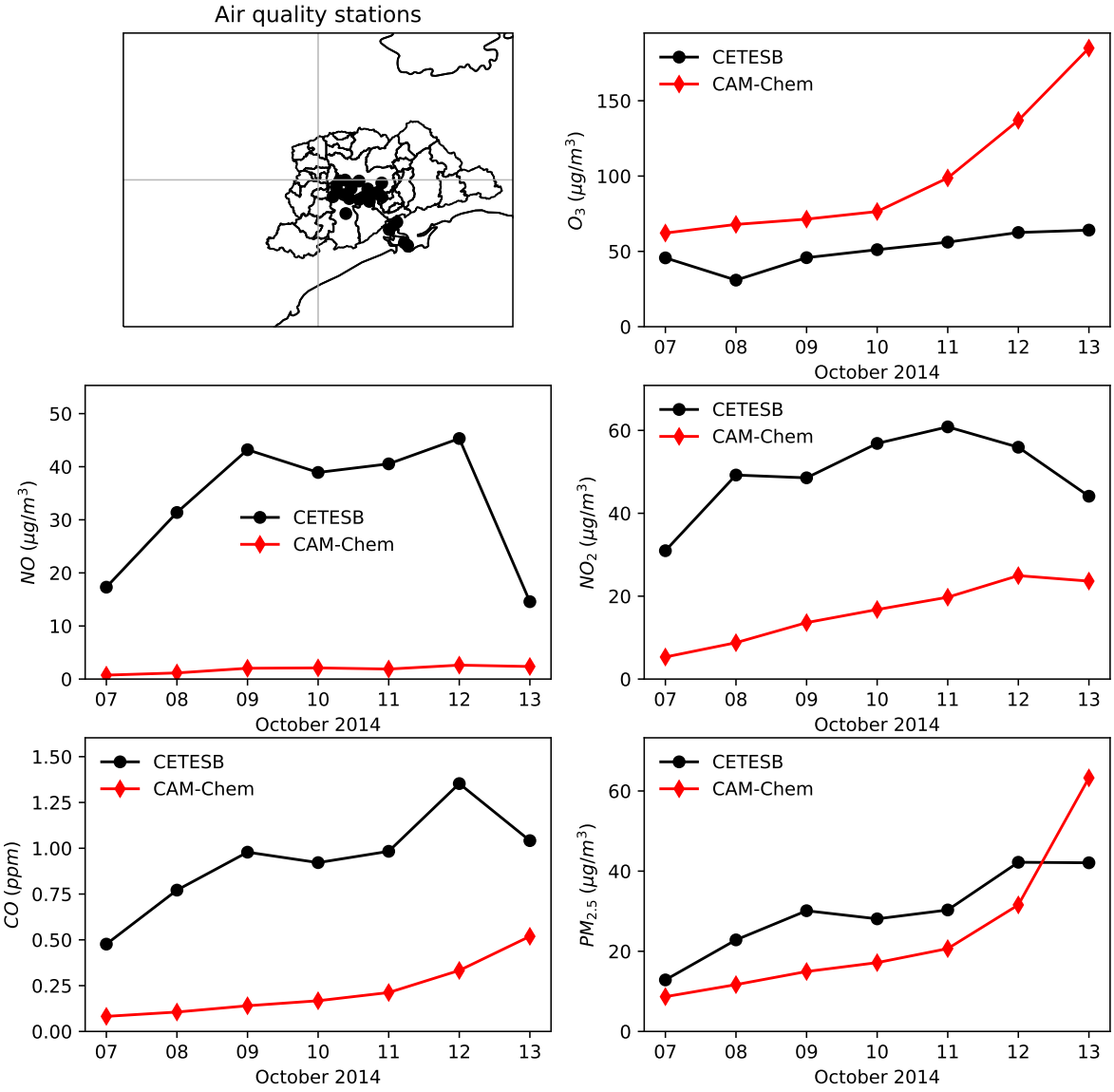

Figure 3.10: Comparison between CAM-Chem daily average simulations in cell D and spatial average of CETESB air quality daily averages. The Top-left map shows the air quality stations used to calculate the pollutants averages in cell D.

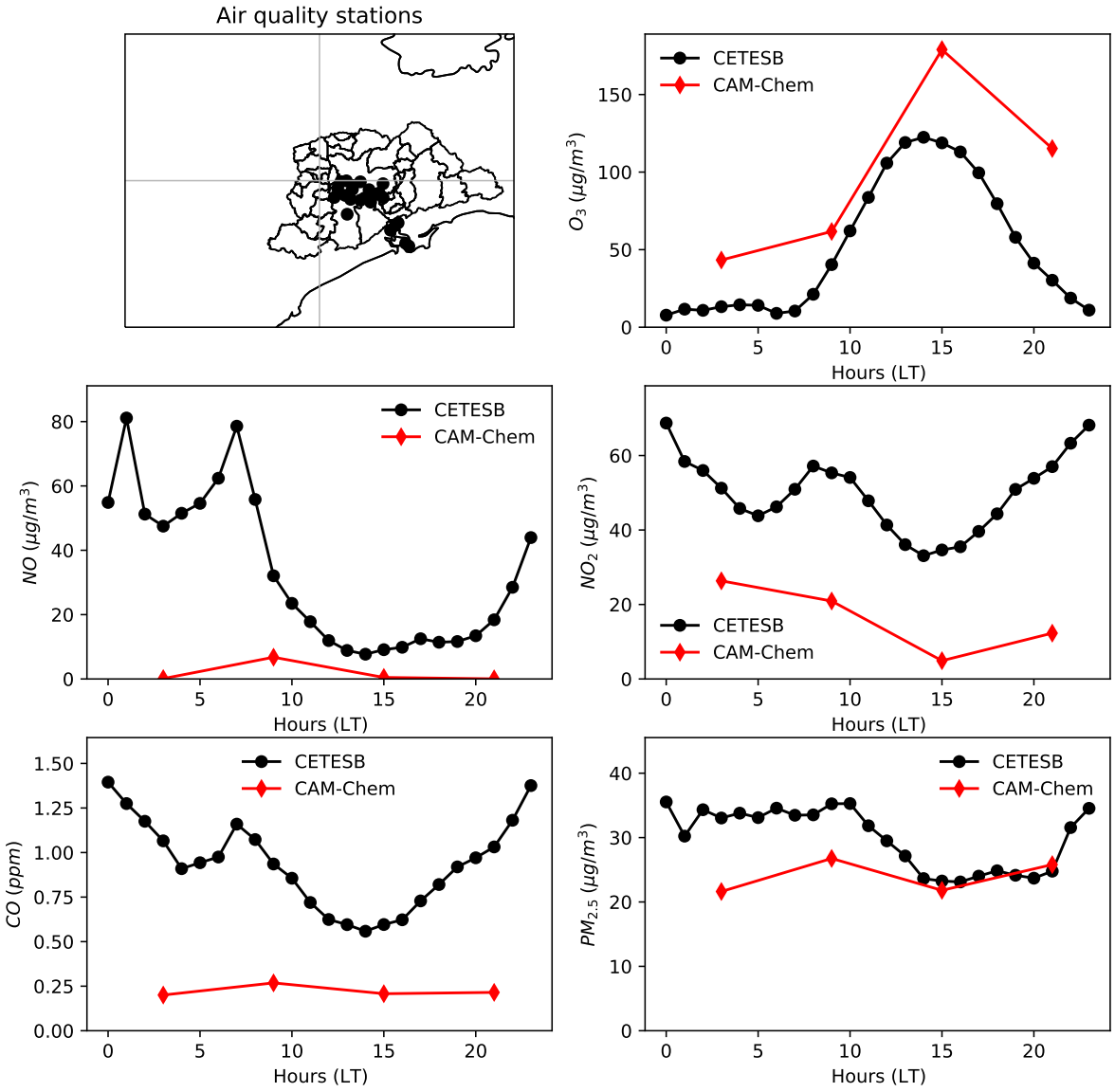

Figure 3.11: Diurnal cycle of CAM-Chem results in cell D and CETESB air quality measurements. The Top-left map shows the air quality stations used to calculate the pollutants averages in cell D.

3.1.4 Analysis of CAM-Chem results

We can see that, in the suburban area, CAM-Chem correctly simulate pollutant concentration, whereas, inside MASP, the CAM-Chem has more difficulty to do so. This is explained by the influence of anthropogenic emissions, which are more concentrated in cells B and D. The underestimation of primary pollutant concentration suggests there is a lack of CO and NO_X emissions. Nevertheless, O_3 is simulated correctly in every cell.

The Emissions of Atmospheric Compounds and Compilation of Ancillary Data (ECCAD) allows us to examine the Community Emissions Data System (CEDS) which constitutes the base of anthropogenic emission for CMIP6 (Emmons et al., 2020). For São Paulo city, CEDS reports 0.207 Tg of NO_X emissions and 0.617 Tg of NMVOC emission for 2014, resulting in a NO_X/MNVOC ratio of 0.33. During the process of emission calibration for WRF-Chem, we found that a ratio of ~ 0.4 (in mass concentration) was optimal for ozone formation. So O_3 good performance can be attributed to a good representation of NO_X/MNVOC ratio from CMIP6 emission inventory, together with the use of MOZART-T1 chemical mechanism.

CAM-Chem correct simulation of the suburban area suggests that CAM-Chem can be used to estimate the background concentration of urban areas. Together with the good representation of oceanic values, imply a suitable model to be used as chemical boundary conditions and initial concentration for MASP.

Finally, we believe that CAM-Chem can be used to get good estimates of maximum O_3 concentration and daily $PM_{2.5}$ averages at a city scale.

In the following section, we present the simulations using WRF-Chem for regional and urban domains. The regional domain used updated chemical boundary conditions from CAM-Chem simulations.

3.2 WRF-Chem air quality simulation over Southeast Brazil and the MASP

We present the results of WRF-Chem simulation at regional (domain 1) and urban (domain 2) scales. Although CETESB air quality network has over 68 automatic air quality stations in the São Paulo state, we present temporal series of observations from those air quality stations that have a complete set of parameters, that is, they provide the measurements of O_3, NO, NO_2, and CO or Temperature, Relative humidity, wind speed and directions. These stations are displayed in Figure 3.12. Including the location of Cubatão because it presents a behavior characteristic of industrial activity. Nevertheless, all the CETESB air quality stations were considered in the model performance statistics.

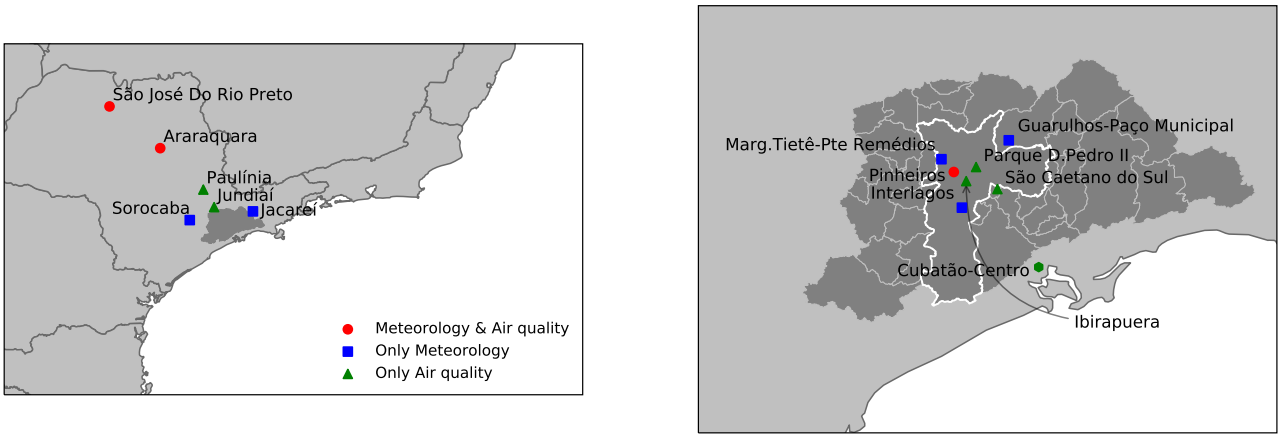

Figure 3.12: Location of air quality stations used for model evaluation of the domain 1 (left) and domain 2 (right). São Paulo city is highlighted in white.

3.2.1 The effect of chemical boundary conditions on the simulations results

We used CAM-Chem output to feed WRF-Chem with dynamic chemical boundary conditions (CBC). In Gavidia-Calderón et al. (2018), the effect of using this CBC from MOZART-4 was evaluated for wet and dry seasons over MASP. They found that in the dry season, the same study period presented here, the impact of CBC on ozone representation is low. In this case, over MASP, for O_3 there is a difference of 3 $\mu g\ m^{-3}$ ($\sim$ 1.5 ppb), for NO the difference is -0.92 $\mu g\ m^{-3}$ ($\sim$ 0.7 ppb), for NO_2 is 0.69 $\mu g\ m^{-3}$ ($\sim$ 0.37 ppb), and for CO is 0.001 ppm (Fig. 3.14).

Default WRF-Chem chemical boundary conditions are an idealized profile based on

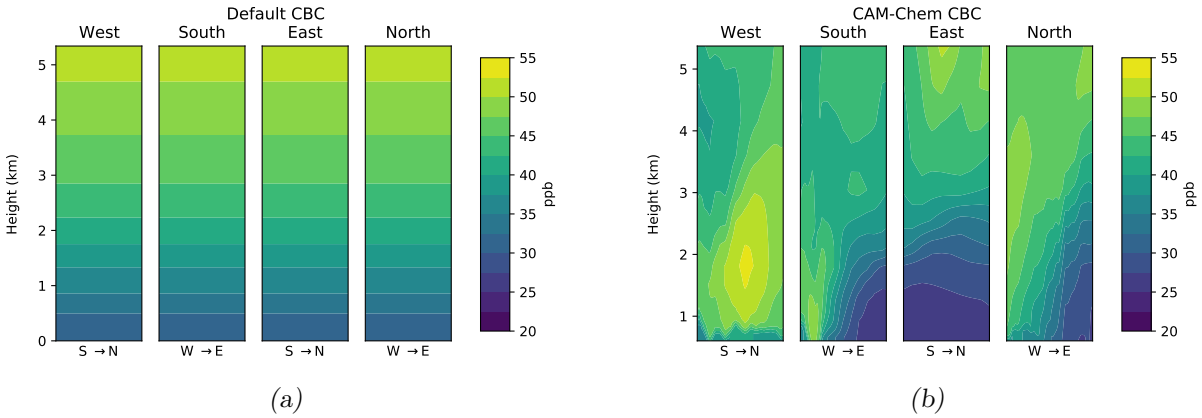

Figure 3.13: (a) NALROM WRF-Chem default profile and (b) mean tropospheric ozone lateral boundary (CAM-Chem) condition for each simulation period

NOAA-Aeronomy Laboratory Regional Oxidation Model (NALROM) simulation (Peckham, 2018) (See Fig. 3.13). When using CBM-Z chemical mechanism, this idealized profile at the surface level presents an O_3 concentration of 30 ppb ($\sim$ 60 $\mu g\ m^{-3}$), CO is 80 ppb (0.08 ppm), NO is 0.0054 ($\sim$ 0.00675 $\mu g\ m^{-3}$) ppb and, NO_2 is 0.0162 ppb ($\sim$ 0.030456 $\mu g\ m^{-3}$) (See Fig. 3.13 a).

Figure 3.14 illustrates the difference between running WRF-Chem with default CBC or using CBC based on CAM-Chem. During the studied period, the predominant wind presented a north-east direction, meaning that the North and East boundaries are the ones that will affect the most the simulation inside the domain. Blue values in figure 3.14 means that WRF-Chem with default CBC results presented lower concentrations than when using CAM-Chem CBC; red colors means the opposite. In the previous section, from CAM-Chem we obtained over South Atlantic O_3 concentration of 50 $\mu g\ m^{-3}$, 10 $\mu g\ m^{-3}$ lower than default CBC. Hence, there is a positive difference in the north-east area that decreases downwind. O_3 is transported in these borders because over the ocean there aren't enough NO emissions that can consume it.

The differences for NO and NO_2 are low as they react with continental pollutants and emissions during their transportation from the northern borders. In the north-west part of the domain, the difference is negative. Default CBC, being static boundary condition, don't have temporal and spatial variation, whereas CAM-Chem CBC do. So, this difference happens because CAM-Chem simulates O_3, NO, CO, and NO_2 formed in the continent, which then is advected into the domain.

Regarding the temporal variation of the effect of using CAM-Chem as CBC, in figure D.1 in the appendix section, we observe that the difference for ozone simulation is higher during the daytime rather than nighttime, the opposite behavior happens for NO, NO_2, and CO when higher differences happen during nighttime.

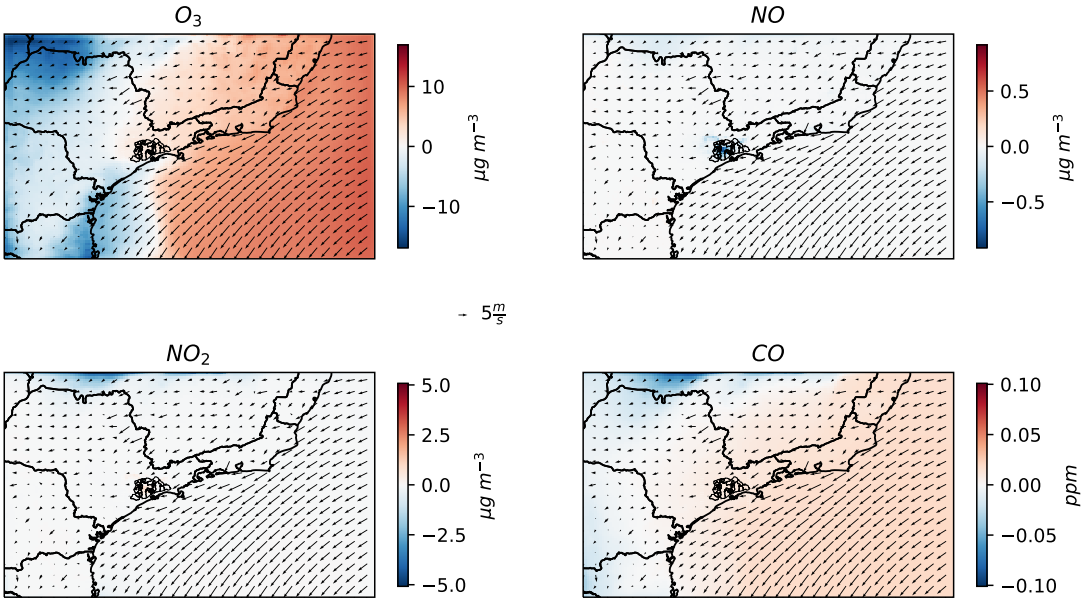

Figure 3.14: Mean concentrations difference between simulation using default CBC and simulation using CAM-Chem as CBC.

3.2.2 Regional: Suburban vs urban pollutants concentrations

Working with a regional domain can help us to address the difference between suburban (outside MASP) and urban areas. In this section, we evaluate WRF-Chem performances in simulating meteorological and air quality parameters for São Paulo State. We are using all the information available in the CETESB air quality network for model evaluation.

3.2.2.1 Meteorological prediction

Table 3.4 shows the performance statistics for the verification of meteorological parameters accuracy. WRF-Chem successfully reaches the expected benchmark for simple and complex terrain for T2 and RH2. For WS, the model reaches expected benchmarks for the complex terrain, while WD only passed the ME benchmark. The wind topographic correction helped to reach the WS benchmark for complex terrain but is still insufficient to reach WD mean bias benchmark. Based on MB index, there is a sightly underestimation

of T2, RH2, and an overestimation of WS. When we analyze the wind components, it is observed for wind direction that there is a deviation toward the South.

Table 3.4 - Performance statistics for predicted meteorological parameters against CETESB measurements for WRF-Chem regional domain

	N	$\bar{O}$	$\bar{M}$	σ_O	σ_M	MB	ME	RMSE	NMB	NME	R	IOA
T2 (K)	3933	297.11	296.01	6.29	5.83	-0.41	1.65	2.04	-0.14	0.55	0.95	0.97
RH2 (%)	3888	51.03	50.22	23.27	20.14	-1.53	8.56	11.43	-3.00	16.78	0.87	0.93
WS (m s^{-1})	4415	1.99	2.99	0.91	1.57	1.20	1.51	1.92	60.44	75.56	0.39	0.50
WD (°)	4382	-	-	-	-	-22.84	50.66	-	-	-	-	-
U10 (m s^{-1})	4382	-0.75	-1.73	1.31	1.91	-1.08	1.71	2.11	144.82	-228.03	0.50	0.61
V10 (m s^{-1})	4382	0.34	-0.55	1.55	2.12	-0.93	1.55	2.01	-269.91	448.82	0.60	0.71

N : numbers of observation (O) and prediction (M); $\bar{O}$: observations mean; $\bar{M}$: prediction mean; σ_O: observation standard deviation; σ_M: prediction standard deviation; MB: mean bias; MAGE: Mean absolute gross error; RMSE: Root mean square error; NMB: Normal mean bias (%); NME: Normal mean error (%); R: Pearson correlation coefficient; IOA: index of agreement.

Figure 3.15, shows the spatial distribution of observations (dots) and model prediction, Pearson coefficient, and mean bias between modeled and observation for T2, RH2, and WS. We note that T2 and RH2 are spatially well simulated and the correlation is positive over the domain. For RH2 the correlation is not high near Santos station (the closest point to the coastline), probably caused by a mismatch in land type. Also, it is possible to observe the opposite behavior between T2 and RH2, when T2 presents a positive bias, RH2 registered a negative bias. This situation is clearer in the center of São Paulo State. Regarding WS, the overestimation of the wind speed is registered over the domain but is higher inside the rural areas.

Figures 3.16 and 3.17 show temporal series of meteorological parameters for four suburban stations and MASP stations, respectively. When analyzing the spatial distribution differences in figure 3.15, we have that T2 is better simulated at the urban stations. WRF-Chem represents the daily minimum temperature but fails to reach the daily maximum temperature. WS is better represented in the urban areas, regional stations like Araraquara and São José do Rio Preto, present a larger overprediction of WS. Furthermore, the wind vector is better simulated during daylight hours and the bigger difference happens during nighttime. These difference between suburban and urban representation of meteorological parameters is explained by the description of surface and land properties in the model.

Limitations on the representation of the radiative properties of urban areas can explain the underestimation of T2. The overestimation of wind speed is less in the urban area due to the use of the roughness parameter given by the urban parameterization (Liao et al., 2014).

Overall, based on the benchmark indexes, the WRF-Chem model performs very well simulating meteorological parameters at this scale.

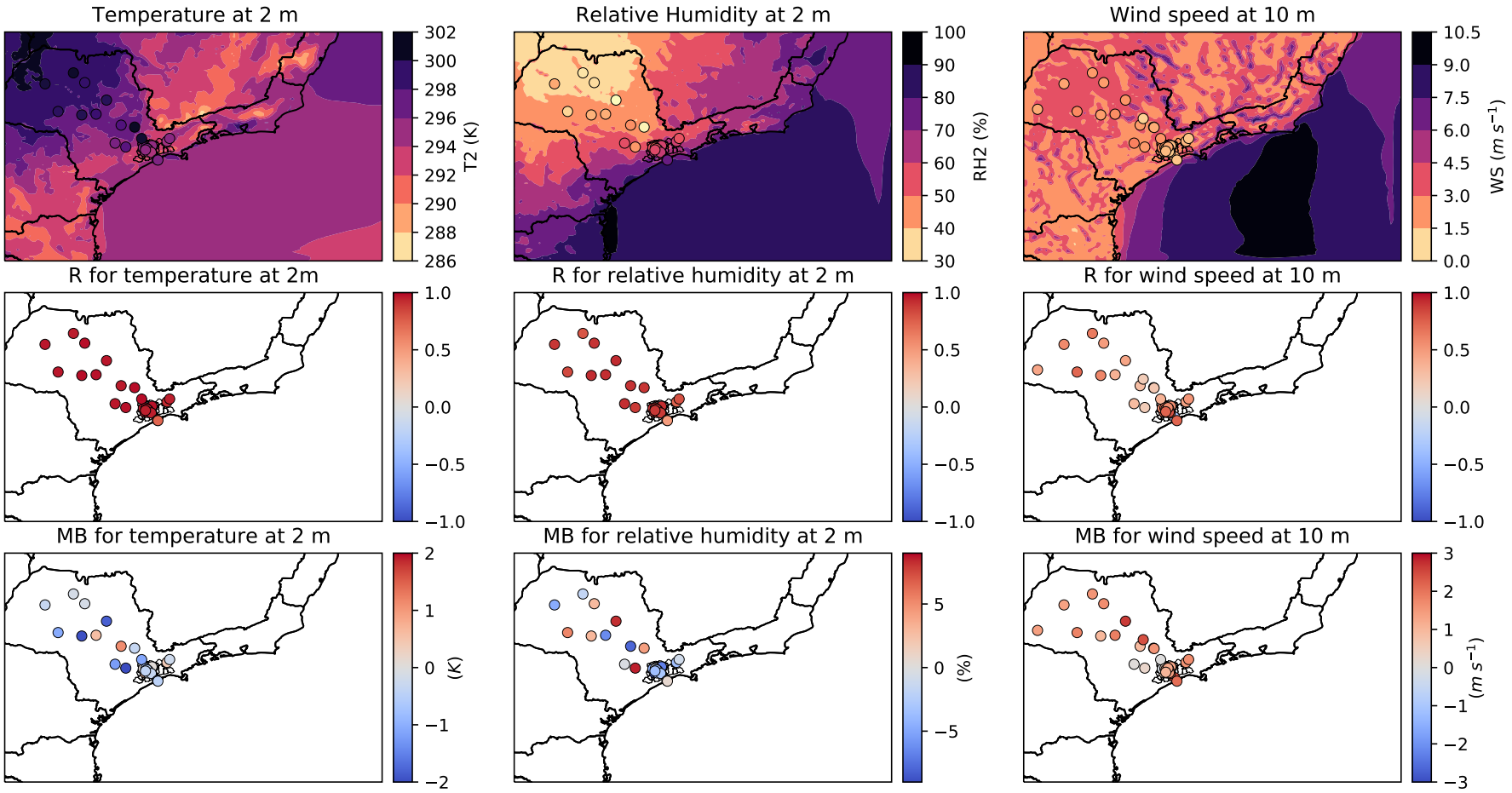

Figure 3.15: Spatial distribution of averaged hourly observations and WRF-Chem predictions, Pearson correlation coefficient, and Mean bias for T2, RH2 and WS in the regional domain

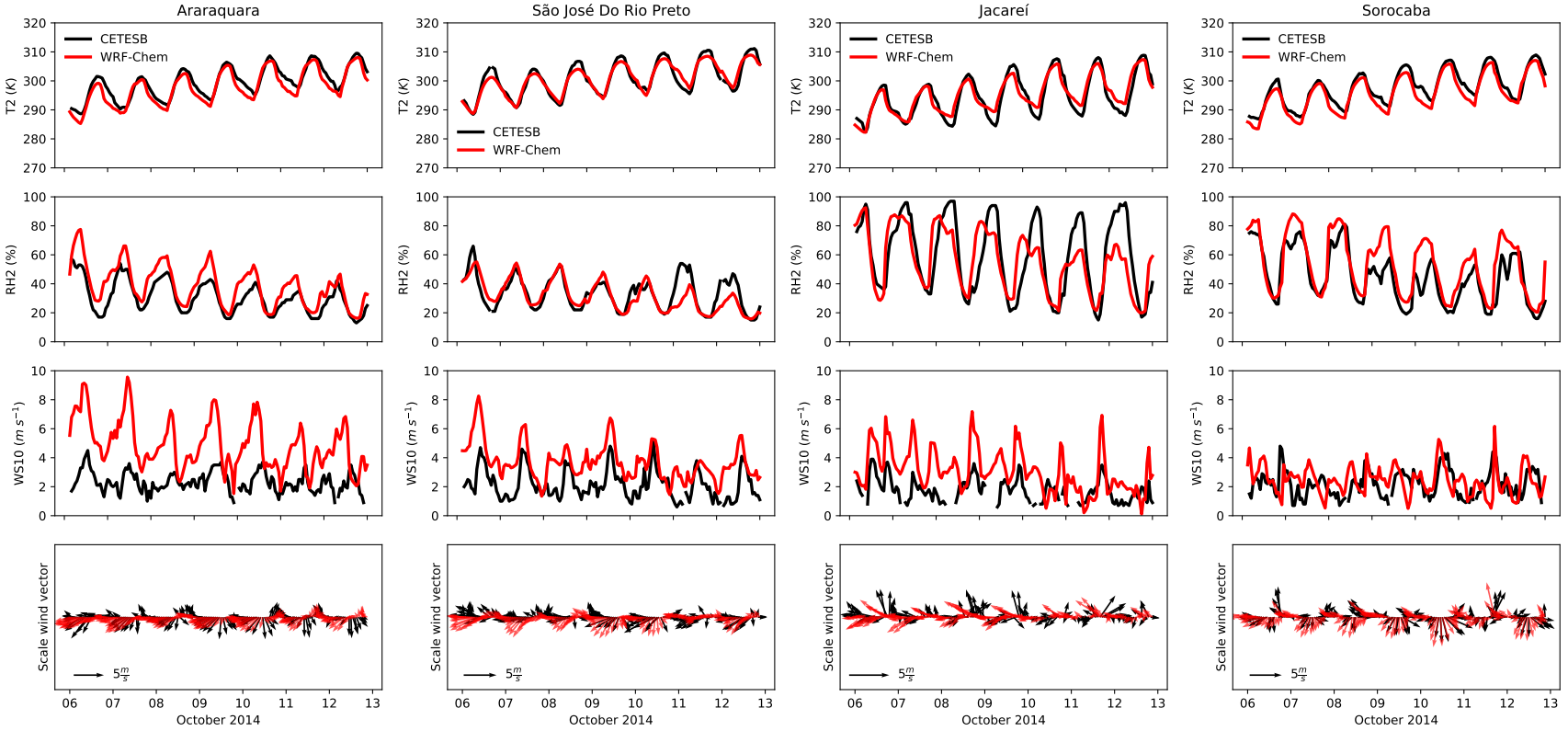

Figure 3.16: Comparison between WRF-Chem meteorological parameters in the regional domain and CETESB observations for stations in the suburban area

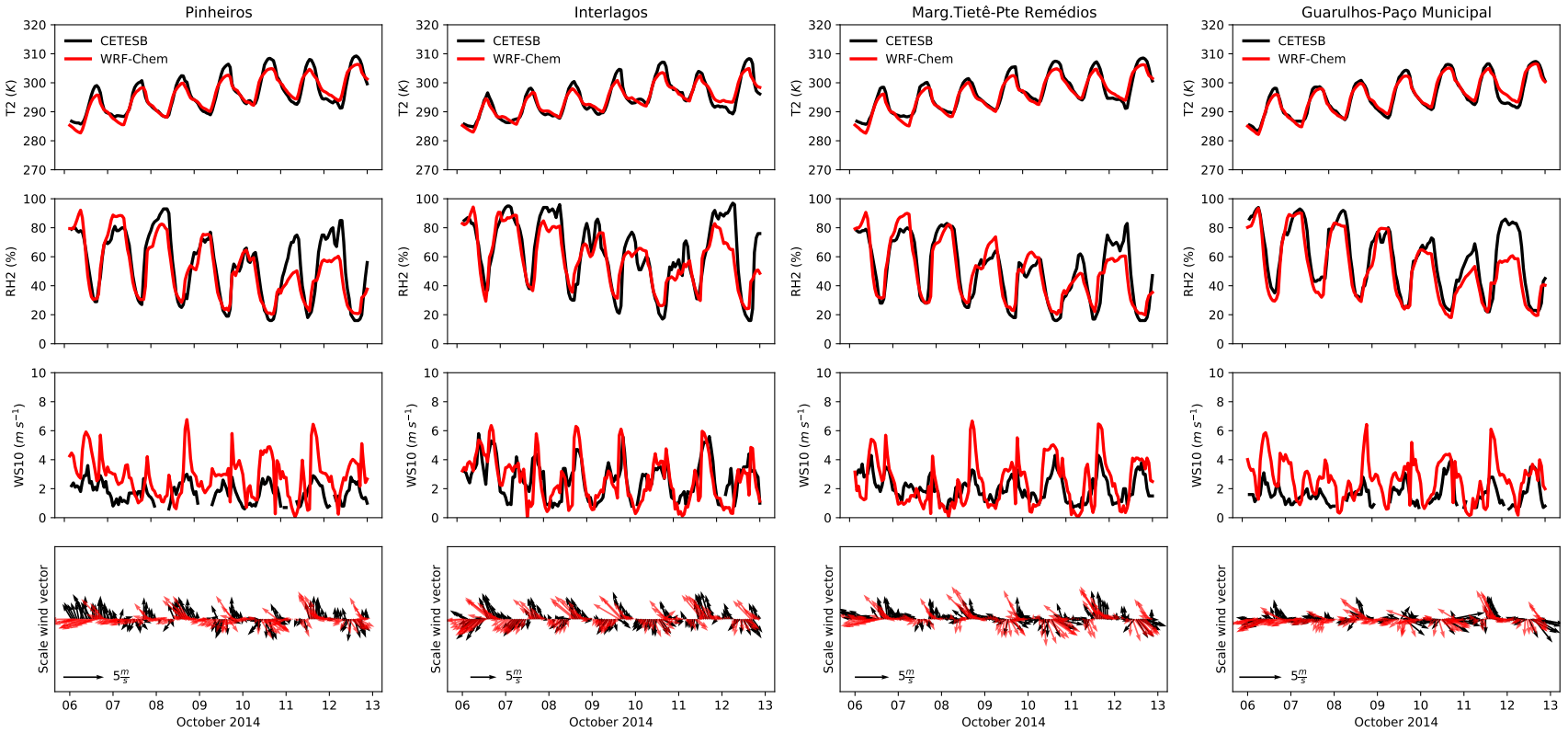

Figure 3.17: Comparison between WRF-Chem meteorological parameters in the regional domain and CETESB observations for stations inside MASP

3.2.2.2 Air quality prediction

Table 3.5 shows the performance statistics for the verification of air pollutant concentration accuracy. Ozone simulation reaches the recommended goal benchmarks for the Pearson correlation coefficient and the criteria benchmark for NMB, nevertheless, WRF-Chem doesn't reach the benchmark for NME. There is an underestimation of the concentration of all pollutants, and all are positively correlated with WRF-Chem simulated values.

Figure 3.18 shows the spatial distribution of observations (dots) and model prediction, Pearson coefficient, and mean bias for O_3, NO, NO_2, and CO. Stronger values of R are located inside MASP, whereas lower values are registered in the other regions of São Paulo state. This behavior is clearer when considering NO. The predicted concentration underestimation occurs in all the model domain.

Table 3.5 - Performance statistics for predicted pollutants concentration against CETESB measurements for WRF-Chem regional domain

	N	$\bar{O}$	$\bar{M}$	σ_O	σ_M	MB	ME	RMSE	NMB	NME	R	IOA
O_3 ($\mu g\ m^{-3}$)	6269	58.30	53.48	48.69	35.70	-2.93	22.96	29.15	-5.02	39.38	0.81	0.87
NO ($\mu g\ m^{-3}$)	5639	22.87	11.14	44.72	30.73	-10.04	22.86	47.82	-43.90	99.95	0.32	0.54
NO_2 ($\mu g\ m^{-3}$)	5639	42.80	20.68	29.70	19.35	-20.46	24.26	33.00	-47.81	56.69	0.52	0.64
NO_X (ppb)	5639	41.22	21.38	45.95	33.76	-17.49	30.11	49.74	-42.44	73.04	0.38	0.60
CO (ppm)	2663	0.92	0.37	0.55	0.40	-0.30	0.52	0.70	-33.15	56.36	0.31	0.54

N : numbers of observation (O) and prediction (M); $\bar{O}$: observations mean; $\bar{M}$: prediction mean; σ_O: observation standard deviation; σ_M: prediction standard deviation; MB: mean bias; MAGE: Mean absolute gross error; RMSE: Root mean square error; NMB: Normal mean bias (%); NME: Normal mean error (%); R: Pearson correlation coefficient; IOA: index of agreement.

Figure 3.19 and figure 3.20[1] show the diurnal variation of observation and WRF-Chem prediction of pollutant concentration in the regional and suburban stations, respectively. CO is only measured in one air quality stations outside MASP. WRF-Chem reproduces well the variation of O_3 and NO_2 concentrations during the day. NO concentrations are well represented during the daylight, but bigger differences occur at nighttime hours. In the suburban stations closer to MASP (i.e. Jundiaí and Paulínia), the underestimation of the O_3 concentrations starts around 9 Local Time (LT), whereas in MASP the underestimation

[1] Missing hours in CETESB diurnal cycle are caused by the calibration of pollutant analyzers in the stations. That information is discarded by CETESB.

starts after 11 LT, also, in the farthest stations (i.e. Araraquara and São Jose do Rio Preto), we observe an overestimation of ozone concentration during night time hours, whereas during the daylight there is an underestimation. Without the use of CAM-Chem as CBC, the O_3 underestimation could have been more pronounced in air quality stations located in the Northwest part of São Paulo state (See Figure D.2). There is a high peak of concentration at 6 hours both for CO and NO, both primary pollutants. This can be caused by errors in the emission temporal profile, but also in an underestimation of the planetary boundary layer height.

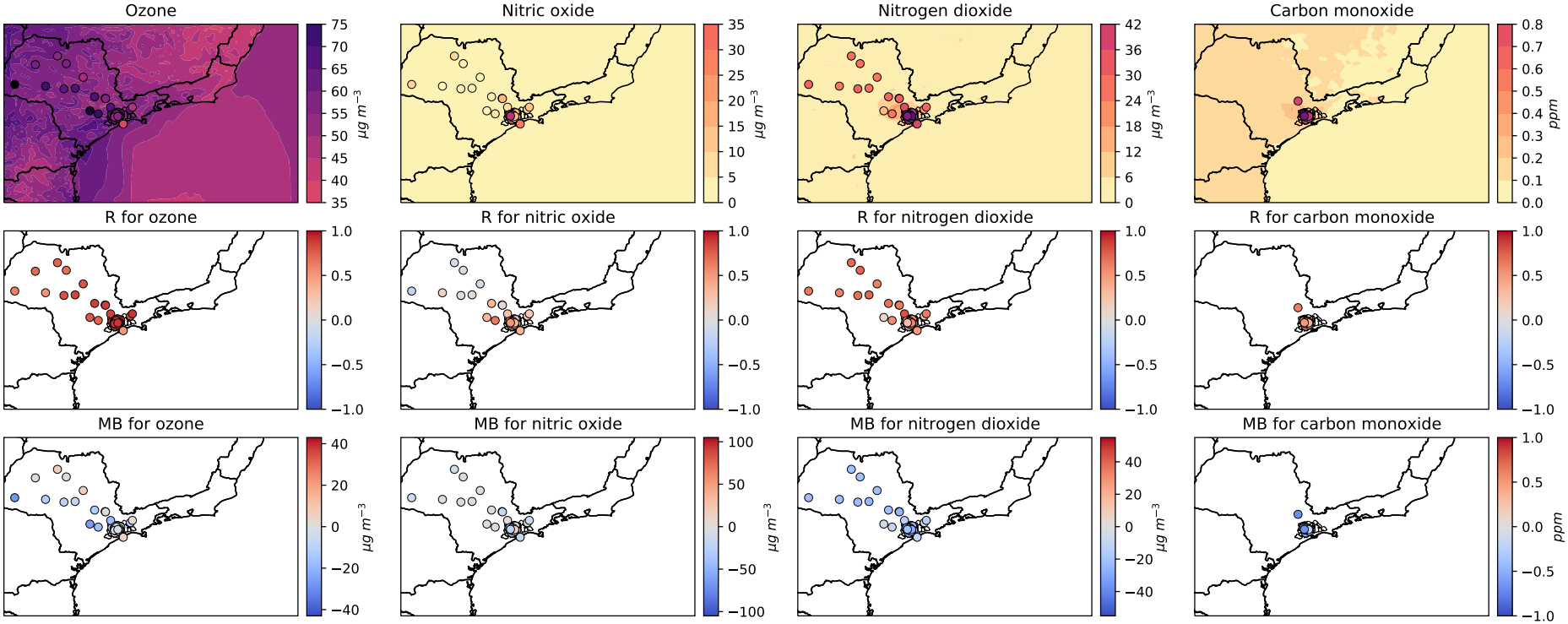

Figure 3.18: Spatial distribution of averaged hourly observations and WRF-Chem predictions, Pearson correlation coefficient, and Mean bias for O_3, NO, NO_2, and CO in the regional domain.

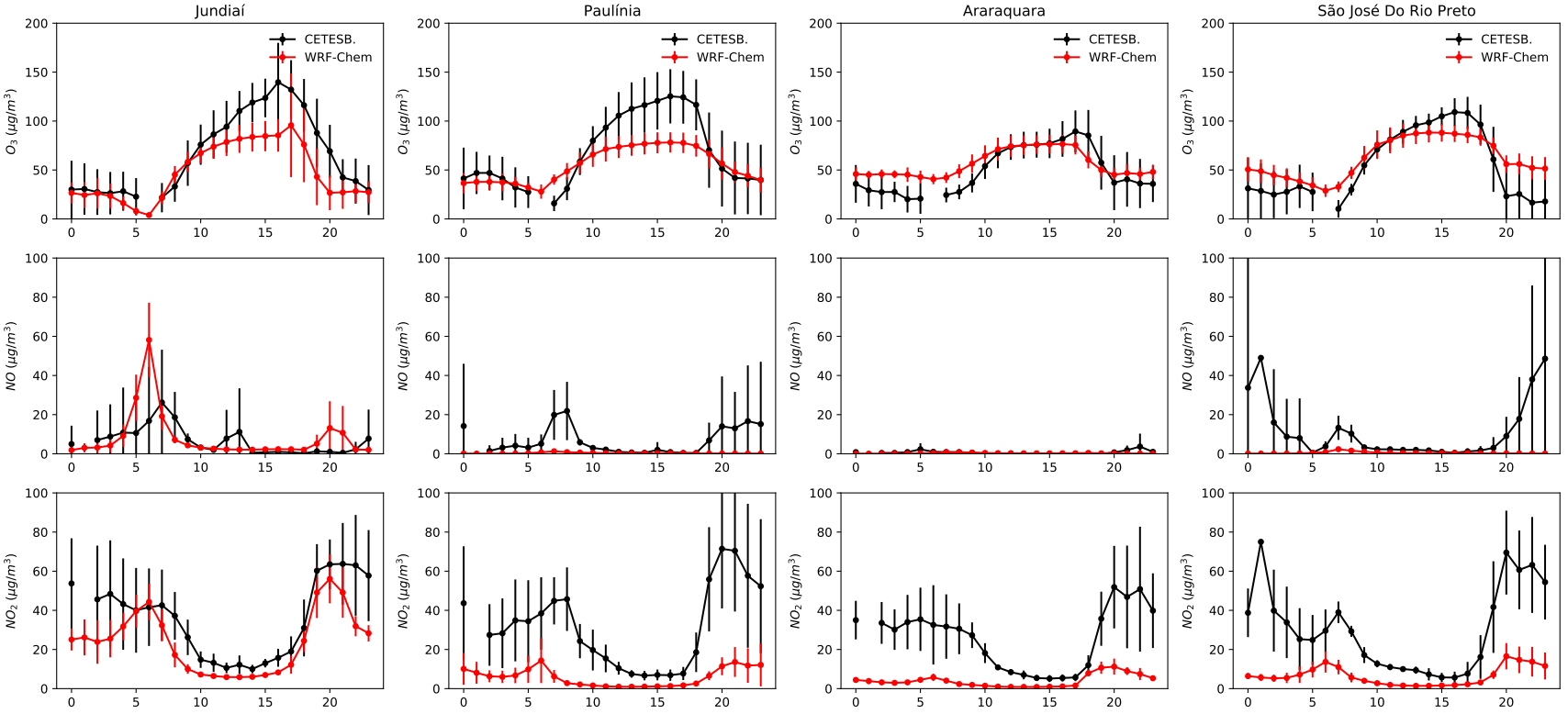

Figure 3.19: Comparison between WRF-Chem pollutant concentration predictions in the regional domain and CETESB observations for stations in the suburban area

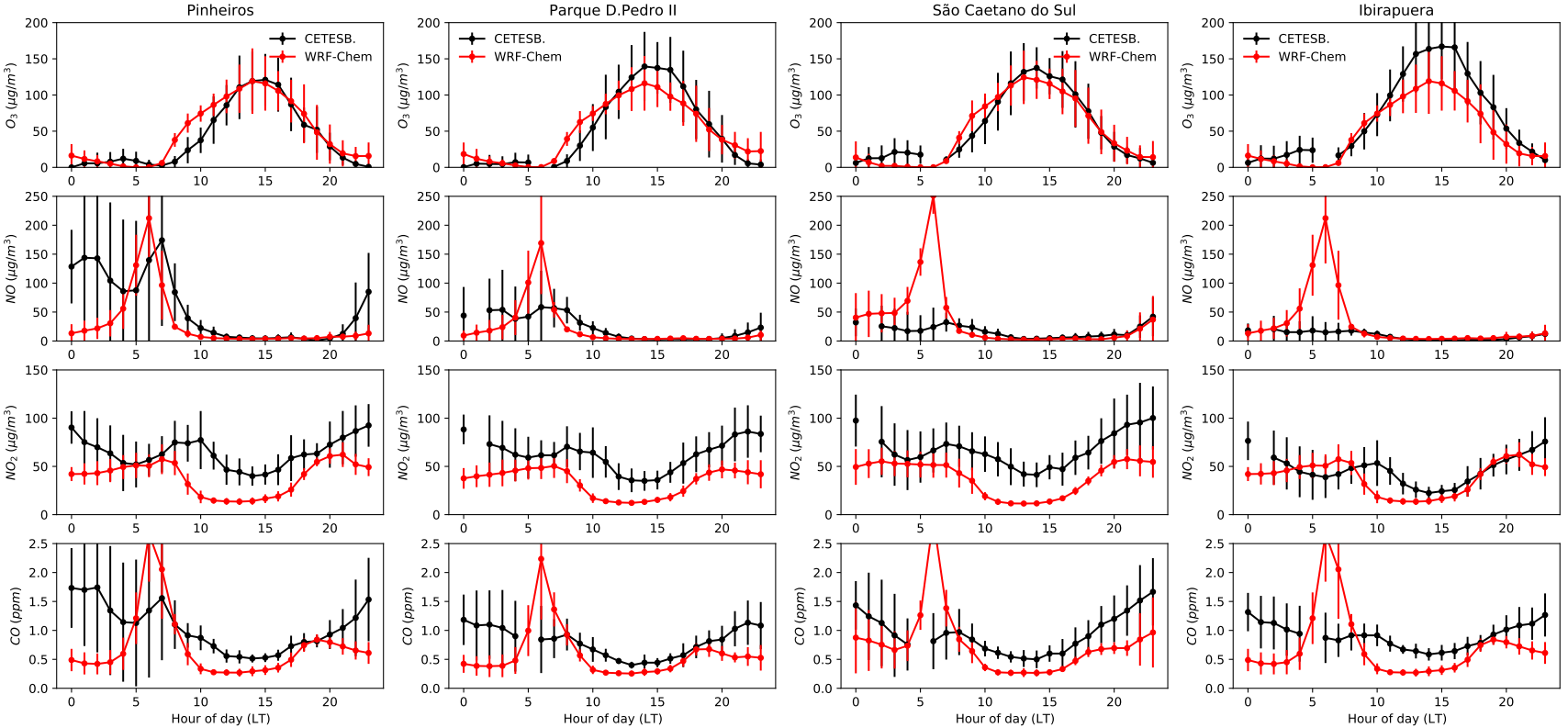

Figure 3.20: Comparison between WRF-Chem pollutant concentration predictions in the regional domain and CETESB observations for stations inside MASP

3.2.3 Urban scale: inside MASP simulations

The second WRF-Chem domain focuses on the MASP region. The objective of this session is to study in more detail how the WRF-Chem behaves at the urban scale.

3.2.3.1 Meteorological prediction

Table 3.6 shows the performance statistics for the verification of meteorological parameters accuracy in domain 2. We have that WRF-Chem reaches the benchmark for simple and complex terrain for T2 and RH2, the complex terrain benchmarks for WS, and only satisfies the ME complex terrain benchmark for WD, nevertheless, the MB was closer to the benchmark than domain 2 simulations. Inside MASP, there is an improvement in the representation of the meteorological parameters when increasing the spatial resolution to 3 km. The Pearson correlation coefficient for T2, RH2, and WS (Fig. 3.22), is higher and the underestimation of wind speed is lower; and the inclination of wind direction towards south is less than in domain 1 (See table E.1 in Appendix, where it was used the air quality station inside domain 2 to make the verification for domain 1).

Table 3.6 - Performance statistics for predicted meteorological parameters against CETESB measurements for WRF-Chem urban domain

	N	$\bar{O}$	$\bar{M}$	σ_O	σ_M	MB	ME	RMSE	NMB	NME	R	IOA
T2 (K)	2357	295.72	295.33	5.93	5.56	-0.03	1.65	2.07	-0.01	0.56	0.94	0.97
RH2 (%)	2303	59.09	53.94	22.61	20.38	-3.89	9.63	12.66	-6.59	16.30	0.85	0.91
WS (m s^{-1})	2453	1.86	2.80	0.90	1.59	1.10	1.46	1.83	58.97	78.20	0.44	0.53
WD (°)	2430	-	-	-	-	-12.96	53.64	-	-	-	-	-
U10 (m s^{-1})	2430	-0.55	-1.41	1.24	1.97	-0.80	1.66	2.11	143.60	-300.08	0.43	0.59
V10 (m s^{-1})	2430	0.42	-0.17	1.51	2.11	-0.54	1.39	1.81	-129.00	334.66	0.65	0.75

N : numbers of observation (O) and prediction (M); $\bar{O}$: observations mean; $\bar{M}$: prediction mean; σ_O: observation standard deviation; σ_M: prediction standard deviation; MB: mean bias; MAGE: Mean absolute gross error; RMSE: Root mean square error; NMB: Normal mean bias (%); NME: Normal mean error (%); R: Pearson correlation coefficient; IOA: index of agreement.

Figure 3.22 shows the spatial distribution of observations and WRF-Chem predictions, the Pearson correlation, and the Mean Bias of the evaluated meteorological parameters for T2, RH2, and WS. WRF-Chem represents well the spatial distribution of these parameters. The center of São Paulo city, which is highly urbanized, presents the highest temperature and it is drier than its surroundings (i.e. urban heat island effect). All parameters are

positively correlated, with the exception of wind speed in Cubatão station. Temperature overestimation is heterogeneous around the domain, with clearer greater bias in northeast stations. WRF-Chem simulates drier conditions inside MASP, and WS is overestimated over all the domain. Figure 3.22 shows the temporal series of these parameters.

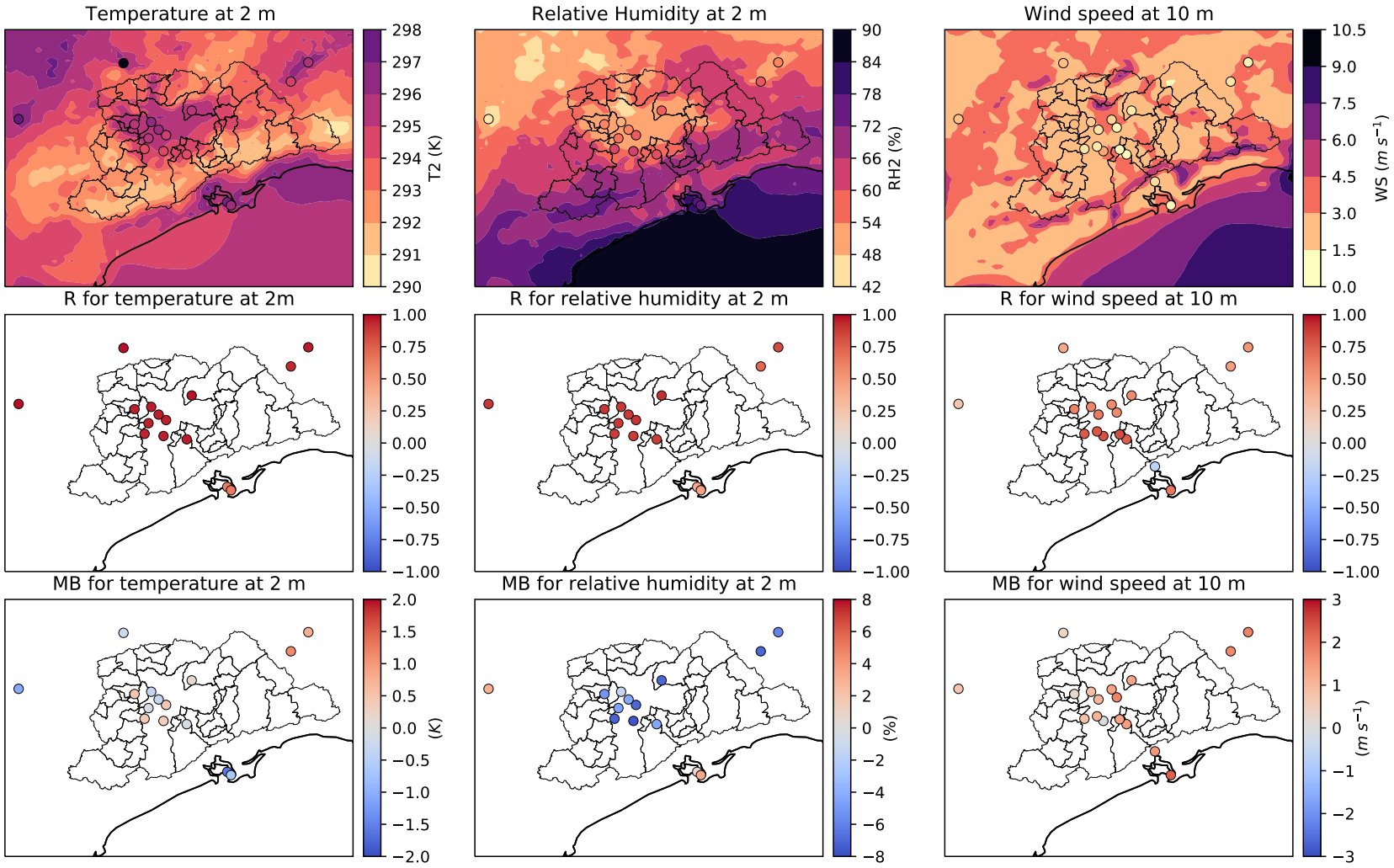

Figure 3.21: Spatial distribution of averaged hourly observations and WRF-Chem predictions, Pearson correlation coefficient, and Mean bias for T2, RH2 and WS in the urban domain

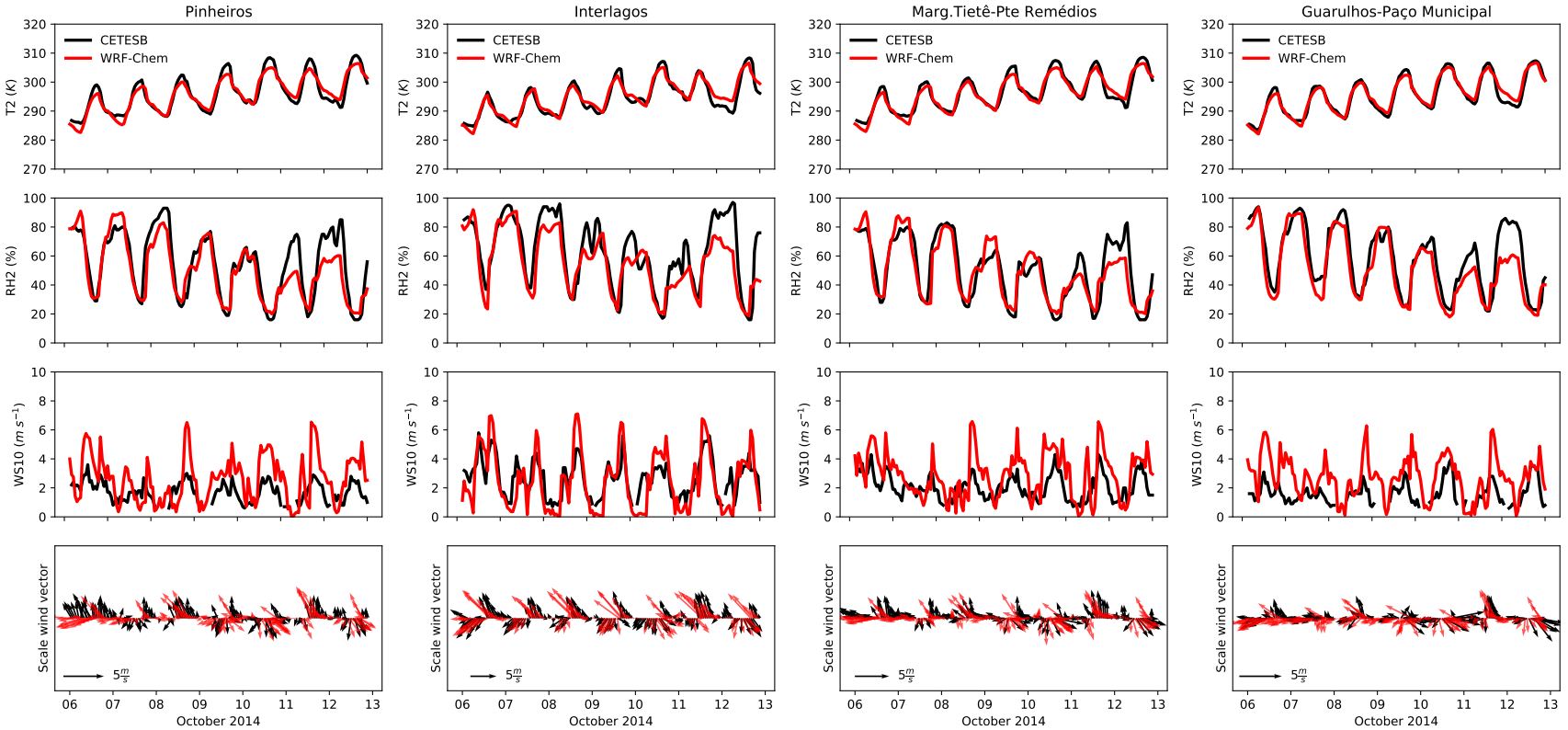

Figure 3.22: Comparison between WRF-Chem meteorological parameters in the urban domain and CETESB observations for stations inside MASP for the urban domain.

Table 3.7 - Performance statistics for predicted pollutants concentration against CETESB measurements for WRF-Chem urban domain

	N	$\bar{O}$	$\bar{M}$	σ_O	σ_M	MB	ME	RMSE	NMB	NME	R	IOA
O_3 ($\mu g\ m^{-3}$)	4423	55.09	50.66	51.74	42.37	-2.74	22.51	29.16	-4.97	40.86	0.83	0.90
NO ($\mu g\ m^{-3}$)	3964	30.22	19.29	50.62	42.94	-8.62	32.73	60.48	-28.53	108.30	0.24	0.50
NO_2 ($\mu g\ m^{-3}$)	3964	49.55	30.12	29.25	20.82	-17.75	25.47	34.30	-35.82	51.39	0.37	0.58
NO_X (ppb)	3964	50.73	33.75	49.86	43.91	-14.16	38.44	60.57	-27.91	75.78	0.26	0.54
CO (ppm)	2516	0.92	0.53	0.56	0.51	-0.24	0.53	0.75	-26.12	56.97	0.27	0.52

N : numbers of observation (O) and prediction (M); $\bar{O}$: observations mean; $\bar{M}$: prediction mean; σ_O: observation standard deviation; σ_M: prediction standard deviation; MB: mean bias; MAGE: Mean absolute gross error; RMSE: Root mean square error; NMB: Normal mean bias (%); NME: Normal mean error (%); R: Pearson correlation coefficient; IOA: index of agreement.

3.2.3.2 Air quality predictions

Table 3.7 shows the performance statistics for the verification of air pollutant concentration accuracy in the domain 2. Like the domain 1 results, O_3 simulations reach the goal benchmark for the Pearson correlation coefficient, and the criteria benchmark for NMB.

Figure 3.25 shows the spatial distribution of observed and WRF-Chem prediction, Pearson correlation coefficient, and MB for O_3, NO, NO_2, and CO in domain 2. NO is concentrated inside São Paulo city, whereas O_3, NO_2, and CO concentrations are distributed in all the domain. Pearson correlation coefficient is positive in all domain for O_3; while for NO and NO_2, the correlations are stronger in the center of the city. In most of the stations, there is an underestimation of pollutants concentrations. A special exception occurs in Cubatão where there is a significant overestimation of the model simulated values. This location is an industrial pole and the emissions sources are not correctly assigned.

Figure 3.24 shows the temporal series of pollutants at four stations located in MASP. In more urbanized areas like Pinheiros and Parque D. Pedro II the representation of magnitude as well as the diurnal cycle presented a good performance. Figure 3.25 shows the diurnal concentration cycle of pollutants. WRF-Chem simulate correctly the diurnal variation of O_3 and NO_2. It is more evident the peak of concentration at 6 LT for the primary pollutants CO and NO, as in domain 1.

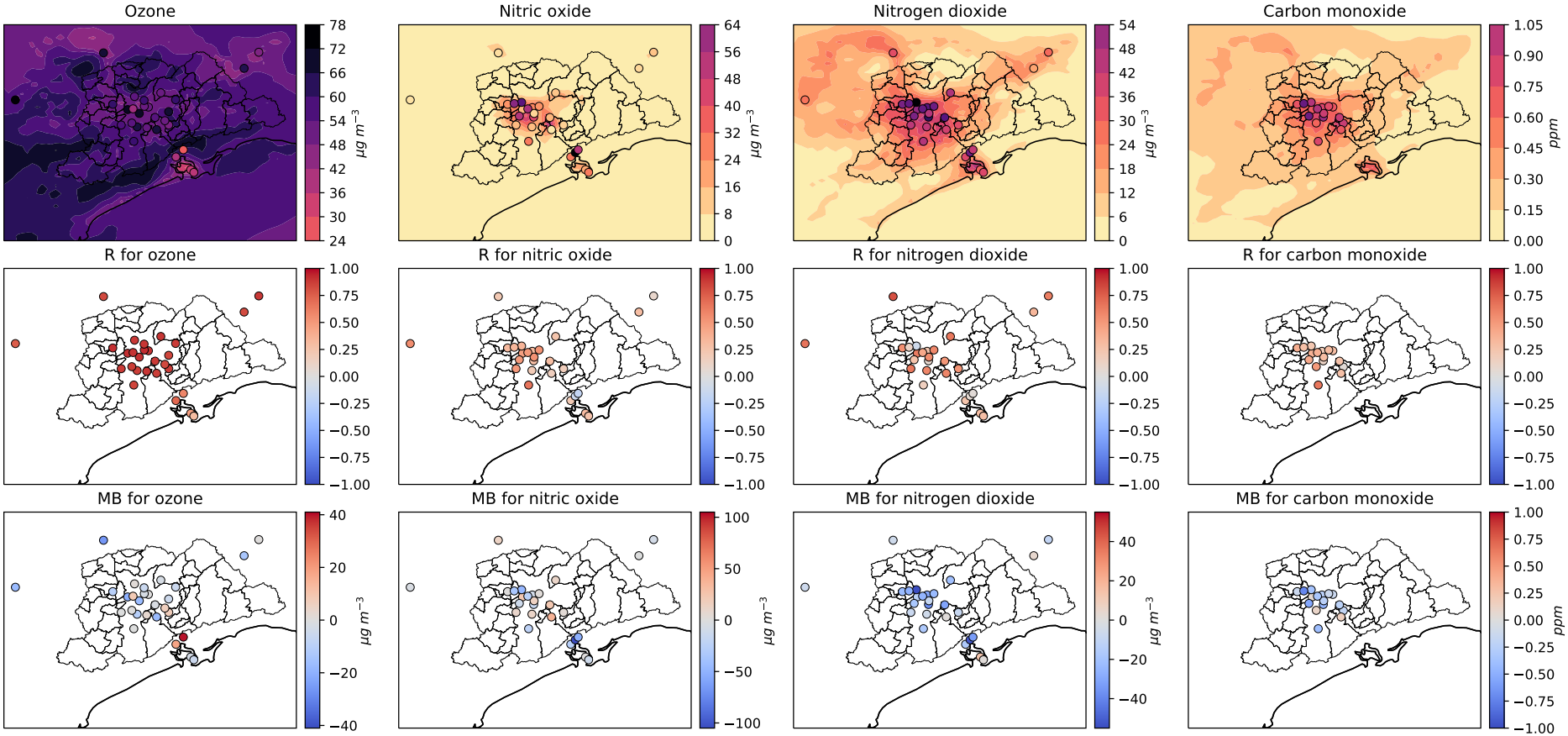

Figure 3.23: Spatial distribution of averaged hourly observations and WRF-Chem predictions, Pearson correlation coefficient, and Mean bias for O_3, NO, NO_2, and CO in the urban domain

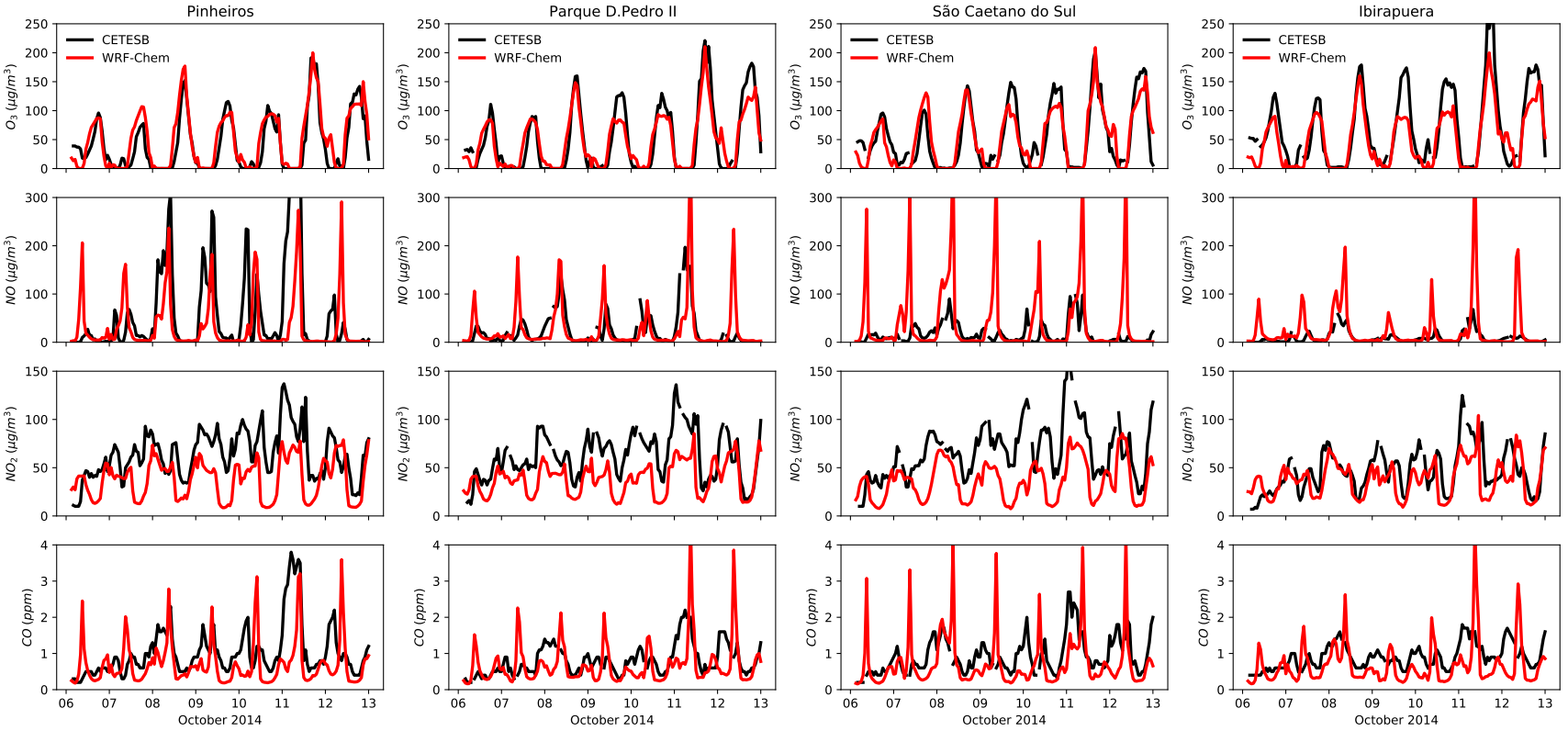

Figure 3.24: Comparison between WRF-Chem pollutant concentration predictions in the urban domain and CETESB observations time series for stations inside MASP

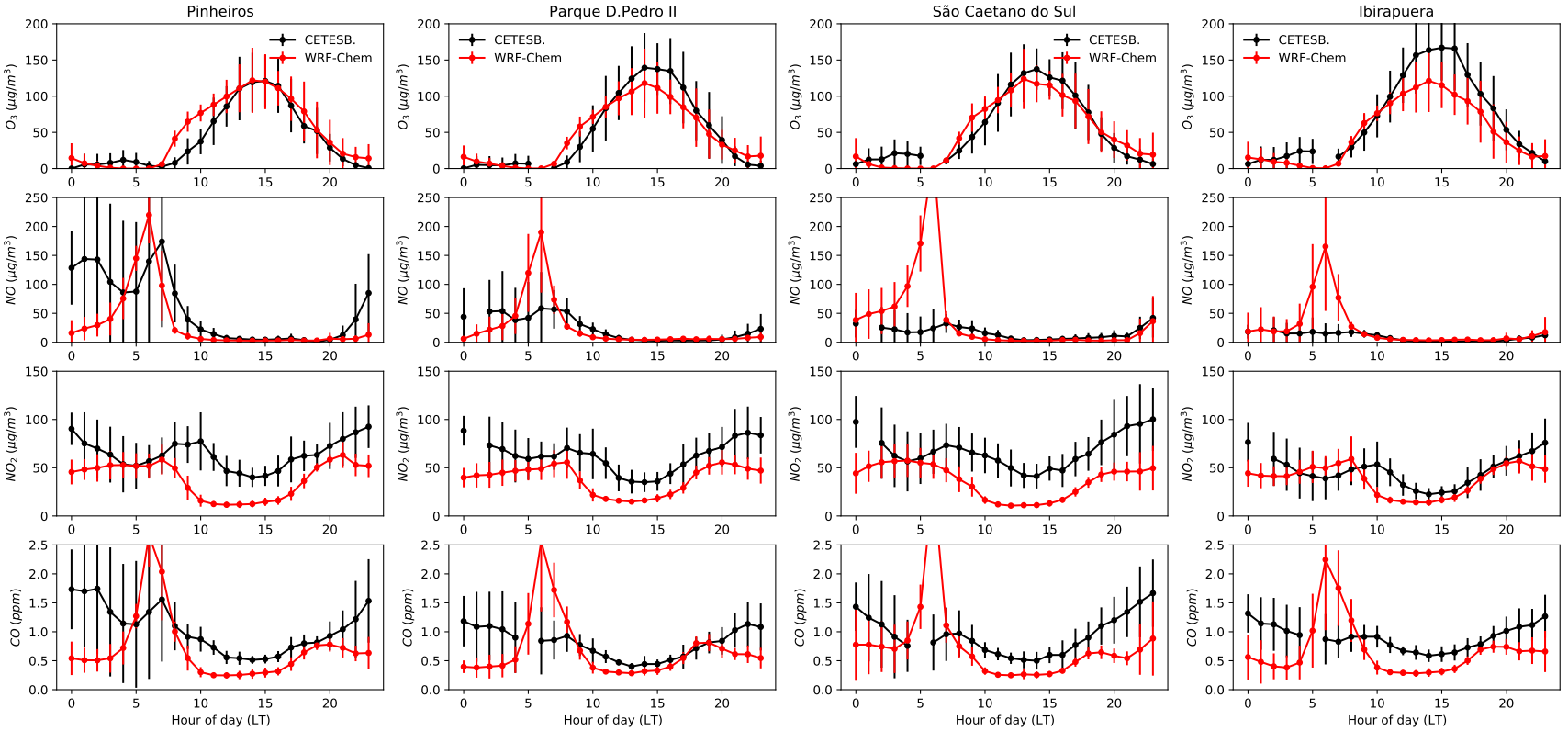

Figure 3.25: Comparison between WRF-Chem pollutant concentration predictions in the urban domain and CETESB observations for stations inside MASP for urban domain.

3.2.4 Analysis of WRF-Chem simulations

Underestimation of ozone can be explained by imprecisions in meteorology and emission estimates. The underestimation of T2 maximum values could have limited the representation of the production of biogenic VOC emissions (Monks et al., 2009), reducing the formation of ozone in the MASP, as it is under a VOC limited regime (Carvalho et al., 2015; Andrade et al., 2017). This situation can be more clearly observed at Ibirapuera station, which is located in a Park and ozone formation is highly influenced by biogenic emissions.

The representation of the PBL height poses a huge constraint on the simulations of pollutant concentrations. In figure 3.24, we can see that the three first days of the week present a better representation of pollutants. During these days WRF-Chem underestimate the PBL height, as we can see in figure E.1, where we used the inversion base height from sounding launched at the Campo de Marte to estimate the PBL height. Further, in domain 2 it was simulated a higher PBL height. As noted in Misenis and Zhang (2010), YSU parameterization tends to overestimate the PBL height, and also PBL parameterization schemes still have trouble representing residual boundary layer at night hours (McNider and Pour-Biazar, 2020).

Wind speed favors air pollutant dispersion, the overestimation of wind speed decrease the concentration during the day. The overestimation of the wind speed over MASP with WRF-Chem was also reported in Vara-Vela et al. (2016, 2017); Pellegatti Franco et al. (2019)

The other factor is the spatial disaggregation of the vehicular emissions. The methodology of using road length in each cell to spatially disaggregate the total emissions forces emission regimes predefined by the total emission estimates. In this case, the ratio of NO_X/VOC emission was ~ 0.4, which is valid in urban areas, but not suitable for suburban or rural areas.

CBC also affect the O_3 underestimation. As seen in the previous section, CBC from CAM-Chem advected less O_3 from the east border producing an underprediction of 3 $\mu g\ m^{-3}$.

Even when the increase of spatial resolution resulted in better meteorological variables representation, there wasn't an increase in pollutant concentration representation perfor-

mance. However, the results are very close and are consistent with Tie et al. (2010), where they indicate that an increase in emission resolution results in a modest impact on ozone representation.

Our results are consistent with previous air quality simulations over MASP, for the dry season. With R $\geq$ 0.7, and model underestimation of O_3 as shown in Vara-Vela et al. (2016); Hoshyaripour et al. (2016); Vara-Vela et al. (2017); Pellegatti Franco et al. (2019), see Table 3.8.

Table 3.8 - Performance statistic from different O_3 simulation studies in MASP ($\mu g\ m^{-3}$)

Reference	Season	AQS	MB	RMSE	R
Hoshyaripour et al. (2016)	August 2012	3	-	23.8	0.73
Vara-Vela et al. (2016)	August 2012	6	-0.85	27.45	0.63
Gavidia-Calderón et al. (2018)	Oct 30 - Nov 1 2006	12	16.38	31.32	0.81
Vara-Vela et al. (2017)	September 2014	6	-5.32	28.12	0.71
Pellegatti Franco et al. (2019)	Nov 1-3 2013	4	-2.8	-25.68	-
This work	Oct 6-13 2014	27	-2.7	29.1	0.83

AQS: Number of Air quality considered; MB: Mean Bias; RMSE: Root mean square error; R: Pearson Correlation Coefficient.

There is a need for the evaluation of pollutant exposure of the population at the street level. With the knowledge accumulated through many years of application of Chemical Transport Models for the description of the formation and transport of pollutants, we start the application of a street-network model to specific neighborhoods within São Paulo City. The next session will discuss the difficulties and applicability of the MUNICH model in São Paulo.

3.3 Local scale air quality modeling: MUNICH

In this section, we present the O_3, NO_X, NO, and NO_2 simulations with MUNICH, with the idea of having a street-in-grid model to simulate the pollutants dispersion at urban canopy as shown in Kim et al. (2018). First, we calibrated VEIN input emissions by studying Pinheiros neighborhood (a residential-commercial area in the West part of São Paulo City) by using background concentration from the Ibirapuera air quality station. Later, we used WRF-Chem urban domain simulation to retrieve pollutant concentrations for Pinheiros location as background concentration.

3.3.1 Control case for the Pinheiros neighborhood

Figure 3.26 shows the MUNICH simulation using VEIN original emissions (Vehicular Emission Model) for MASP. MUNICH pollutants simulations are very close to background concentrations. This leads to an overprediction of O_3 and underprediction of NO and NO_X. The background concentrations come from Ibirapuera station, and they represent the concentration of O_3, NO_2 and NO outside the domain (i.e. over the building rooftop).

This is produced by emission underestimation and a strong dependence on background concentrations. The emission underestimation is caused by emission factors calculated derived from dynamometer experiments. The drive cycle considered for the evaluation of emissions factors do not represent real-drive emissions (Ropkins et al., 2009). Also, the number of vehicles could have been underestimated in VEIN. The underestimation of NO_X is caused by the underestimation of NO concentrations. Nevertheless, NO_2 concentration magnitudes are well represented.

The diurnal cycle of MUNICH simulations, observations, and background concentrations are shown in figure 3.27. MUNICH simulated well the diurnal variation of O_3 and NO_2 concentrations inside the urban canyon. For NO and NO_X, the concentrations during the day and until midnight are well simulated, while the morning peak at six hours is underestimated. After midnight, higher concentrations of NO_X happens by the increase of heavy-duty vehicle circulation that run with diesel. In Pinheiros neighborhood, light-duty vehicles are predominant, but it is close to a highway with heavy traffic of trucks (Marginal Pinheiros). This situation explains the high NO_X concentrations that are transported from the highway. The difference between MUNICH simulation and background concentration

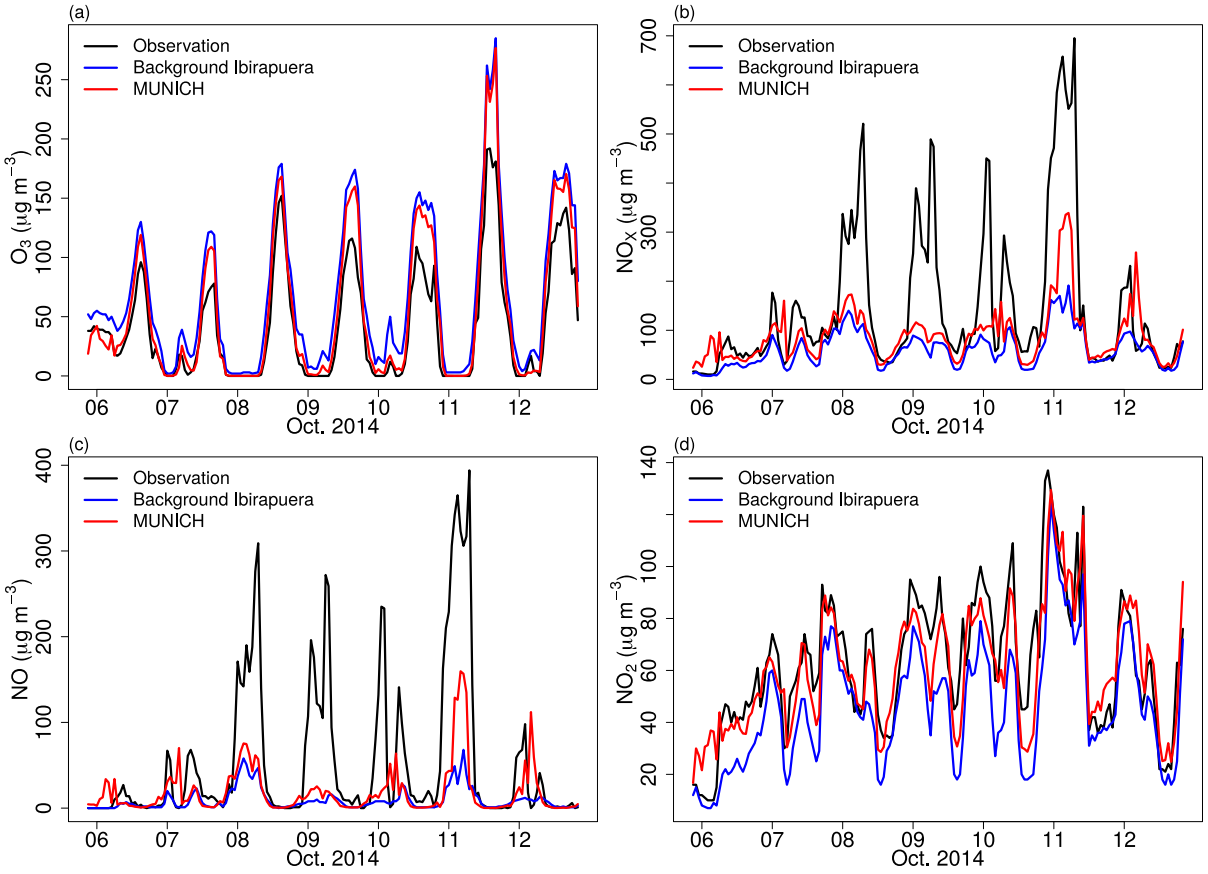

Figure 3.26: Comparison of MUNICH results against background and observation concentrations for (a) O_3 , (b) NO_X , (c) NO, and (d) NO_2 for Pinheiros urban canyon control case.

for O_3, NO_X, NO, and NO_2 are -13.1 $\mu g\ m^{-3}$, 28.6 $\mu g\ m^{-3}$, 9.2 $\mu g\ m^{-3}$, and 14.4 $\mu g\ m^{-3}$, respectively.

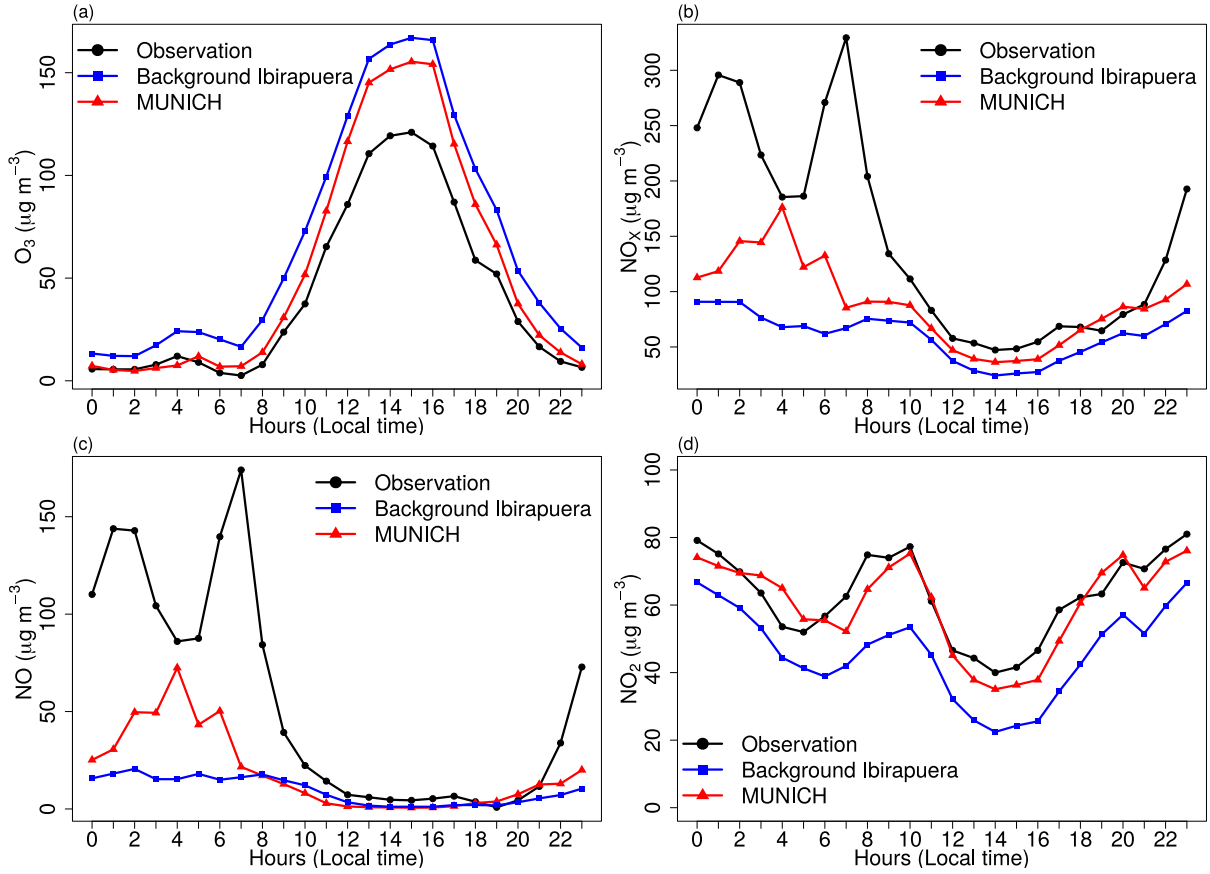

Figure 3.27: Diurnal profile of MUNICH results, background, and concentrations for (a) O_3 , (b) NO_X , (c) NO, and (d) NO_2 for Pinheiros urban canyon control case.

3.3.2 Emission adjustment scenario

We doubled the NO_X and VOCs emissions from VEIN to try to improve the model results, this scenario is called MUNICH-Emiss. We achieved an overall improvement of MUNICH simulations. Figure 3.28 shows the comparison among MUNICH-Emiss, background concentrations, and observations. O_3 continues to be overpredicted due to the higher values of O_3 and the lower values NO background concentrations (i.e. reducing O_3 consumption). Still, the simulated O_3 concentration during the night is well represented and daily peak concentrations are now closer to observations.

NO_X and NO concentrations are still underpredicted, while NO_2 magnitude is closer to the observations. NO_X underprediction is caused by the underprediction of NO, particularly during October 8^{th}, 9^{th}, and, 10^{th} where high values of NO were measured. Never-

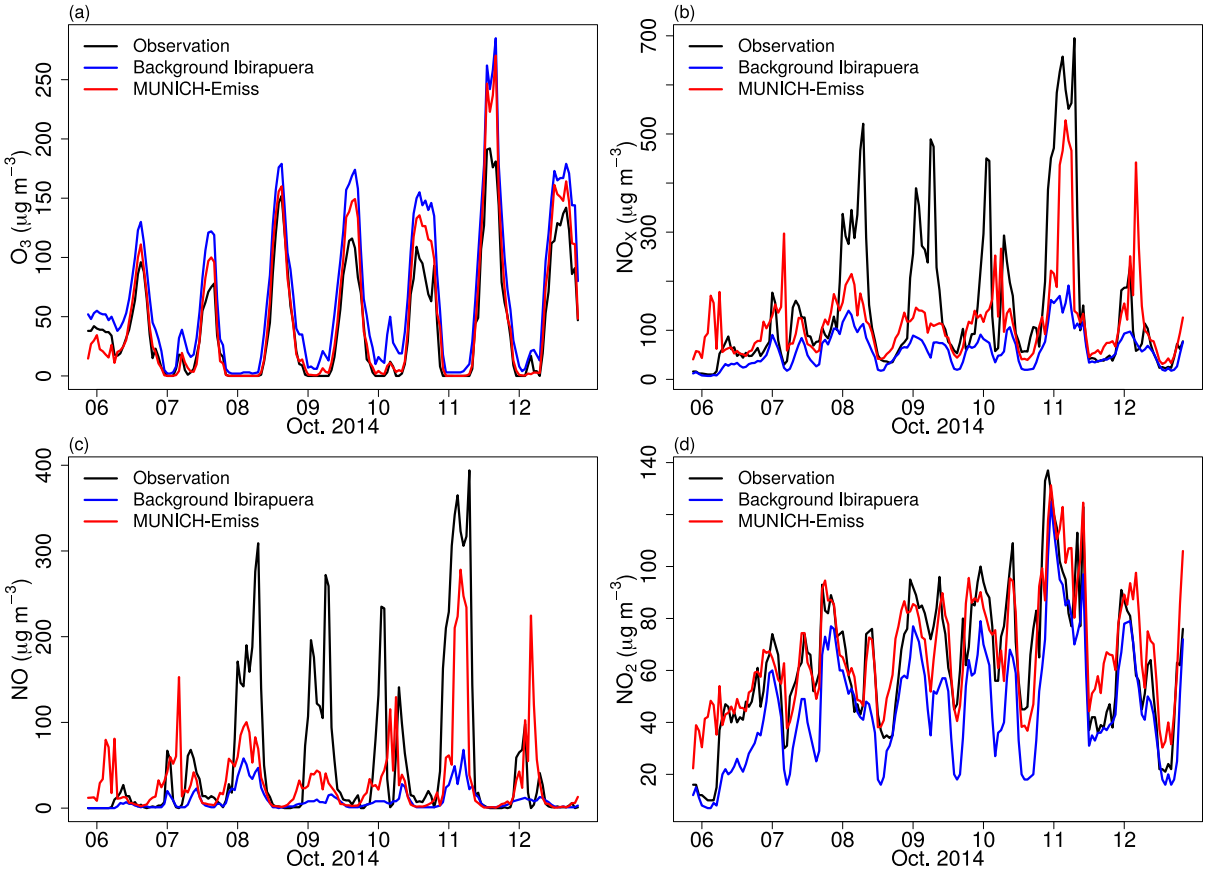

Figure 3.28: Comparison of MUNICH results against background and observation concentrations of (a) O_3 , (b) NO_X , (c) NO, and (d) NO_2 for Pinheiros urban canyon from the MUNICH-Emiss simulation.

theless, MUNICH can better simulate the high concentration during Saturday 11^{th}. This high simulated NO concentration occurs from the influence of meteorology as MUNICH uses the same emission profile for the weekend (same emission from Saturday to Sunday) and weekdays (same emission from Monday to Friday).

Figure 3.29 presents the diurnal profiles for MUNICH-Emiss. MUNICH-Emiss profiles resulted in simulations that are closer to the observations profiles, with an improvement in the representation of the peak concentrations magnitude of NO_X, NO, and NO_2. The difference over the period between simulated and the background concentrations for O_3, NO_X, NO and NO_2 are -17.9 $\mu\ gm^{-3}$, -57.3 $\mu g\ m^{-3}$, 23.6 $\mu\ gm^{-3}$, and 21.1 $\mu g\ m^{-3}$, respectively, showing bigger differences than in the control case scenario. The reaction of O_3 with the additional NO from the emissions increment, which also formed NO_2, results in a lower O_3 overestimation and a better NO_2 simulation.

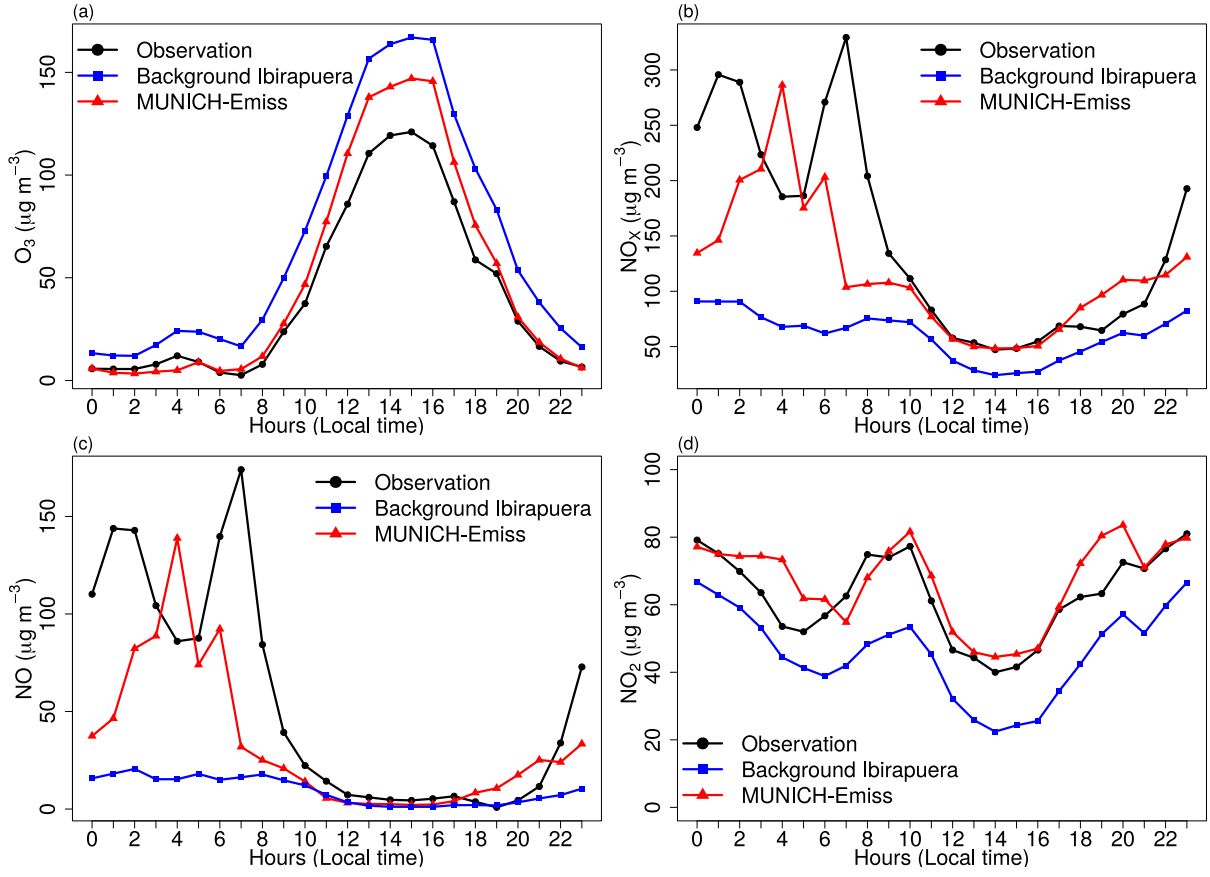

Figure 3.29: Diurnal profile of MUNICH results, background, and concentration for (a) O_3 , (b) NO_X , (c) NO, and (d) NO_2 for Pinheiros urban canyon from the MUNICH-Emiss simulation.

Table 3.9 shows the performance statistics for each scenario and background concentrations from Ibirapuera station. The performance statistics from the MUNICH-Emiss case

show lower values of MB, NMGE, and RMSE for O_3, NO_X, and NO; NO_2 presents a slight increase in these indicators. Every simulation scenario shows high values of R (≥ 0.7) for each pollutant in every case. This indicates that the temporal variations of emission and background concentration are in the same phase as the observations. In MUNICH control case and MUNICH-Emiss simulations, NO_2 and O_3 are better simulated. MUNICH-Emiss scenario performs better and also reaches the recommendations of Hanna and Chang (2012) for O_3, NO_2, NO, and NO_X, whereas MUNICH control case didn't reach the benchmarks for NO.

Table 3.9 - Statistical indicators for O_3 , NO_X , NO, and NO_2 comparison among background concentration, MUNICH simulation, and MUNICH-Emiss against observation from Pinheiros AQS.

		$\bar{M}$	$\bar{O}$	σ_M	σ_O	MB	NMB	NME	RMSE	R	FB	NMSE	FAC2	NAD
O_3 ($\mu g\ m^{-3}$)	Background	67.6	41.5	63.2	47.5	26.1	0.6	0.6	32.4	1.0	0.5	0.4	0.5	0.2
	MUNICH	54.5	41.5	62.1	47.5	13.0	0.3	0.3	22.2	1.0	0.3	0.2	0.6	0.1
	MUNICH-Emiss	49.7	41.5	59.5	47.5	8.2	0.2	0.3	18.0	1.0	0.2	0.2	0.6	0.1
	MUNICH-WRF_Chem	39.3	41.5	45.0	47.5	-2.3	-0.1	0.33	18.8	0.9	0.05	0.2	0.4	0.02
NO_X ($\mu g\ m^{-3}$)	Background	60.3	146.4	37.3	150.3	-86.0	-0.6	0.6	149.6	0.8	0.8	2.5	0.5	0.4
	MUNICH	88.9	146.4	57.4	150.3	-57.4	-0.4	0.5	128.5	0.7	0.5	1.3	0.7	0.2
	MUNICH-Emiss	117.6	146.4	85.6	150.3	-28.8	-0.2	0.5	120.0	0.6	0.2	0.8	0.7	0.1
	MUNICH-WRF_Chem	122.9	146.4	126.9	150.3	-23.4	-0.2	0.6	137.3	0.5	0.2	1.0	0.5	0.1
NO ($\mu g\ m^{-3}$)	Background	9.5	54.6	12.7	88.9	-45.1	-0.8	0.8	91.5	0.8	1.4	16.2	0.3	0.7
	MUNICH	18.7	54.6	28.7	88.9	-35.9	-0.7	0.8	80.7	0.7	1.0	6.4	0.1	0.5
	MUNICH-Emiss	33.1	54.6	48.5	88.9	-21.5	-0.4	0.8	74.5	0.6	0.5	3.1	0.3	0.2
	MUNICH-WRF_Chem	47.7	54.6	77.4	88.9	-6.8	-0.1	0.9	80.4	0.5	0.1	2.5	0.2	0.1
NO_2 ($\mu g\ m^{-3}$)	Background	45.8	62.7	23.4	25.9	-16.8	-0.3	0.3	21.2	0.9	0.3	0.2	0.9	0.2
	MUNICH	60.3	62.7	22.8	25.9	-2.4	0.0	0.2	13.3	0.9	0.0	0.0	1.0	0.0
	MUNICH-Emiss	66.9	62.7	22.0	25.9	4.2	0.10	0.2	14.8	0.8	0.1	0.1	0.9	0.0
	MUNICH-WRF_Chem	49.7	62.7	18.8	25.9	-12.9	-0.2	0.3	27.2	0.5	0.2	0.2	0.8	0.1

$\bar{M}$: prediction mean; $\bar{O}$: observations mean; σ_M: prediction standard deviation; σ_O: observation standard deviation; MB: mean bias; NMB: Normal mean bias (unitless ratio); NME: Normal mean error (unitless ratio); RMSE: Root mean square error; R: Pearson correlation coefficient; FB: Fractional mean bias; NMSE: Normalized mean-square error; FAC2: Fraction of prediction within a factor of two; NAD: Normalized absolute difference.

Figure 3.30 displays O_3 and NO_X mean hourly concentration in the Pinheiros neighborhood. The red diamond shows the location of Pinheiros air quality station. As the VEIN model can distribute spatially the emissions, there is a variation of concentrations in different streets. For instance, the orange diamond points to the location of a traffic light, where traffic jams frequently occur, producing lower O_3 concentrations due to the higher NO emissions.

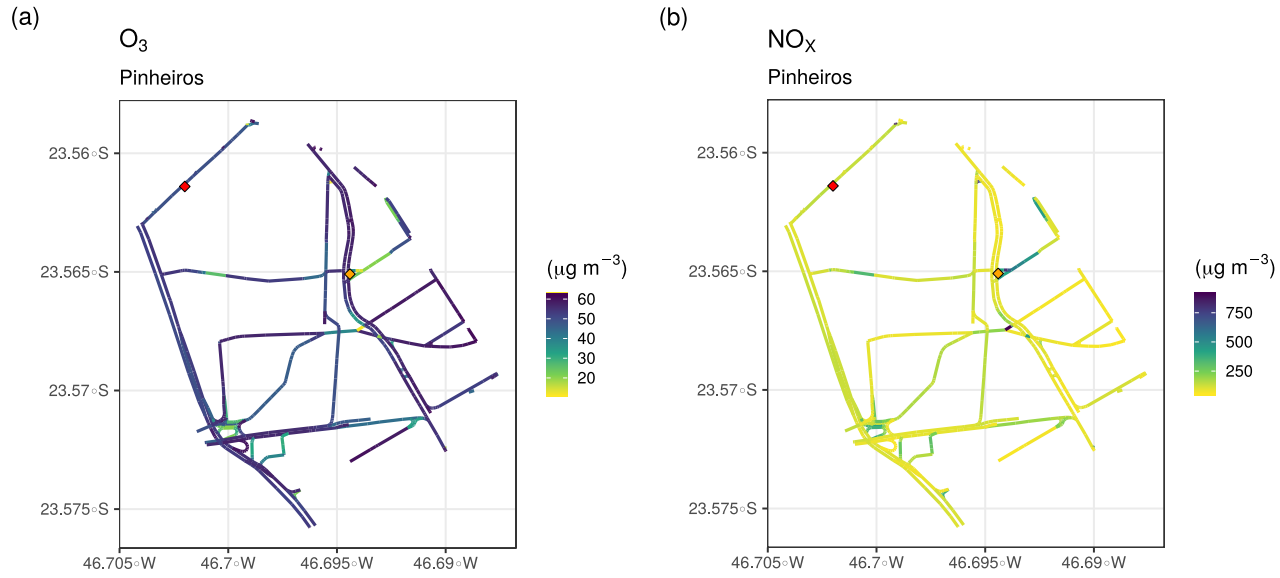

Figure 3.30: Hourly mean simulated concentration of (a) O_3 and (b) NO_X for Pinheiros neighborhood. Red diamond denotes the location of the Pinheiros AQS and orange diamond denotes traffic light location.

3.3.3 Running MUNICH using WRF-Chem D02 output

We can't use observation as background concentration when we try to build an air quality forecasting system. In Kim et al. (2018) and in Lugon et al. (2020), the background concentration came from a Polair3D CTM (described by Boutahar et al. (2004)). We decided to replicate it by using WRF-Chem simulations from domain 2, to feed MUNICH with meteorological information and background pollutants concentrations. For the background concentration, model results for Pinheiros were extracted from WRF-Chem output and we ran the MUNICH-WRF_Chem scenario using the original emissions estimated with VEIN.

Figure 3.31 and 3.32 show the results. MUNICH-WRF_Chem results for O_3 are worst than with WRF-Chem (now the background), nevertheless it improves the representation of NO and NO_2 in Pinheiros. These results suggest that background concentration highly affect MUNICH results, and in the MUNICH-Emiss scenario, the emission adjustments also compensate for the low values of NO_X background concentration from Ibirapuera station.

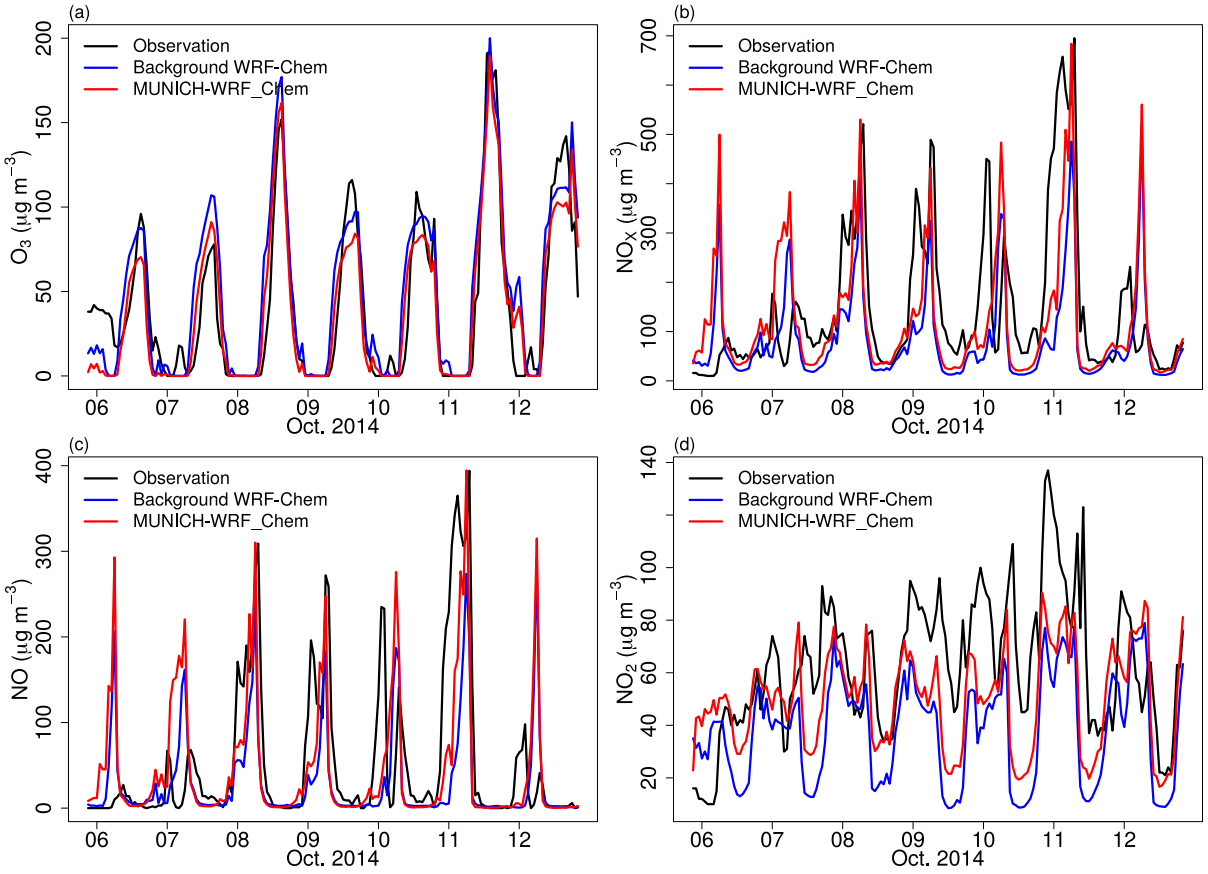

Figure 3.31: Comparison of MUNICH results against background and observation concentrations of (a) O_3 , (b) NO_X , (c) NO, and (d) NO_2 for Pinheiros urban canyon from the MUNICH-WRF_Chem simulation

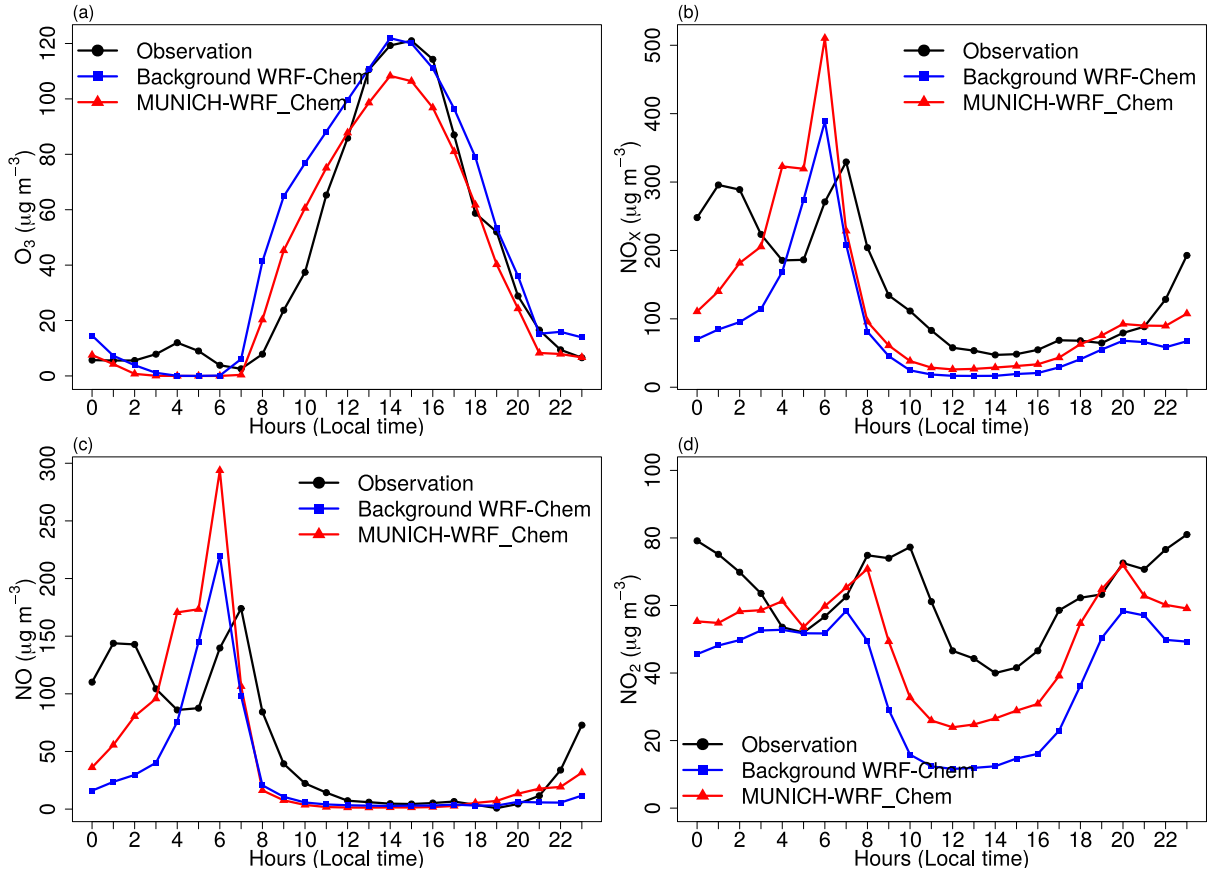

Figure 3.32: Diurnal profile of MUNICH results, background, and concentration for (a) O_3 , (b) NO_X , (c) NO, and (d) NO_2 for Pinheiros urban canyon from the MUNICH-WRF_Chem simulation

3.3.4 Discussion about MUNICH simulation results

The results showed the capacity of the MUNICH coupled with WRF-Chem to represent the concentration of the pollutants at street levels. Results showed that MUNICH simulations considering adjusted emissions can better represent the temporal variation of O_3, NO_X, NO, and NO_2 concentrations inside urban canyons. Nevertheless, the results are highly dependent on background concentrations and emission rates. This background concentration dependence is stronger for secondary pollutants such as O_3, and primary pollutants are more affected by emission rates. The reason for the significant contribution of background concentration is that MUNICH is based in SIRANE, and SIRANE also presents a significant contribution from background concentration (Soulhac et al., 2012).

The main cause of O_3 overprediction in MUNICH and MUNICH-Emiss scenarios is the high value of background O_3 concentration measured in Ibirapuera AQS. In Pinheiros neighborhood, the underprediction of NO_X concentration is caused by the underprediction of NO concentration during the second half of the week. MUNICH with the adjusted emissions fulfills the performance criteria.

O_3 concentrations simulated in Pinheiros are smaller than background concentrations, the same results are reported by Wu et al. (2020). As noted in Krecl et al. (2016), this behavior is caused by the high NO_X emissions inside the street urban canyons, which rapidly deplete the formed O_3 and the O_3 concentration over the rooftop (i.e, background concentration).

More simulations with improved emissions must be performed but the results presented here show the potential of using multi-scale simulations for describing the concentrations at the urban canopy.

Chapter 4

Summary and conclusions

"Begin at the beginning," the King said, very gravely, "and go on till you come to the end: then stop."
Lewis Carroll, Alice in Wonderland

We used CAM-Chem, WRF-Chem, and MUNICH models to study the air quality inside the Metropolitan Area of São Paulo (MASP) at a global, regional, and local scale from October 6^{th} to 14^{th}, 2014. Together they form a multi-scale air quality forecast system. CAM-Chem provides dynamic chemical boundary conditions (CBC) for WRF-Chem, and WRF-Chem provides the meteorological information and background concentration that MUNICH requires to calculate pollutant concentration inside the urban canyons.

We found that CAM-Chem is suitable to be used as CBC for WRF-Chem and can also represent secondary pollutants (i.e. O_3 and $PM_{2.5}$) at regional and diurnal scales. To run WRF-Chem, we developed a simplified method to disaggregate spatially and temporally vehicular emissions based on total emissions, road length, and activity; and we also implemented a new tool to build the WRF-Chem anthropogenic emission file. Furthermore, we performed the first simulation of O_3 and NO_X concentration inside the MASP urban canyons using the MUNICH model. Finally, we developed a set of tools to automate and perform model evaluation using all the available air quality and meteorology measurements of the São Paulo State Environmental Agency (CETESB) air quality network.

Our results showed that besides providing chemical initial and boundary conditions, CAM-Chem can simulate coherently the concentration of O_3 and $PM_{2.5}$ for the whole MASP, presenting a mean bias (MB), a Pearson coefficient (R), and index of aggreement (IOA) of 32 $\mu g\ m^{-3}$, 0.83, and 0.81 for O_3, respectively; and of -6.8 $\mu g\ m^{-3}$, 0.73, and

0.79 for $PM_{2.5}$, respectively. Contrarily, it underestimates and fails to simulate primary pollutant concentration with R lower than 0.56 and IOA lower than 0.52. Therefore, CAM-Chem can be used for feasible estimates of O_3 and $PM_{2.5}$ concentrations at 6 hour, 12 hour and daily averages at the scale of macro-regions. Also, as CAM-Chem performs better in suburban areas, it can serve as a first estimate of urban background concentrations.

In the case of WRF-Chem, both regional (ΔX = 9 km) and urban (ΔX = 3 km) simulations achieved the meteorological benchmark of performance (e.g. ± 0.5 K mean bias for temperature, ± 10% mean bias for relative humidity, and ± 1.5 ms^{-1} mean bias of wind speed) for T2, RH2, WS, and only the mean gross error (ME) benchmark for wind direction. For this reason, WRF-Chem meteorology simulation demonstrated to be suitable for air quality modeling. We focused our analysis on O_3, NO, NO_2, and CO. WRF-Chem underestimates the concentration of these pollutants, with a normalized mean bias (NMB) of -5 % for O_3 and NMB lower than -35 % for primary pollutants. Nevertheless, WRF-Chem successfully represents their diurnal variation, especially during the daylight. The underestimation can be explained by the underestimation of T2, which reduces the biogenic emission of VOC; by the overestimation of PBL height; by the overestimation of wind speed, which facilitates pollutant dispersion; and errors in the emissions estimates. WRF-Chem reproduces better pollutant concentrations inside the MASP rather than in the suburban areas, mainly due to the disaggregation strategy that favors denser roads in urban areas. Ozone concentrations are well simulated achieving goal benchmarks for R (R $>$ 0.75)and NMB (NMB $<$ ± 5%).

We used MUNICH to simulate O_3 and NO_X concentration inside Pinheiros neighborhoods urban canyons. To calibrate MUNICH input we performed two simulations using measurements from Ibirapuera air quality station (AQS) as background concentration, a WRF meteorological simulation with the finest domain with a horizontal grid resolution of 1km, and emissions inside the street links calculated by the VEIN model (Control case scenario); and the second simulation was performed by doubling VEIN emissions (MUNICH_Emiss scenario). In the control case, MUNICH overpredicts O_3 (NMB = 30%) and underpredicts NO_X (NMB = -40%) concentrations. Once emissions are calibrated by a factor of two, the concentration simulations perform better (i.e. NMB_{O_3} = 20 % and NMB_{NO_X} = -20 %), and NO_2 concentrations are better simulated (NMB $\sim$ 0%). MUNICH results are highly dependent on the provided background concentrations and they are the main

cause of O_3 overprediction and NO_X underprediction. Finally, we tested running MUNICH using the original VEIN emissions and WRF-Chem urban domain results (ΔX = 3 km) to provide meteorological input and background concentrations (MUNICH-WRF_Chem) as a part of this multi-scale modeling system. This scenario produces the best O_3 simulation (NMB = -10 %), and similar performance as the MUNICH_Emiss scenario for NO_X, confirming the strong dependence of MUNICH on the background concentration.

Figure 4.1 summarized the results of this research. Comparing global air quality output against one station seems forceful, but still it gave us an idea of how CAM-Chem simulates air pollutants in the urban area. WRF-Chem simulates reasonably well O_3, NO, and NO_2, and when using MUNICH with WRF-Chem as background concentration, even when we get an underprediction of O_3, there is an improvement in the representation of NO, NO_2, and O_3 daily average.

During the development of this work, *qualR*, *wrf_sp_eval*, and *PyChEmiss* programs were developed. *qualR* allows us to use all CETESB air quality network available information for model evaluation, while *wrf_sp_eval*, automatize the performance statistics calculations for WRF-Chem simulation over the MASP. Both have the potential to be adapted for other cities. PyChEmiss successfully built WRF-Chem emission files from local emission inventories total values and can be used in other cities. We believed that these tools can improve the air quality data analysis and modeling over MASP and they can be accessed in `https://github.com/quishqa/` .

Now that we have a set of models that can simulate pollutant concentrations even at street level, it's necessary to step further and, as noted by Kumar et al. (2018), create services. An example of these services is the translation of forecast concentration to an Air Quality Index that is better understood by the population. Another example, is to use model output to address human health impact of pollutant exposure, as the work of Gao et al. (2018), where human mortality by $PM_{2.5}$ was estimated using a one-year simulation with WRF-Chem in China and India. With this set of models, exposure can be addressed from country to street level.

In the spirit of reproducible science (Lowndes et al., 2017; Munafò et al., 2017), all the code used to make the figures and tables in this thesis, to process model input and output, and to perform other useful tasks, are freely available in the repository `https://github.com/quishqa/FromGlob2LocSP`. We also hope that these scripts become a helpful hand in

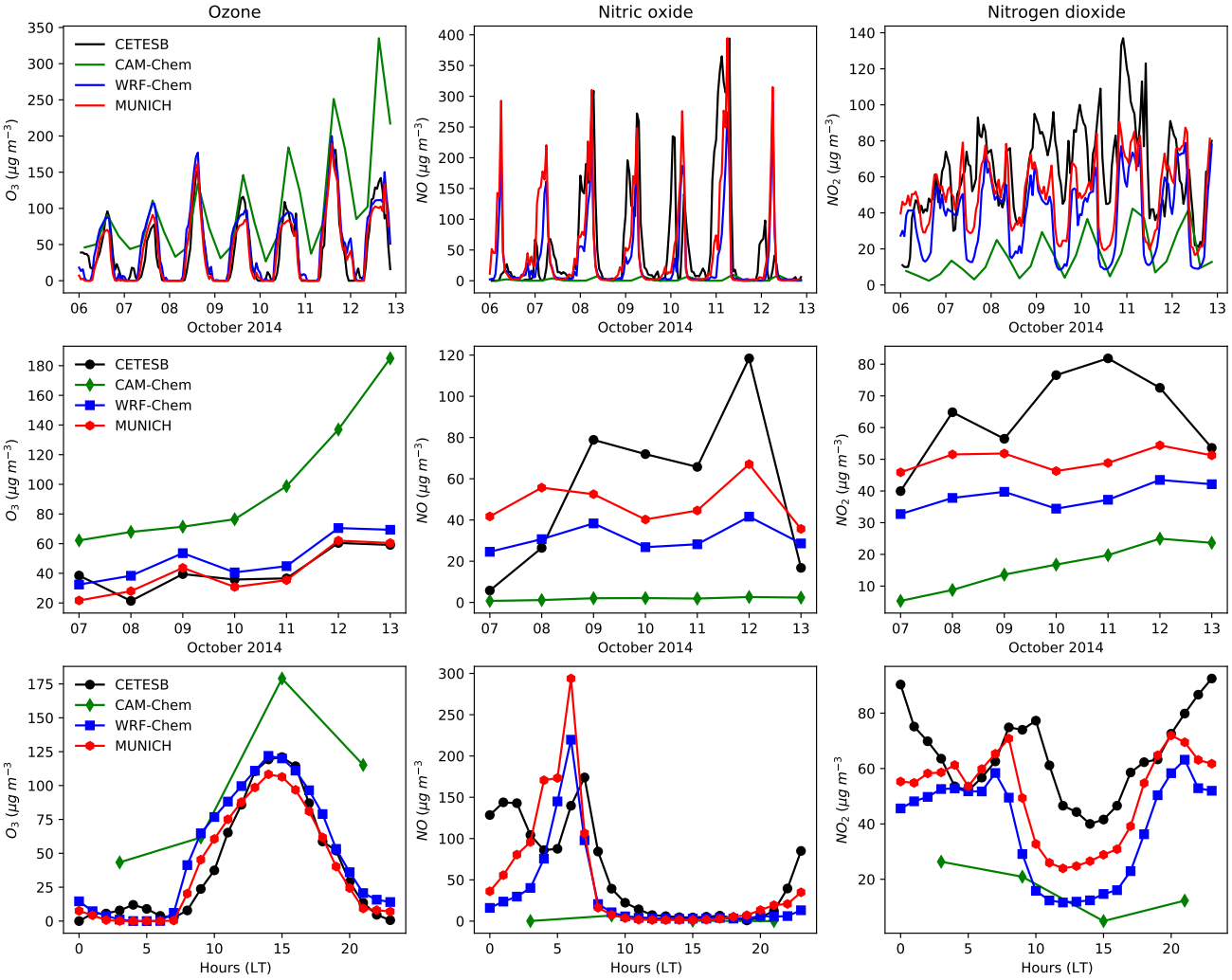

Figure 4.1: Comparison of O_3, NO, and NO_2 simulations with the models used in this research and observation from Pinheiros air quality station. Columns shows pollutants plots and rows different temporal averages (i.e. Hourly, daily averages and diurnal cycle).

the establishment of an air quality modeling system in other cities.

4.1 Future works

More efforts are needed to improve the accuracy of the simulations. We still need to achieve the normalized mean error (NME) benchmark for O_3 (NME < 25 %). Further analysis on emission inventories at different scales is needed, that is, it is necessary to try to complete local vehicular emission with newer versions of global emission inventories like EDGAR5 (Crippa et al., 2020). We believe that this can be achieved by improving the spatial disaggregation of global emission inventories, by using for example, night-light products, or a better proxy, to spatial disaggregate domestic emission. As a matter of fact, emission factors estimated based on measurements in real conditions, like ambient air and tunnels, have shown that there is an underprediction of the emissions by the vehicles in official inventories

It is important to enhance the description of the land/use cover data, as it impacts the meteorological variables prediction, which will also impact the pollutant predictions. Based on Pellegatti Franco et al. (2019), we could increase the WUDAPT area description for a regional domain that covers the Sâo Paulo state, this could improve wind representation in the suburban areas. Further, WUDAPT building height can be upgraded by using in-situ measurement or by using the new capabilities that Google Earth offers.

There is the need to automate the coupling between these models, at least in a one-way approach. This implies trying to run the models with the same or similar chemical mechanism and to assess the impact of mapping species in different chemical mechanisms. On the other hand, there is also the possibility to couple MUNICH to WRF-Chem, to build a street-in-grid model like SinG.

Finally, we need to upgrade our model evaluation protocol to include satellite information, evaluate other meteorological parameters (i.e. solar radiation and precipitation), and summarize model performance statistics in plots like soccer or Taylor plot diagrams.

Chapter 5

Other lessons learned

But if it is true that the act of observing changes the thing which is observed (because of Quantum), it's even more true that it changes the observer.

Terry Pratchett, Soul Music

This part was written for those few who totally read the thesis and for those students who only read the abstract and the conclusions (Surprise! There is one more chapter). Well, I've been working with air quality models since my undergrad education, I started with AERMOD (the one version with a graphical interface) and now I ended up working with WRF-Chem and MUNICH models (in a bash terminal). It feels like a long way, but it also feels like the start of a journey, atmospheric sciences and numerical models are advancing really fast.

In this time, I learned how to run those models, their basic equations, and numerical approximations; but in a two-way nesting approach, models also teach me great lessons that I want to share with you, new student who only read the abstract and the conclusion of every thesis and papers.

First, models taught me to not get discouraged by errors. When running a model, errors will appear since the installation, and they'll continue to appear until the post-processing. Don't get frustrated, even when society curse errors, they are actually great teachers, but that doesn't mean to get stuck in the error, the idea is to make new errors until you get the 'SUCCESS COMPLETE WRF' message (Please see This comic[1]). This also can be applied in life.

[1] In: `https://twitter.com/nathanwpyle/status/1176860147223867393`

Now, you face the very famous expectation versus reality situation, and you will experience that *reality always beats fiction*. I still remember the first time I ran WRF, only the meteorology part, I was expecting to solve the weather forecast of Lima city, I was wrong. Once you have installed the model, the trial and error starts, testing is basic, test parameterizations schemes, grid spatial resolutions, etc. Then, armed with your performance statistics, you'll be getting closer to reality.

The last point brings me to the following: models teach you humility: Even when we are getting closer, when you got a calibrated and tested model, reality beats models again. But this is good, there is always something to learn and keep improving. As Professor Guy Brasseur once told "The history of the science is the history of failed models[2]."

WRF-Chem and MUNICH are open-source, they run in Linux. So, working with these models bring me the opportunity to learn many open-source resources as bash shell and programming language. Learn a programming language, it will help you to automatize many repetitive processes and to deal with the processing of huge amounts of data, so you'll have more time for your result analyses. In the spirit of open-source, you'll realize that science is a cooperative activity, so don't be afraid to ask for help and to share your code and results.

Last but not least, it's important not only to focus on the modeler world, as noted by Wainwright and Mulligan (2013), if you got the opportunity to participate in field campaigns, far from the computer, go for it. You'll get a lot of practical knowledge that will be useful when analyzing model input and model results. Also, this applies the other way around, non-modellers also need to get involved in models.

I almost forgot, *the devil is in the details*. I learned that the hard way, and here I'm talking, with a great emphasis, about units. Always double-check your calculations. Background concentrations and emissions are ingested with particular units depending on the model. So, always verify the correct units and make the transformation with care (and love too). Obviously, those errors are easier to spot when you got experience in the field dealing with pollutant measurements.

In summary, in addition to learning about how the world works, models can teach you, the hard way, to be patient, to be humble, to cooperate, and much more. I'm also grateful for that. Now, go and compile WRF.

[2] In: `https://ams.confex.com/ams/2020Annual/meetingapp.cgi/Paper/364222`

Bibliography

Albuquerque T. T., Andrade M. D. F., Ynoue R. Y., Moreira D. M., Andreão W. L., Soares F., WRF-SMOKE-CMAQ modeling system for air quality evaluation in São Paulo megacity with a 2008 experimental campaign data, Environmental Science and Pollution Research, 2018, vol. 25, p. 36555

Albuquerque T. T., West J., de F. Andrade M., Ynoue R. Y., Andreão W. L., dos Santos F. S., Maciel F. M., Pedruzzi R., de O. Mateus V., Martins J. A., Martins L. D., Nascimento E. G. S., Moreira D. M., Analysis of PM2.5 concentrations under pollutant emission control strategies in the metropolitan area of São Paulo, Brazil, Environmental Science and Pollution Research, 2019, vol. 26, p. 33216

Andrade M. d. F., Kumar P., de Freitas E. D., Ynoue R. Y., Martins J., Martins L. D., Nogueira T., Perez-Martinez P., de Miranda R. M., Albuquerque T., Gonçalves F. L. T., Oyama B., Zhang Y., Air quality in the megacity of São Paulo: Evolution over the last 30 years and future perspectives, Atmospheric Environment, 2017, vol. 159, p. 66

Andrade M. d. F., Ynoue R. Y., Freitas E. D., Todesco E., Vara Vela A., Ibarra S., Martins L. D., Martins J. A., Carvalho V. S. B., Air quality forecasting system for Southeastern Brazil, Frontiers in Environmental Science, 2015, vol. 3, p. 1

Baklanov A., Molina L. T., Gauss M., Megacities, air quality and climate, Atmospheric Environment, 2016, vol. 126, p. 235

Baklanov A., Schlünzen K., Suppan P., Baldasano J., Brunner D., Aksoyoglu S., Carmichael G., Douros J., Flemming J., Forkel R., Galmarini S., Gauss M., Grell G., Hirtl M., Joffre S., Jorba O., Kaas E., Kaasik M., Kallos G., Kong X., Korsholm U., Kur-

ganskiy A., Online coupled regional meteorology chemistry models in Europe: current status and prospects, Atmospheric Chemistry and Physics, 2014, vol. 14, p. 317

Barnard J. C., Chapman E. G., Fast J. D., Schmelzer J. R., Slusser J. R., Shetter R. E., An evaluation of the FAST-J photolysis algorithm for predicting nitrogen dioxide photolysis rates under clear and cloudy sky conditions, Atmospheric Environment, 2004, vol. 38, p. 3393

Boutahar J., Lacour S., Mallet V., Quelo D., Roustan Y., Sportisse B., Development and validation of a fully modular platform for numerical modelling of air pollution: POLAIR, International Journal of Environment and Pollution, 2004, vol. 22, p. 17

Boylan P., Helmig D., Oltmans S., Ozone in the Atlantic Ocean marine boundary layer, Elem Sci Anth, 2015, vol. 3, p. 1

Brasseur G. P., Jacob D. J., Modeling of Atmospheric Chemistry. Cambridge University Press Cambridge, 2017, 606

Briber B., Hutyra L., Dunn A., Raciti S., Munger J., Variations in Atmospheric CO2 Mixing Ratios across a Boston, MA Urban to Rural Gradient, Land, 2013, vol. 2, p. 304

Buchholz R. R., Emmons L. K., Tilmes S., Team T. C. D., , 2019 CESM2.1/CAM-chem Instantaneous Output for Boundary Conditions `https://doi.org/10.5065/NMP7-EP60.`

Carpentieri M., Salizzoni P., Robins A., Soulhac L., Evaluation of a neighbourhood scale, street network dispersion model through comparison with wind tunnel data, Environmental Modelling and Software, 2012, vol. 37, p. 110

Carslaw D. C., Ropkins K., openair — An R package for air quality data analysis, Environmental Modelling & Software, 2012, vol. 27-28, p. 52

Carvalho D., Rocha A., Gómez-Gesteira M., Santos C., A sensitivity study of the WRF model in wind simulation for an area of high wind energy, Environmental Modelling and Software, 2012, vol. 33, p. 23

Carvalho V. S. B., Freitas E. D., Martins L. D., Martins J. A., Mazzoli C. R., Andrade M. d. F., Air quality status and trends over the Metropolitan Area of São Paulo, Brazil as

a result of emission control policies, Environmental Science & Policy, 2015, vol. 47, p. 68

CETESB, 2015 Technical report Emissões veiculares no estado de São Paulo 2014 `https://cetesb.sp.gov.br/veicular/relatorios-e-publicacoes/`. CETESB São Paulo

CETESB, 2020 Technical report Qualidade do ar no estado de São Paulo 2019 `https://cetesb.sp.gov.br/ar/publicacoes-relatorios/`. CETESB Sao Paulo

Chen F., Kusaka H., Bornstein R., Ching J., Grimmond C. S. B., Grossman-Clarke S., Loridan T., Manning K. W., Martilli A., Miao S., Sailor D., Salamanca F. P., Taha H., Tewari M., Wang X., Wyszogrodzki A. A., Zhang C., The integrated WRF/urban modelling system: development, evaluation, and applications to urban environmental problems, International Journal of Climatology, 2011, vol. 31, p. 273

Ching J., Mills G., Bechtel B., See L., Feddema J., Wang X., Ren C., Brousse O., Martilli A., Neophytou M., Mouzourides P., Stewart I., Hanna A., Ng E., Foley M., Alexander P., Aliaga D., Niyogi D., Shreevastava A., Bhalachandran P., Masson V., Hidalgo J., Fung J., Andrade M., WUDAPT: An Urban Weather, Climate, and Environmental Modeling Infrastructure for the Anthropocene, Bulletin of the American Meteorological Society, 2018, vol. 99, p. 1907

Crippa M., Solazzo E., Huang G., Guizzardi D., Koffi E., Muntean M., Schieberle C., Friedrich R., Janssens-Maenhout G., High resolution temporal profiles in the Emissions Database for Global Atmospheric Research, Scientific Data, 2020, vol. 7, p. 121

Darmenov A. S., Silva A., The Quick Fire Emissions Dataset (QFED): Documentation of versions 2.1, 2.2 and 2.4, NASA Technical Report Series on Global Modeling and Data Assimilation, NASA/TM-2015-104606, Technical Report Series on Global Modeling and Data Assimilation, 2015, vol. 38

Dasu T., Johnson T., Exploratory Data Mining and Data Cleaning 1 edn. John Wiley & Sons, Inc, 2003, 203

De Freitas E. D., Martins L. D., Da Silva Dias P. L., De Fátima Andrade M., A simple photochemical module implemented in RAMS for tropospheric ozone concentration forecast

in the metropolitan area of São Paulo, Brazil: Coupling and validation, Atmospheric Environment, 2005, vol. 39, p. 6352

Dominutti P. A., Nogueira T., Borbon A., Andrade M. d. F., Fornaro A., One-year of NMHCs hourly observations in São Paulo megacity: meteorological and traffic emissions effects in a large ethanol burning context, Atmospheric Environment, 2016, vol. 142, p. 371

Emery C., Liu Z., Russell A. G., Odman M. T., Yarwood G., Kumar N., Recommendations on statistics and benchmarks to assess photochemical model performance, Journal of the Air and Waste Management Association, 2017, vol. 67, p. 582

Emery C., Tai E., Yarwood G., , 2001 Technical report Enhanced meteorological modeling and performance evaluation for two Texas ozone episodes. ENVIRON International Corporation

Emmons L. K., Schwantes R. H., Orlando J. J., Tyndall G., Kinnison D., Lamarque J. F., Marsh D., Mills M. J., Tilmes S., Bardeen C., Buchholz R. R., Conley A., Gettelman A., Garcia R., Simpson I., Blake D. R., Meinardi S., Pétron G., The Chemistry Mechanism in the Community Earth System Model Version 2 (CESM2), Journal of Advances in Modeling Earth Systems, 2020, vol. 12, p. 1

Emmons L. K., Walters S., Hess P. G., Lamarque J.-F., Pfister G. G., Fillmore D., Granier C., Guenther A., Kinnison D., Laepple T., Orlando J., Tie X., Tyndall G., Wiedinmyer C., Baughcum S. L., Kloster S., Description and evaluation of the Model for Ozone and Related chemical Tracers, version 4 (MOZART-4), Geoscientific Model Development Discussions, 2009, vol. 2, p. 1157

Gao M., Beig G., Song S., Zhang H., Hu J., Ying Q., Nielsen C. P., Mcelroy M. B., The impact of power generation emissions on ambient PM 2 . 5 pollution and human health in China and India, Environment International, 2018, vol. 121, p. 250

Gavidia-Calderón M., Ibarra-espinosa S., Kim Y., Zhang Y., Andrade M. D. F., Sciences A., Paulo S., Engieneering E., Simulation of O 3 and NO X in Sao Paulo street urban canyons with, Geoscientific Model Development Discussions, 2020, pp 1–32

Gavidia-Calderón M., Vara-Vela A., Crespo N. M., Andrade M. F., Impact of time-dependent chemical boundary conditions on tropospheric ozone simulation with WRF-Chem: An experiment over the Metropolitan Area of São Paulo, Atmospheric Environment, 2018, vol. 195, p. 112

Grell G. A., Peckham S. E., Schmitz R., McKeen S. A., Frost G., Skamarock W. C., Eder B., Fully coupled "online" chemistry within the WRF model, Atmospheric Environment, 2005, vol. 39, p. 6957

Guenther A., Karl T., Harley P., Wiedinmyer C., Palmer P. I., Geron C., Estimates of global terrestrial isoprene emissions using MEGAN (Model of Emissions of Gases and Aerosols from Nature), Atmospheric Chemistry and Physics, 2006, vol. 6, p. 3181

Guenther A. B., Jiang X., Heald C. L., Sakulyanontvittaya T., Duhl T., Emmons L. K., Wang X., The model of emissions of gases and aerosols from nature version 2.1 (MEGAN2.1): An extended and updated framework for modeling biogenic emissions, Geoscientific Model Development, 2012, vol. 5, p. 1471

Hanna S., Chang J., , 2012 Acceptance criteria for urban dispersion model evaluation

Harris C. R., Millman K. J., van der Walt S. J., Gommers R., Virtanen P., Cournapeau D., Wieser E., Taylor J., Berg S., Smith N. J., Kern R., Picus M., Hoyer S., van Kerkwijk M. H., Brett M., Haldane A., del R'ıo J. F., Wiebe M., Peterson P., Oliphant T. E., Array programming with NumPy, Nature, 2020, vol. 585, p. 357

Harrison R. M., Urban atmospheric chemistry: a very special case for study, npj Climate and Atmospheric Science, 2018, vol. 1, p. 1

Hoesly R. M., Smith S. J., Feng L., Klimont Z., Janssens-Maenhout G., Pitkanen T., Seibert J. J., Vu L., Andres R. J., Bolt R. M., Bond T. C., Dawidowski L., Kholod N., Kurokawa J.-i., Li M., Liu L., Lu Z., Moura M. C. P., O'Rourke P. R., Zhang Q., Historical (1750–2014) anthropogenic emissions of reactive gases and aerosols from the Community Emissions Data System (CEDS), Geoscientific Model Development, 2018, vol. 11, p. 369

Hong S.-Y., Noh Y., Dudhia J., A New Vertical Diffusion Package with an Explicit Treatment of Entrainment Processes, Monthly Weather Review, 2006, vol. 134, p. 2318

Hoshyaripour G., Brasseur G., Andrade M. F., Gavidia-Calderón M., Bouarar I., Ynoue R. Y., Prediction of ground-level ozone concentration in São Paulo, Brazil: Deterministic versus statistic models, Atmospheric Environment, 2016, vol. 145, p. 365

Hoyer S., Hamman J. J., xarray: N-D labeled Arrays and Datasets in Python, Journal of Open Research Software, 2017, vol. 5, p. 1

Iacono M. J., Delamere J. S., Mlawer E. J., Shephard M. W., Clough S. A., Collins W. D., Radiative forcing by long-lived greenhouse gases: Calculations with the AER radiative transfer models, Journal of Geophysical Research Atmospheres, 2008, vol. 113, p. 2

Ibarra-Espinosa S., Ynoue R., Giannotti M., Ropkins K., de Freitas E. D., Generating traffic flow and speed regional model data using internet GPS vehicle records, MethodsX, 2019, vol. 6, p. 2065

Ibarra-Espinosa S., Ynoue R., O'Sullivan S., Pebesma E., Andrade M. D. F., Osses M., VEIN v0.2.2: an R package for bottom–up vehicular emissions inventories, Geoscientific Model Development, 2018, vol. 11, p. 2209

Ibarra-Espinosa S., Ynoue R. Y., Ropkins K., Zhang X., de Freitas E. D., High spatial and temporal resolution vehicular emissions in south-east Brazil with traffic data from real-time GPS and travel demand models, Atmospheric Environment, 2020, vol. 222, p. 117136

Ibarra-Espinosa S., Zhang X., Xiu A., Gao C., Wang S., Ba Q., Gao C., Chen W., A comprehensive spatial and temporal vehicular emissions for northeast China, Atmospheric Environment, 2021, vol. 244, p. 117952

Instituto Brasileiro de Geografia e Estatistica, 2019 Estimativa da população residente no Brasil. Diretoria de Pesquisas-DPE `https://www.ibge.gov.br/pt/inicio.html`

Jacobson M. Z., Fundamentals of Atmospheric Modeling 2 edn. Cambridge University Press, 2005

Kaduwela A., Luecken D., Carter W., Derwent R., New directions: Atmospheric chemical mechanisms for the future, Atmospheric Environment, 2015, vol. 122, p. 609

Kim Y., Wu Y., Seigneur C., Roustan Y., Multi-scale modeling of urban air pollution : development and application of a Street-in-Grid model by coupling MUNICH and, Geoscientific Model Development, 2018, pp 1–24

Krecl P., Targino A. C., Wiese L., Ketzel M., de Paula Corrêa M., Screening of short-lived climate pollutants in a street canyon in a mid-sized city in Brazil, Atmospheric Pollution Research, 2016, vol. 7, p. 1022

Kumar R., Peuch V. H., Crawford J. H., Brasseur G., Five steps to improve air-quality forecasts, Nature, 2018, vol. 561, p. 27

Lelieveld J., van Aardenne J., Fischer H., de Reus M., Williams J., P. W., Increasing Ozone over the Atlantic Ocean, Science, 2004, vol. 304, p. 1483

Liao J., Wang T., Wang X., Xie M., Jiang Z., Huang X., Zhu J., Impacts of different urban canopy schemes in WRF/Chem on regional climate and air quality in Yangtze River Delta, China, Atmospheric Research, 2014, vol. 145-146, p. 226

Lin J. W. B., Why python is the next wave in earth sciences computing, Bulletin of the American Meteorological Society, 2012, vol. 93, p. 1823

Lowndes J. S., Best B. D., Scarborough C., Afflerbach J. C., Frazier M. R., O'Hara C. C., Jiang N., Halpern B. S., Our path to better science in less time using open data science tools, Nature Ecology and Evolution, 2017, vol. 1

Lugon L., Sartelet K., Kim Y., Vigneron J., Chrétien O., Nonstationary modeling of NO2, NO and NO in Paris using the Street-in-Grid model: coupling local and regional scales with a two-way dynamic approach, Atmospheric Chemistry and Physics, 2020, vol. 20, p. 7717

McNider R. T., Pour-Biazar A., Meteorological modeling relevant to mesoscale and regional air quality applications: a review, Journal of the Air and Waste Management Association, 2020, vol. 70, p. 2

McRae G. J., Goodin W. R., Seinfeld J. H., Development of a second-generation mathematical model for Urban air pollution-I. Model formulation, Atmospheric Environment (1967), 1982, vol. 16, p. 679

Martins L. D., Andrade M. D. F., Ozone formation potentials of volatile organic compounds and ozone sensitivity to their emission in the megacity of São Paulo, Brazil, Water, Air, and Soil Pollution, 2008, vol. 195, p. 201

Misenis C., Zhang Y., An examination of sensitivity of WRF/Chem predictions to physical parameterizations, horizontal grid spacing, and nesting options, Atmospheric Research, 2010, vol. 97, p. 315

Monk K., Guérette E.-A., Paton-Walsh C., Silver J. D., Emmerson K. M., Utembe S. R., Zhang Y., Griffiths A. D., Chang L. T.-C., Duc H. N., Trieu T., Scorgie Y., Cope M. E., Evaluation of Regional Air Quality Models over Sydney and Australia: Part 1—Meteorological Model Comparison, Atmosphere, 2019, vol. 10, p. 374

Monks P., Granier C., Fuzzi S., Stohl A., Williams M., Akimoto H., Amann M., Baklanov A., Baltensperger U., Bey I., Blake N., Blake R., Carslaw K., Cooper O., Dentener F., Fowler D., Fragkou E., Frost G., Generoso S., Ginoux P., Grewe V., Guenther A., Hansson H., Henne S., Atmospheric composition change – global and regional air quality, Atmospheric Environment, 2009, vol. 43, p. 5268

Morrison H., Thompson G., Tatarskii V., Impact of cloud microphysics on the development of trailing stratiform precipitation in a simulated squall line: Comparison of one- and two-moment schemes, Monthly Weather Review, 2009, vol. 137, p. 991

Munafò M. R., Nosek B. A., Bishop D. V., Button K. S., Chambers C. D., Percie Du Sert N., Simonsohn U., Wagenmakers E. J., Ware J. J., Ioannidis J. P., A manifesto for reproducible science, Nature Human Behaviour, 2017, vol. 1, p. 1

Oke T. R., Mills G., Christen A., Voogt J. A., Urban Climates. Cambridge University Press Cambridge, 2017

Peckham S., WRF/Chem Version 3.9.1.1 User's Guide. National Oceanic and Atmospheric Administration [National Center for Atmospheric Research], 2018

Pellegatti Franco D. M., Andrade M. d. F., Ynoue R. Y., Ching J., Effect of Local Climate Zone (LCZ) classification on ozone chemical transport model simulations in Sao Paulo, Brazil, Urban Climate, 2019, vol. 27, p. 293

Pérez-Martínez P. J., de Fátima Andrade M., de Miranda R. M., Traffic-related air quality trends in São Paulo, Brazil, Journal of Geophysical Research: Atmospheres, 2015, vol. 120, p. 6290

Pielke R. A., Mesoscale Meteorological Modeling third edn. Academic Press, 2013

Pulles T., Heslinga D., The Art of Emission Inventorying. TNO-Environment and Geosciences, 2007

R Core Team, 2020 R: A Language and Environment for Statistical Computing. R Foundation for Statistical Computing Vienna, Austria

Rao S. T., Luo H., Astitha M., Hogrefe C., Garcia V., Mathur R., On the limit to the accuracy of regional-scale air quality models, Atmospheric Chemistry and Physics, 2020, vol. 20, p. 1627

Rao S. T., Porter P. S., Mobley J. D., Hurley F., Understanding the spatio-temporal: Variability in air pollution concentrations, EM: Air and Waste Management Association's Magazine for Environmental Managers, 2011, pp 42–48

Reboredo B., Arasa R., Codina B., Evaluating Sensitivity to Different Options and Parameterizations of a Coupled Air Quality Modelling System over Bogotá, Colombia. Part I: WRF Model Configuration, Open Journal of Air Pollution, 2015, vol. 04, p. 47

Riojas-Rodríguez H., Da Silva A. S., Texcalac-Sangrador J. L., Moreno-Banda G. L., Air pollution management and control in Latin America and the Caribbean: Implications for climate change, Revista Panamericana de Salud Publica/Pan American Journal of Public Health, 2016, vol. 40, p. 150

Ropkins K., Beebe J., Li H., Daham B., Tate J., Bell M., Andrews G., Real-World Vehicle Exhaust Emissions Monitoring: Review and Critical Discussion, Critical Reviews in Environmental Science and Technology, 2009, vol. 39, p. 79

Sánchez-Ccoyllo O. R., Ynoue R. Y., Martins L. D., de Fátima Andrade M., Impacts of ozone precursor limitation and meteorological variables on ozone concentration in São Paulo, Brazil, Atmospheric Environment, 2006, vol. 40, p. 552

Scovronick N., França D., Alonso M., Almeida C., Longo K., Freitas S., Rudorff B., Wilkinson P., Air Quality and Health Impacts of Future Ethanol Production and Use in São Paulo State, Brazil, International Journal of Environmental Research and Public Health, 2016, vol. 13, p. 695

Seigneur C., Air pollution: Current challenges and future opportunities, AIChE Journal, 2005, vol. 51, p. 356

Seigneur C., Dennis R., , 2011 in Hidy G. M., Brook J. R., Demerjian K. L., Molina L. T., Pennell W. T., Scheffe R. D., eds, , Technical Challenges of Multipollutant Air Quality Management. Springer Science+Business Media B.V Chapt. 9 pp 299–337

Seinfeld J. H., Air pollution: A half century of progress, AIChE Journal, 2004, vol. 50, p. 1096

Seinfeld J. H., Pandis S. N., Atmospheric Chemistry and Physics: From Air Pollution to Climate Change 3 edn. John Wiley & Sons, 2016, 1152

Simon H., Baker K. R., Phillips S., Compilation and interpretation of photochemical model performance statistics published between 2006 and 2012, Atmospheric Environment, 2012, vol. 61, p. 124

Skamarock W., Klemp J., Dudhia J., Gill D., Zhiquan L., Berner J., Wang W., Powers J., Duda M. G., Barker D. M., Huang X.-Y., A Description of the Advanced Research WRF Model Version 4, NCAR Technical Note NCAR/TN-475+STR, 2019, p. 145

Soulhac L., Salizzoni P., Cierco F. X., Perkins R., The model SIRANE for atmospheric urban pollutant dispersion; part I, presentation of the model, Atmospheric Environment, 2011, vol. 45, p. 7379

Soulhac L., Salizzoni P., Mejean P., Didier D., Rios I., The model SIRANE for atmospheric urban pollutant dispersion; PART II, validation of the model on a real case study, Atmospheric Environment, 2012, vol. 49, p. 320

Spiegelhalter D., The Art of Statistics: Learning from Data. Penguin Books Limited, 2019

Stewart I. D., Oke T. R., Local climate zones for urban temperature studies, Bulletin of the American Meteorological Society, 2012, vol. 93, p. 1879

Tang Y., Carmichael G. R., Thongboonchoo N., Chai T., Horowitz L. W., Pierce R. B., Al-Saadi J. A., Pfister G., Vukovich J. M., Avery M. A., Sachse G. W., Ryerson T. B., Holloway J. S., Atlas E. L., Flocke F. M., Weber R. J., Huey L. G., Dibb J. E., Streets D. G., Brune W. H., Influence of lateral and top boundary conditions on regional air quality prediction: A multiscale study coupling regional and global chemical transport models, Journal of Geophysical Research Atmospheres, 2007, vol. 112, p. 1

Tewari M., Chen F., Wang W., Dudhia J., LeMone M. A., Mitchell K., Ek M., Gayno G., Wegiel J., Cuenca R. H., Implementation and verification of the unified NOAH land surface model in the WRF model. In 20th Conference on weather analysis and forecasting/16th conference on numerical weather prediction , 2004, p. 11

Tie X., Brasseur G., Ying Z., Impact of model resolution on chemical ozone formation in Mexico City: Application of the WRF-Chem model, Atmospheric Chemistry and Physics, 2010, vol. 10, p. 8983

United Nations The World 's Cities in 2018. , 2018, 34

Vallero D., Fundamentals of Air Pollution 5 edn. Academic Press, 2014, 996

Vara-Vela A., Andrade M. F., Kumar P., Ynoue R. Y., Muñoz A. G., Impact of vehicular emissions on the formation of fine particles in the Sao Paulo Metropolitan Area: A numerical study with the WRF-Chem model, Atmospheric Chemistry and Physics, 2016, vol. 16, p. 777

Vara-Vela A., de Fátima Andrade M., Zhang Y., Kumar P., Ynoue R. Y., Souto-Oliveira C. E., da Silva Lopes F. J., Landulfo E., Modeling of Atmospheric Aerosol Properties in the São Paulo Metropolitan Area: Impact of Biomass Burning, Journal of Geophysical Research: Atmospheres, 2018, vol. 123, p. 9935

Vara-Vela A., Muñoz A., Lomas A., González C. M., Gavidia-Calderon M., Andrade M. d. F., The Another Assimilation System for WRF-Chem (AAS4WRF): a new mass-conserving emissions pre-processor for WRF-Chem regional modelling. In Conference: 2017 AGU Fall Meeting , 2017

Vardoulakis S., Fisher B. E., Pericleous K., Gonzalez-Flesca N., Modelling air quality in street canyons: A review, Atmospheric Environment, 2003, vol. 37, p. 155

Wainwright J., Mulligan M., eds, Environmental Modelling: Finding Simplicity in Complexity 2 edn. Wiley, 2013, 494

Warner T. T., Numerical Weather and Climate Prediction first edn. Cambridge University Press Cambridge, 2010

Wes McKinney Data Structures for Statistical Computing in Python. In Proceedings of the 9th Python in Science Conference , 2010, p. 56

Williams J., Keßel S. U., Nölscher A. C., Yang Y., Lee Y., Yáñez-Serrano A. M., Wolff S., Kesselmeier J., Klüpfel T., Lelieveld J., Shao M., Opposite OH reactivity and ozone cycles in the Amazon rainforest and megacity Beijing: Subversion of biospheric oxidant control by anthropogenic emissions, Atmospheric Environment, 2016, vol. 125, p. 112

Wu L., Chang M., Wang X., Hang J., Zhang J., Development of a Real-time On-road emission (ROE v1.0)model for street-scale air quality modeling based on dynamic traffic big data, Geoscientific Model Development, 2020, pp 23–40

Zaveri R. A., A new lumped structure photochemical mechanism for large-scale applications, Journal of Geophysical Research Atmospheres, 1999, vol. 104, p. 30387

Zhang Y., Online-coupled meteorology and chemistry models: history, current status, and outlook, Atmospheric Chemistry and Physics, 2008, vol. 8, p. 2895

Zheng Y., Alapaty K., Herwehe J. A., Del Genio A. D., Niyogi D., Improving high-resolution weather forecasts using the Weather Research and Forecasting (WRF) model with an updated Kain-Fritsch scheme, Monthly Weather Review, 2016, vol. 144, p. 833

Zhong J., Cai X. M., Bloss W. J., Coupling dynamics and chemistry in the air pollution modelling of street canyons: A review, Environmental Pollution, 2016, vol. 214, p. 690

Zhuang J., raphael dussin Jüling A., Rasp S., , 2020 JiaweiZhuang/xESMF: v0.3.0 Adding ESMF.LocStream capabilities

Appendix

Appendix A

Air pollutants concentration in Pinheiros air quality station

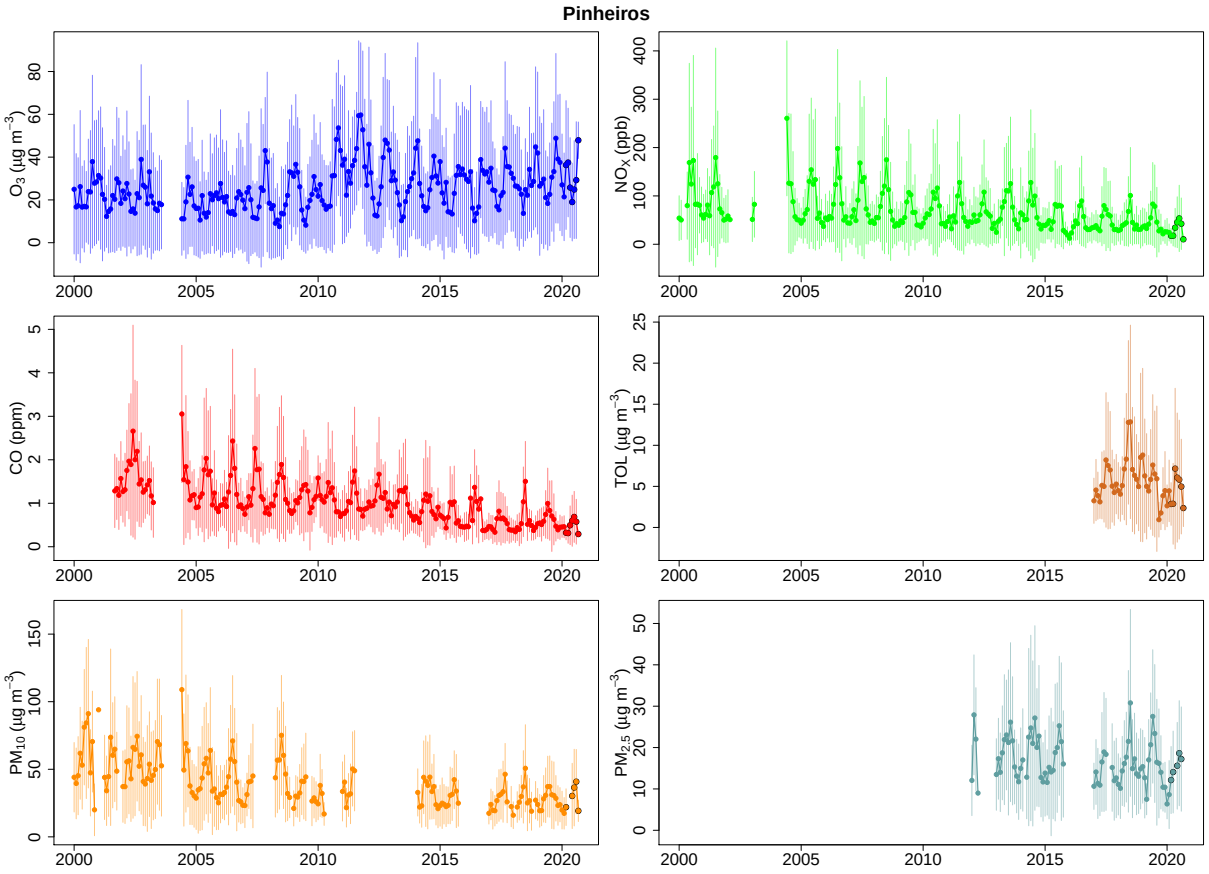

Figure A.1: Monthly variation of air pollutants in Ibirapuera air quality station.

Appendix B

Performance statistics

B.1 For pollutant concentration and meteorological parameters

Table B.1 - Model performance statistics.

Name and abbreviation	Definition	Observations
Mean bias (MB)	$\frac{1}{N}\sum_{i=1}^{N}(M_i - O_i)$	Evaluated variable units
Mean Absolute Gross Error (MAGE)	$\frac{1}{N}\sum_{i=1}^{N}\lvert M_i - O_i\rvert$	Evaluated variable units
Root mean square error (RMSE)	$\sqrt{\frac{1}{N}\sum_{i=1}^{N}(M_i - O_i)^2}$	Evaluated variable units
Normalized mean bias (NMB)	$\frac{\sum_{i=1}^{N}(M_i - O_i)}{\sum_{i=1}^{N} O_i} \times 100$	$-100\% \leq NMB \leq \infty$
Normalized mean error (NME)	$\frac{\sum_{i=1}^{N}\lvert M_i - O_i\rvert}{\sum_{i=1}^{N} O_i} \times 100$	$0\% \leq NME \leq \infty$
Correlation coefficient (R)	$\frac{\sum[(M_i - \overline{M}) \times ((O_i - \overline{O})]}{\sqrt{\sum(M_i - \overline{M})^2 \times \sum(O_i - \overline{O})^2}}$	$-1 \leq R \leq 1$

Continue next page...

Table B.1 - Continuation

Name and abbreviation	Definition	Observations
Index of agreement (IOA)	$1 - \frac{\sum((M_i - O_i)^2}{\sum(\lvert M_i - \bar{O}\rvert + \lvert O_i - \bar{O}\rvert)^2}$	$0 \leq IOA \leq 1$
Fractional mean bias (FB)	$2\overline{(O_i - M_i)}/(\bar{O} + \bar{M})$	
Normalized mean-square error (NMSE)	$\overline{(O_i - M_i)^2}/(\bar{O} \times \bar{M})$	
Fraction of prediction within a factor of two (FAC2)	$0.5 < M_i/O_i < 2$	
Normalized absolute difference (NAD)	$\overline{\lvert O_i - M_i\rvert}/(\bar{O} + \bar{M})$	

B.2 Consideration for wind direction

As suggested by Warner (2010) when doing model verification, only wind speeds with values higher than 0.5 m/s were selected in the verification process, and to consider the periodic nature of wind direction, Mean Absolute Gross Error (MAGE) and Mean Bias (MB) were calculated as indicated by Reboredo et al. (2015) and Carvalho et al. (2012) using the following equations[1]:

$$MB = \sum_{i=1}^{N} \frac{D}{N} \tag{B.1}$$

$$ME = \sum_{i=1}^{N} \frac{|D|}{N} \tag{B.2}$$

[1] M_i and O_i, are individual model simulation and its related observation, N is the number of observations

where:

if $M_i < O_i$:

$$D = \begin{cases} M_i - O_i & if|M_i - O_i| < |360 + (M_i - O_i)| \\ 360 + (M_i - O_i) & if|M_i - O_i| > |360 + (M_i - O_i)| \end{cases}$$

and if $M_i > O_i$:

$$D = \begin{cases} M_i - O_i & if|M_i - O_i| < |(M_i - O_i) - 360| \\ (M_i - O_i) - 360 & if|M_i - O_i| > |(M_i - O_i) - 360| \end{cases}$$

Appendix C

CAM-Chem north-east cell results

Table C.1 - Performance statistics for predicted pollutant concentrations against averaged CETESB measurements at CAM-Chem Cell B

	N	$\bar{O}$	$\bar{M}$	σ_O	σ_M	MB	ME	RMSE	NMB	NME	R	IOA
O_3 ($\mu g\ m^{-3}$)	28	55.30	76.63	51.48	50.79	23.66	26.70	34.60	44.66	50.39	0.87	0.88
NO ($\mu g\ m^{-3}$)	28	31.54	1.93	32.49	2.64	-24.04	24.04	32.11	-92.59	92.59	0.49	0.46
NO_2 ($\mu g\ m^{-3}$)	28	54.96	22.37	19.58	16.74	-33.99	34.21	39.81	-60.31	60.70	0.45	0.51
CO (ppm)	28	0.92	0.25	0.42	0.13	-0.68	0.68	0.76	-73.19	73.19	0.56	0.46
$PM_{2.5}$ ($\mu g\ m^{-3}$)	28	38.93	22.52	22.28	13.87	-18.66	21.27	27.49	-45.31	51.66	0.47	0.57

N : numbers of observation (O) and prediction (M); $\bar{O}$: observations mean; $\bar{M}$: prediction mean; σ_O: observation standard deviation; σ_M: prediction standard deviation; MB: mean bias; MAGE: Mean absolute gross error; RMSE: Root mean square error; NMB: Normal mean bias (%); NME: Normal mean error (%); R: Pearson correlation coefficient; IOA: index of agreement.

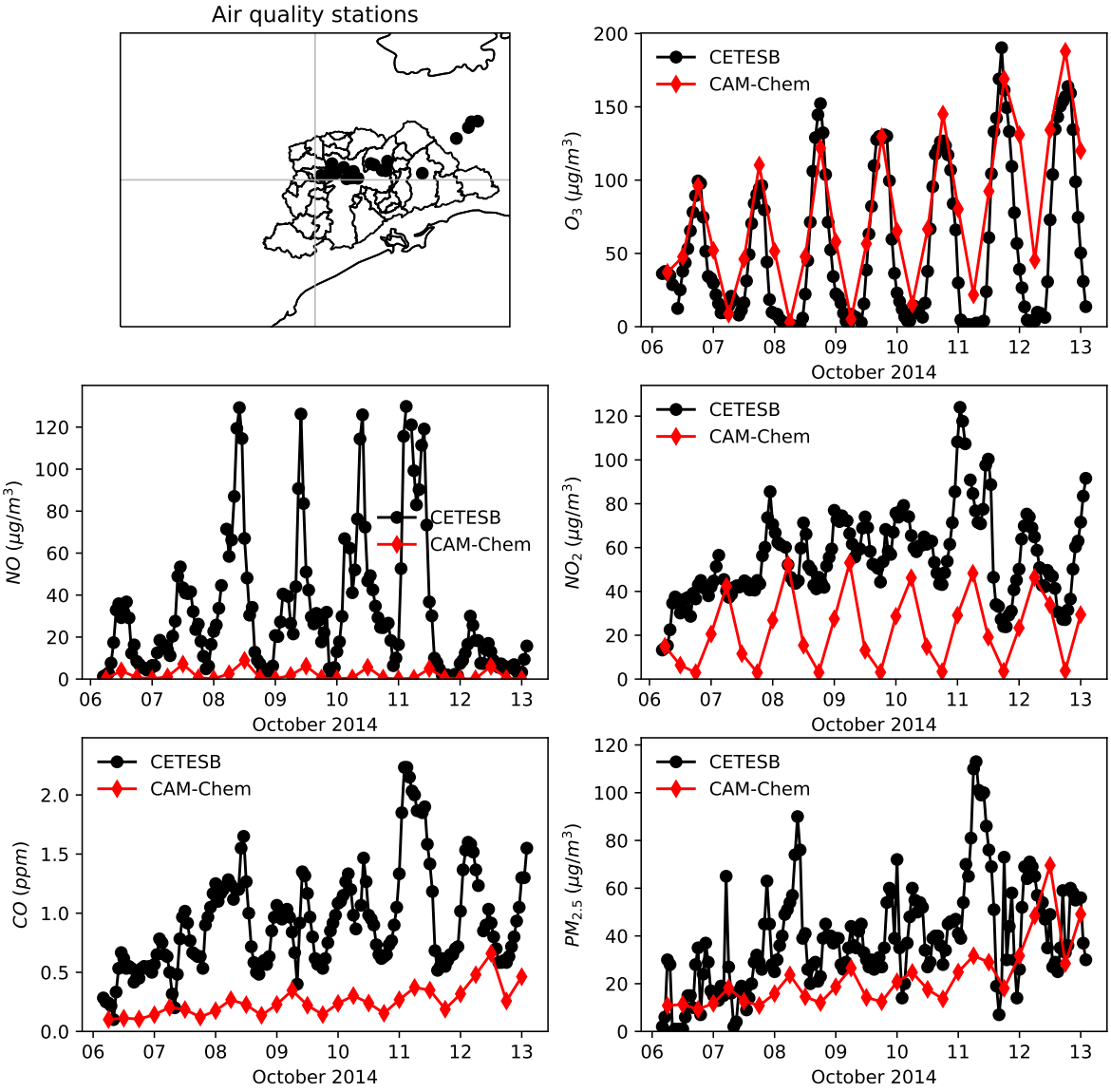

Figure C.1: Comparison between spatial average of CAM-Chem simulations in cell B and spatial average of CETESB air quality stations hourly measurements. The Top-left map shows the air quality stations used to calculate the pollutants averages in cell B.

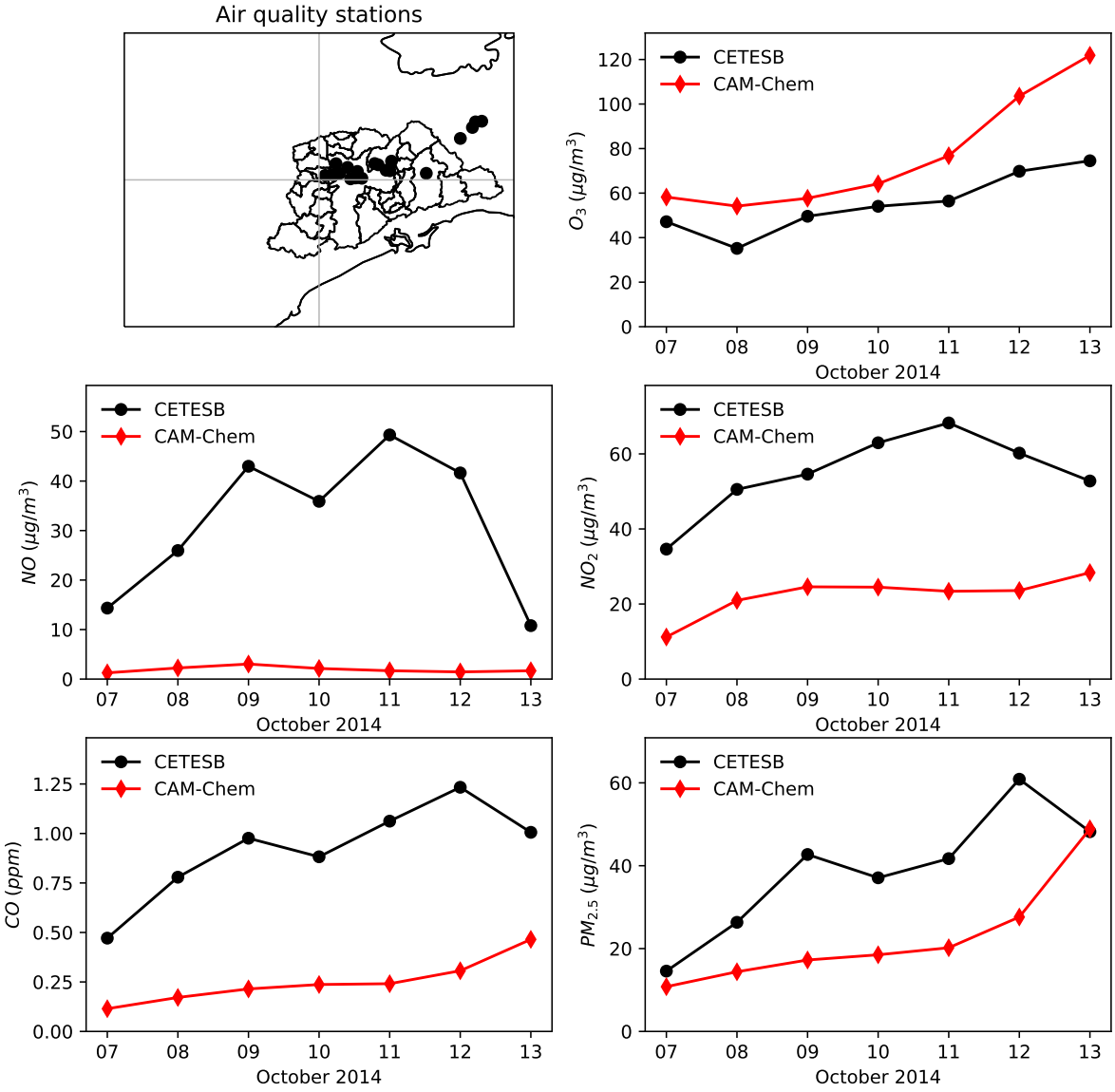

Figure C.2: Comparison between spatial average of CAM-Chem daily average simulations in cell B and spatial average of CETESB air quality daily averages. The Top-left map shows the air quality stations used to calculate the pollutants averages in cell B.

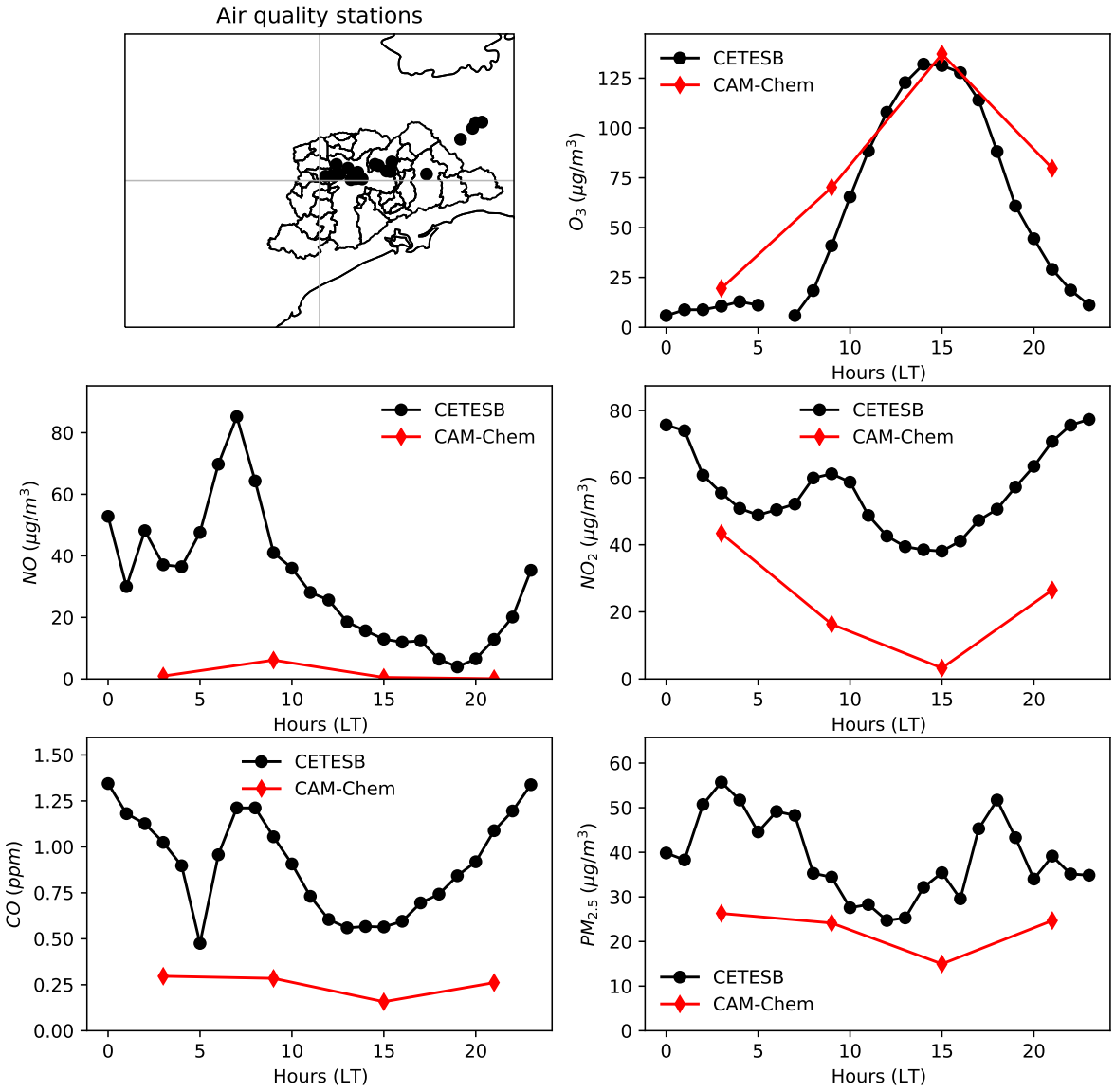

Figure C.3: Diurnal cycle of CAM-Chem results in cell B and CETESB air quality measurements. The Top-left map shows the air quality stations used to calculate the pollutants averages in cell B.

Appendix D

Difference of using CBC during daylight and nighttime

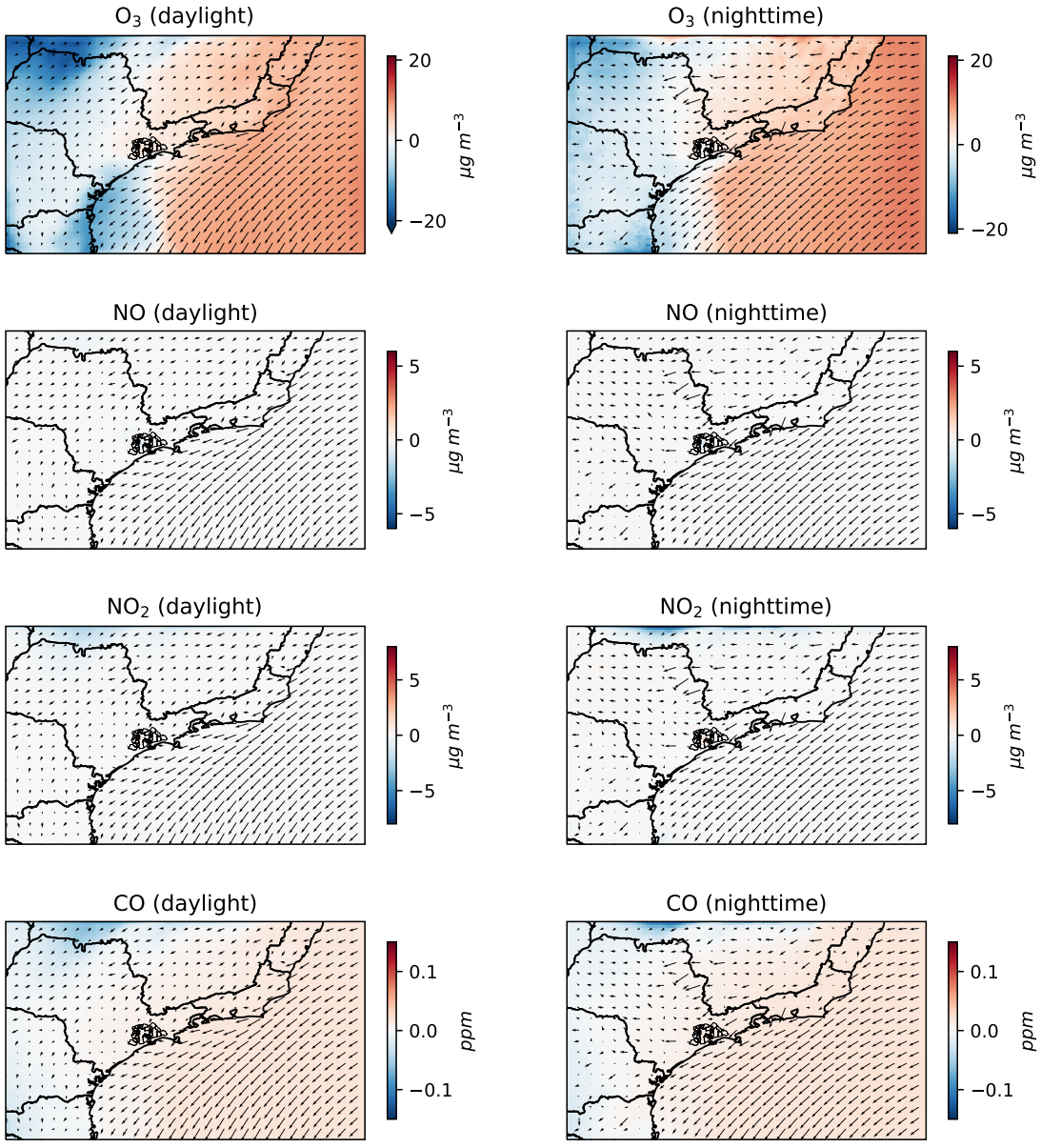

Figure D.1: Spatial difference between WRF-Chem default CBC and WRF-Chem using CAM-Chem CBC

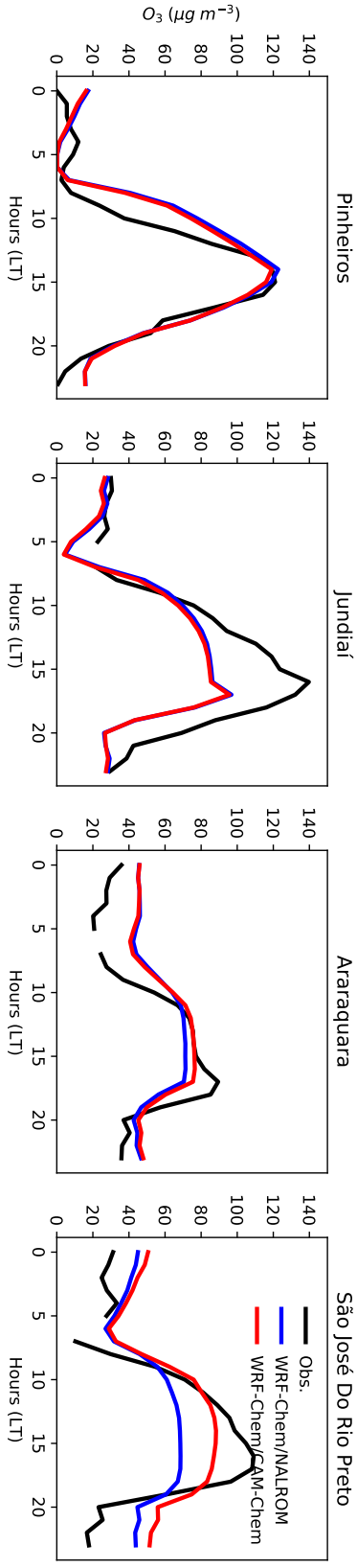

Figure D.2: Comparison between WRF-Chem default CBC and WRF-Chem using CAM-Chem CBC in ozone representation

Appendix E

Comparison between WRF-Chem regional and urban domain

Table E.1 - Statitical indicators for meteorological parameter in the regional domain using same air quality station from urban domain

	N	$\bar{O}$	$\bar{M}$	σ_O	σ_M	MB	ME	RMSE	NMB	NME	R	IOA
T2 (K)	2357	295.72	295.07	5.93	5.57	-0.32	1.67	2.08	-0.11	0.57	0.94	0.97
RH2 (%)	2303	59.09	54.79	22.61	20.38	-2.68	9.55	12.50	-4.53	16.17	0.85	0.91
WS (m s^{-1})	2453	1.86	2.79	0.90	1.59	1.03	1.44	1.85	55.05	77.25	0.35	0.50
WD (°)	2430	-	-	-	-	-17.24	52.42	-	-	-	-	-
U10 (m s^{-1})	2430	-0.55	-1.49	1.24	1.85	-0.86	1.60	2.02	154.60	-288.49	0.41	0.59
V10 (m s^{-1})	2430	0.42	-0.32	1.51	2.15	-0.66	1.42	1.87	-158.51	340.62	0.64	0.74

N : numbers of observation (O) and prediction (M); $\bar{O}$: observations mean; $\bar{M}$: prediction mean; σ_O: observation standard deviation; σ_M: prediction standard deviation; MB: mean bias; MAGE: Mean absolute gross error; RMSE: Root mean square error; NMB: Normal mean bias; NME: Normal mean error; R: Pearson correlation coefficient; IOA: index of agreement.

Table E.2 - Statitical indicators for pollutant concentrations in regional domain using the same air quality station from urban domain

	N	$\bar{O}$	$\bar{M}$	σ_O	σ_M	MB	ME	RMSE	NMB	NME	R	IOA
O_3 ($\mu g\ m^{-3}$)	4423	55.09	52.27	51.74	41.03	-1.08	22.64	29.10	-1.96	41.11	0.83	0.89
NO ($\mu g\ m^{-3}$)	3964	30.22	16.30	50.62	36.24	-12.10	30.26	56.04	-40.04	100.15	0.28	0.53
NO_2 ($\mu g\ m^{-3}$)	3964	49.55	27.59	29.25	19.65	-20.32	25.47	34.25	-41.01	51.41	0.44	0.60
NO_X (ppb)	3964	50.73	29.78	49.86	38.21	-18.52	36.31	56.89	-36.52	71.59	0.31	0.57
CO (ppm)	2516	0.92	0.48	0.56	0.44	-0.28	0.51	0.70	-30.57	55.03	0.32	0.55

N : numbers of observation (O) and prediction (M); $\bar{O}$: observations mean; $\bar{M}$: prediction mean; σ_O: observation standard deviation; σ_M: prediction standard deviation; MB: mean bias; MAGE: Mean absolute gross error; RMSE: Root mean square error; NMB: Normal mean bias; NME: Normal mean error; R: Pearson correlation coefficient; IOA: index of agreement.

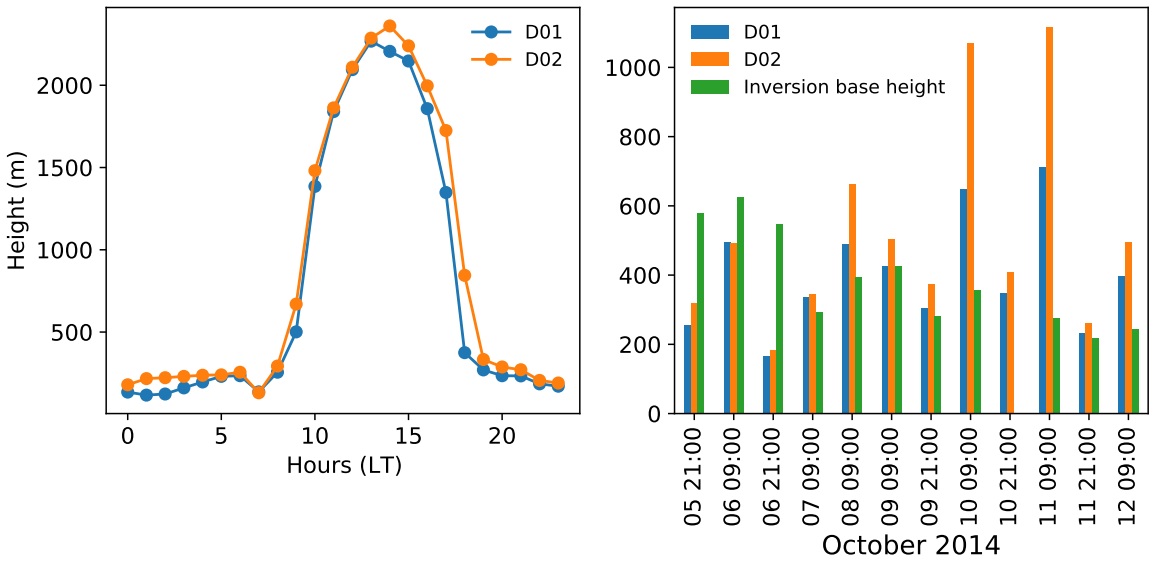

Figure E.1: Comparison of PBL height against inversion base height from soundings launch at Campo de Marte (MASP)

Appendix F

WRF simulation for MUNICH diagnostic run

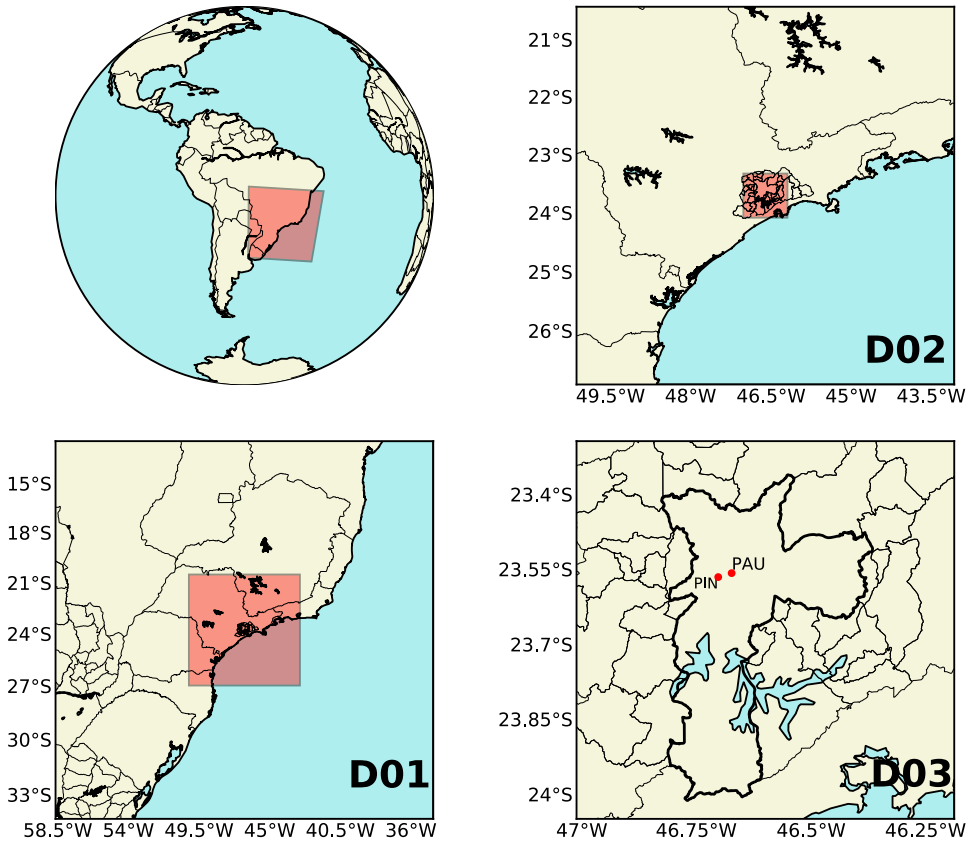

Figure F.1: Three nested WRF simulation domain for MUNICH diagnostic run $\Delta X = 9$ km, 3 km, and 1 km.

Table F.1 - Model Verification. Results outside benchmark are highlighted in bold. MB: mean bias, ME: Mean Absolute Gross Error, IOA: Index of Agreement, $RMSE$: Root mean square error

Parameter	Benchmark for complex terrain	Value
Temperature at 2m	$MB(K) < \pm 1.0$	0.27
(N = 1842)	$ME(K) < 3.0$	1.59
	$IOA \geq 0.8$	0.83
Relative humidity at 2m	$MB(\%) < \pm 10.0$	-5.02
(N = 1843)	$ME(\%) < 20.0$	9.79
	$IOA \geq 0.6$	0.74
Wind Speed at 10m	$MB(ms^{-1}) < \pm 1.5$	0.79
(N = 1885)	$RMSE(ms^{-1}) < 2.5$	1.59
Wind Direction at 10m	$MB(ms^{-1}) < \pm 10.0$	**-16.23**
(N = 1864)	$ME(ms^{-1}) < 55.0$	55

Appendix G

VOC speciation

Table G.1 - VOC speciation fraction

VOC species	Fraction	%
E_ETH	0.04	4.3
E_HC3	0.15	14.7
E_HC5	0.10	10.3
E_HC8	0.11	10.6
E_OL2	0.10	9.6
E_OLT	0.09	9.5
E_OLI	0.10	9.5
E_ISO	0.00	0.1
E_TOL	0.07	6.7
E_XYL	0.06	6.4
E_KET	0.00	0.0
E_CH3OH	0.00	0.0
E_C2H5OH	0.10	9.9
E_HCHO	0.05	4.7
E_ALD	0.04	3.6

ETH: ethane; HC3: propane, alkanes (0.25-0.50), Acetylene, haloalkenes; HC5: alkanes (0.50-1.00), others (0.5-1.0); HC8: alkanes (1.00-2.00), alkanes (> 2.0), alkanes/aromatic mix; OL2: ethene; OLT: propene, alkenes (primary, inter); OLI: alkenes (internal, inter); TOL: benzene, holobenzenes, aromatics (< 2 react), styrenes; XYL: aromatics (> 2 react), alkane/aromatic mix; KET: acetone, higher ketones; CH3OH: methanol; C2H5OH: ethanol; HCHO: formaldehyde; ALD: higher aldehydes